Josip Juraj Strossmayer University of Osijek, Croatia
University of Dubrovnik, Croatia
Ruđer Bošković Institute, Zagreb, Croatia

University Postgraduate Interdisciplinary Doctoral Study
Molecular Biosciences

Ivan Mihaljević

CHARACTERIZATION OF ORGANIC CATION TRANSPORTERS IN ZEBRAFISH (*DANIO RERIO* HAMILTON, 1822)

DOCTORAL THESIS

Osijek, 2015.

TEMELJNA DOKUMENTACIJSKA KARTICA

Sveučilište Josipa Jurja Strossmayera u Osijeku **Doktorski rad**
Sveučilište u Dubrovniku
Institut Ruđer Bošković
Sveučilišni poslijediplomski interdisciplinarni doktorski studij Molekularne bioznanosti

Znanstveno područje: Prirodne znanosti
Znanstveno polje: Biologija

Karakterizacija prijenosnika organskih kationa zebrice (*Danio rerio* Hamilton, 1822)

Ivan Mihaljević

Rad je izrađen u: Institut Ruđer Bošković, Zagreb

Mentor: dr.sc. Tvrtko Smital, znanstveni savjetnik

Kratki sažetak doktorskog rada:

Prijenosnici organskih kationa (OCT, engl. Organic Cation Transporters) su pripadnici SLC22A obitelji unutar nadobitelji SLC (engl. *Solute Cariers*). Ovo istraživanje predstavlja prvu karakterizaciju Slc22 prijenosnika kad riba, s fokusom na njihov fiziološki i ekotoksikološki značaj. Identificirana su dva Oct (Oct1 i Oct2) prijenosnika kod zebrice (*Danio rerio*), koji su pokazali filogenetsku povezanost s OCT ortolozima u sisavaca. Njihova ekspresija u bubregu i jetri upućuje na toksikološku i fiziološki važnu ulogu Oct1 u održavanju homeostaze organskih kationa i obrani od brojnih endo- i ksenobiotika, kao ključan element u ADME procesima.

Broj stranica: 121
Broj slika: 42
Broj tablica: 18
Broj literaturnih navoda: 181
Jezik izvornika: engleski
Ključne riječi: SLC prijenosnici, *Danio rerio*, filogenetska analiza, sintenija, tkivna ekspresija, funkcija, ADME

Datum obrane: 2.7.2015.

Stručno povjerenstvo za obranu:
1. Andreja Ambriović Ristov, dr.sc. znanstvena savjetnica, Institut Ruđer Bošković, predsjednik
2. Tvrtko Smital, dr.sc. znanstveni savjetnik, Institut Ruđer Bošković, mentor i član
3. Vera Cesar, dr.sc. redovita profesorica, Odjel za Biologiju, Sveučilište J.J Strossmayer u Osijeku, član
4.
5.
6. Neda Slade, dr.sc. viša znanstvena suradnica, Institut Ruđer Bošković, zamjena člana

Rad je pohranjen u: Nacionalnoj i sveučilišnoj knjižnici Zagreb, Ul. Hrvatske bratske zajednice 4, Zagreb; Gradskoj i sveučilišnoj knjižnici Osijek, Europska avenija 24, Osijek; Sveučilištu Josipa Jurja Strossmayera u Osijeku, Trg sv. Trojstva 3, Osijek.

BASIC DOCUMENTATION CARD

Josip Juraj Strossmayer University of Osijek, Croatia **PhD thesis**
University of Dubrovnik, Croatia
Ruđer Bošković Institute, Croatia
University Postgraduate Interdisciplinary Doctoral Study of Molecular biosciences

Scientific Area: Natural sciences
Scientific Field: Biology

Characterization of organic cation transporters in zebrafish (*Danio rerio* Hamilton, 1822)

Ivan Mihaljević

Thesis performed at: Institut Ruđer Bošković, Zagreb

Supervisor: Tvrtko Smital, PhD Senior Scientist

Short abstract:

Organic cation transporters (OCTs) are members of SLC22A family within SLC (Solute carrier) protein superfamily which is one of the largest protein superfamilies. This research represents the first characterization of Slc22 transporters in fish, with focus on physiological and ecotoxicological characteristics of Oct transporters in zebrafish (*Danio rerio*). Two Oct genes are identified in zebrafish, and phylogenetic analysis confirmed their relationship with mammalian OCT orthologs. Tissue expression profile showed high expression of Oct1 in kidney and liver, suggesting physiological and ecotoxicological importance of Oct1 in maintenance of organic cation homeostasis and in defense form numerous endo- and xenobiotic compounds, as key element in ADME processes.

Number of pages: 121
Number of figures: 42
Number of tables: 18
Number of references: 181
Original in: English
Key words: SLC transporters, *Danio rerio*, phylogenetic analysis, synteny analysis, tissue expression, function, ADME

Date of the thesis defense: 2.7.2015.

Reviewers:
1. Andreja Ambriović Ristov, PhD, Senior Scientist, Ruđer Bošković Institute, Zagreb
2. Tvrtko Smital, PhD, Senior Scientist, Ruđer Bošković Institute, Zagreb
3. Professor Vera Cesar, PhD, Josip Juraj Strossmayer University of Osijek
4.
5.
6. Neda Slade, PhD, senior research associate, Ruđer Bošković Institute, Zagreb

Thesis deposited in: National and University Library in Zagreb, Ul. Hrvatske bratske zajednice 4, Zagreb, Croatia; City and University Library of Osijek, Europska avenija 24, Osijek, Croatia; Josip Juraj Strossmayer University of Osijek, Trg sv. Trojstva 3, Osijek, Croatia.

Research for this PhD thesis was performed in the Laboratory for Molecular Ecotoxicology, Division of Marine and Environmental Research, Ruđer Bošković Institute, Zagreb, under the supervision of Tvrtko Smital, PhD. This work was supported by the Ministry of Science, Education and Sport of the Republic of Croatia [Project 098-0982934-2745].

Acknowledgments

For excellent mentoring, guidance and for providing me the opportunity and freedom in my research, I thank my supervisor Tvrtko Smital. I am grateful to Marta, Roko and Jovica for all they taught me and for big help and guidance in my research.

I thank Nikola Maraković and Goran Šinko for homology modeling and molecular docking analysis.

Most of all I thank my parents, brother and grandmas for their timeless unconditional love and support. I thank my friends for all the relaxing good times I spent with them.

I thank Sofija for all the love and understanding.

Contents

1. Introduction

1.1. Membrane transporters in Absorption, Distribution, Metabolism and Excretion (ADME)

One of the crucial determinants in absorption, distribution, metabolism and excretion (ADME) of vast number of constantly emerging xenobiotic substances as well as physiological compounds is the cell membrane. Membranes are structures which define main boundaries and connections in living organisms. They are also key regulators of bioavailability of all endo- and xenobiotic compounds. In order to enter a cell, compounds need to cross the selective barrier in a form of cell membrane, which controls the entrance of various nutrients, organic and inorganic ions, as well as various toxicants and drugs that will enter the cell in order to be further metabolized through a series of interconnected processes, and in the end be extruded out of the cells and finally out of the organism.

Essential elements of the cell membrane are proteins embedded in its lipid bilayer through hydrophobic interactions. They play important role in all cellular processes, from receiving the signal molecules and passing on the signaling messages to transporting of physiological compounds in order to be modified or processed by the receiving cells. From the point of ADME processes, crucial membrane proteins responsible primarily for absorption and excretion of endo- and xenobiotics are membrane transporters. Based on their specificities and transport mechanism, membrane transporters regulate both the cell uptake and extrusion of various substrates. Transporter proteins are expressed in all tissues throughout the body, which implies their important role in the maintenance of physiological homeostasis and defensive functions of cells.

The uptake transport proteins represent the initial phase (phase 0) in ADME processes in the cells (Fig. 1.1). This phase represents the entrance of various compounds mediated by polyspecific uptake transporters and it is a rate limiting step of cellular metabolism. Up until recently, it has been considered that lipophilic organic and inorganic molecules pass the membrane by passive diffusion, especially hydrophobic molecules due to specific hydrophobic nature of the membrane lipid bilayer. However, discoveries in the relatively young field of membrane transporters gave a new insight in transport across not only cell membranes, but all membranes in the cell (Nigam, 2015). Two superfamilies of membrane transporters have been identified as relevant ones for these processes: ATP-binding Cassette (ABC) and solute carrier family (SLC) (Shin *et al*., 2015). After the entrance in the cell, compounds go through phase I of the cell metabolism, mediated by enzyme systems responsible for transformation of incoming compounds through series of oxidative and reductive processes. Important enzymatic parts of phase I of the cell metabolism are cytochrome P450 monooxygenases (CYP) and flavin – containing monooxygenases (FMO). Following the first step of transformation, cells need to increase the availability of metabolized compounds through the increase in their solubility in

order to modulate them into more potent substrates of later metabolizing systems or extrusion membrane transporters. The rise of compound solubility in the phase II of cell metabolism is achieved by conjugation with different functional groups of initial non-transformed or already transformed compounds. The usual functional groups which are being conjugated with metabolized compound are glutathione (GSH) added by glutathione s-transferases (GST), glucuronic acid, added by uridine 5'-diphospho-glucuronosyltransferase (UGT) and sulfo group added by sulfotransferases (SULT). In the final phase III of ADME processes metabolized and non-metabolized compounds are extruded out of the cell by ATP-binding Cassette superfamily (ABC) and Multidrug and Toxic compound Extrusion (MATE) family of efflux transporters in order to be further metabolized in other systems or excreted by excretion system (Hodgson, 2010).

The research on membrane transporters as crucial elements of ADME processes is in constant and rapid growth. Due to their essential role, especially in absorption and excretion of pharmaceutical compounds, the efforts have been made to identify new transporters and to determine detailed transport mechanisms and substrate preferences of individual transporters. The research focus is mainly based on drug – drug interactions and determination of the effect different drugs have on numerous membrane transporters (Sun *et al.*, 2014; Kwon *et al.*, 2015). However, endogenous roles of drug transporters, especially in the transport of physiological compounds, such as metabolites and nutrients, are still not fully investigated. Apart from drug - drug interaction, there is growing interest in determination of other types of interaction with membrane transporters, such as drug – metabolite, drug – nutrient or drug – toxin interactions (Nigam, 2015). Understanding the endogenous functions of membrane transporters will provide new insight into the effects of drugs and other xenobiotic compounds on metabolic and developmental processes (Nigam and Bahatnagar, 2013). Additionally, in order to elucidate the impact of membrane transporters on ADME properties of various xeno- and endobiotics, it is necessary to obtain detailed information on transporter expression throughout the organism, especially in primary and toxicologically relevant organs (e.g., liver, kidney, intestine, lungs (gills) and blood–brain barrier (BBB)). Moreover, further investigation of intracellular localization of different types of transporters is necessary for determination of absorptive or exsorptive function of the transporters. Consecutively, combining gathered information about tissue expression and cell localization, together with well-defined interactions with different types of interactors, will provide new insights and valuable information in physiological, pharmacological and ecotoxicological studies of membrane transporters.

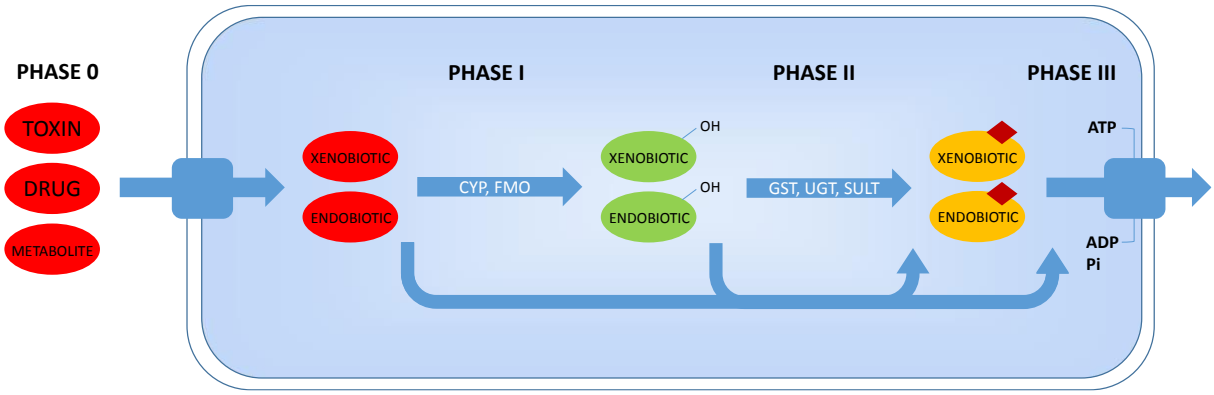

Figure 1.1. Schematic representation of four phases of toxin metabolism in the cell.

1.2. Transporters in blood – tissue barriers

Membrane transporters play crucial roles in the hepatic and renal excretion, intestinal absorption, and transport across blood-tissue barriers. Consequently, they are key mediators in response to environmental and pharmaceutical substances, along with metabolites. Significance of transporters from the SLC family, such as organic cation transporters (OCT/SLC22), organic anion transporters (OAT/SLC22), organic anion transport polypeptides (OATP/SLCO) and MATEs (SLC47), together with extrusion proteins from ABC family, such as P-glycoprotein (ABCB1), multidrug resistance proteins (MRPs/ABCCs), and the breast cancer resistance protein (BCRP/ABCG2), are highly important in characterization of ADME processes. The research on these transporters in ADME studies has been mostly focused on their role in hepatic and renal excretion (Shin *et al*., 2015).

1.2.1. Intestine

Apart from transcellular and paracellular diffusion through intestinal wall (Turner, 2009), membrane transporters play pivotal role in absorption of various essential compounds and nutrients as well as a wide range of drugs and toxins. Numerous polyspecific carriers of organic anions and cations are expressed on apical and basolateral membranes of enterocytes where they play crucial role in absorption, reabsorption and excretion of numerous substances. Compounds are transported into the enterocytes by members of SLC superfamily, OATP, PEPT1 (*SLC15*), ASBT (*SLC10*) and MCT1 (*SLC16*), whereas members of ABC superfamily, MRP2, BCRP and P-gp, pump their substrates out of the enterocytes in the intestinal lumen (Fig. 1.2). The entrance in the blood stream from the enterocytes is mediated by organic solute transporter (OST – *SLC51*) and MRP3, whereas OCT1 mediates transport in opposite direction and contributes to intestinal excretion (Fig. 1.2). In aquatic organisms intestinal absorption accounts for just one fraction of the absorption of foreign compounds. The crucial part of foreign hydrophobic compound absorption in aquatic organisms is dermal absorption, which accounts

for approximately 50% of all uptake (Sukardi *et al.*, 2010). The rest of absorption is mediated through gills, as the most exposed barrier tissue between aquatic environment and living organism (Di Giullio and Hinton, 2008).

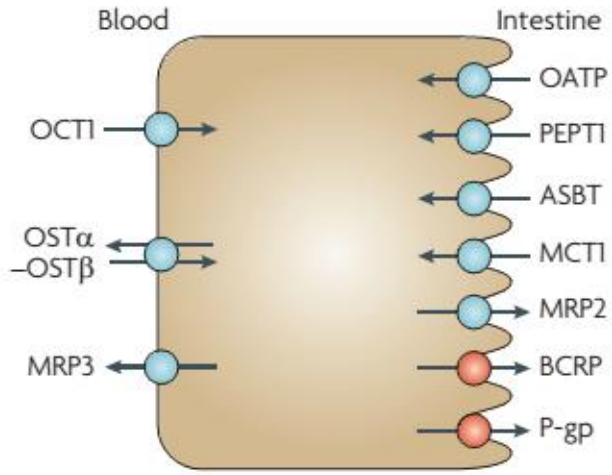

Figure 1.2. Plasma membrane transporter localization on basolateral and luminal membranes of an intestinal epithelial cell (from Giacomini *et al*., 2010).

1.2.2. Liver

After the entrance in the blood stream the compounds are transported into the liver for initial metabolization by the portal blood. Most of the processes connected with previously mentioned phases I and II of xenobiotic metabolism have the highest activity in the liver (Jakoby and Ziegler, 1990). However, in order to be metabolized by phase I and II enzyme systems in the smooth endoplasmic reticulum of the hepatocytes, compounds need to be transported in the hepatocyte by members of SLC21 and SLC22 membrane transporter families, whereas the extrusion of metabolized compounds is governed by MATE1 and ABC superfamily members, including P-glycoprotein (MDR1), MRP2 and BCRP (Fig. 1.3). The uptake of anionic compounds is mediated by three members of SLCO family, OATP1B1, OATP1B3 and OATP2B1 (Smith *et al.,* 2005), with endogenous substrates such as bile salts, bilirubin and estrone-3-sulfate (Hagenbuch and Meier, 2004) and drugs such as statins and angiotensin-II blockers (Hirano *et al*., 2006; Yamashiro *et al*., 2006). Additional anionic species such as prostaglandins, urates, cyclic nucleotides, antibiotics, antiviral drugs and non-steroidal anti-inflammatory drugs (NSAIDs) are transported by OAT2, expressed in the basolateral membrane of hepatocytes (Miyazaki *et al*., 2004). The major hepatic transporter of cationic compounds is OCT1, responsible for uptake and hepatic excretion of various organic cations such as physiological compounds, acetylcholine, corticosterone and progesterone, together with drugs, metformin, cimetidine, quinidine, verapamil

and several antiviral drugs (Koepsell *et al*., 2007). Biliary excretion of endogenous compounds like steroid hormones, conjugated and non-conjugated bile salts, leukotriene C_4, cyclic nucleotides and folic acid, is mediated by members of ABC superfamily (Leslie *et al.*, 2005). The major representatives of these transporters are MDR1, which accepts mostly cationic compounds with one or more plain hydrophobic moieties (Lin and Yamazaki, 2003); BSEP, which eliminate mostly bile salts (Noé *et al*., 2005), pravastatin (Hirano *et al*., 2006) and vinblastine (Lecureur *et al*., 2000); transporters form MRP subfamily, MRP2, located at the canalicular membrane and responsible for extrusion of leukotriene C_4 and wide range of conjugated and non-conjugated metabolites and xenobiotics (Nies and Keppler, 2007), MRP1, MRP3 and MRP4, localized at the basolateral membrane and involved in the efflux of drugs and metabolites back to plasma (Donner and Keppler, 2001); and finally BCRP, expressed in the canalicular membranes of hepatocytes with important role in excretion of xenobiotics and conjugated metabolites (Xia *et al*., 2005).

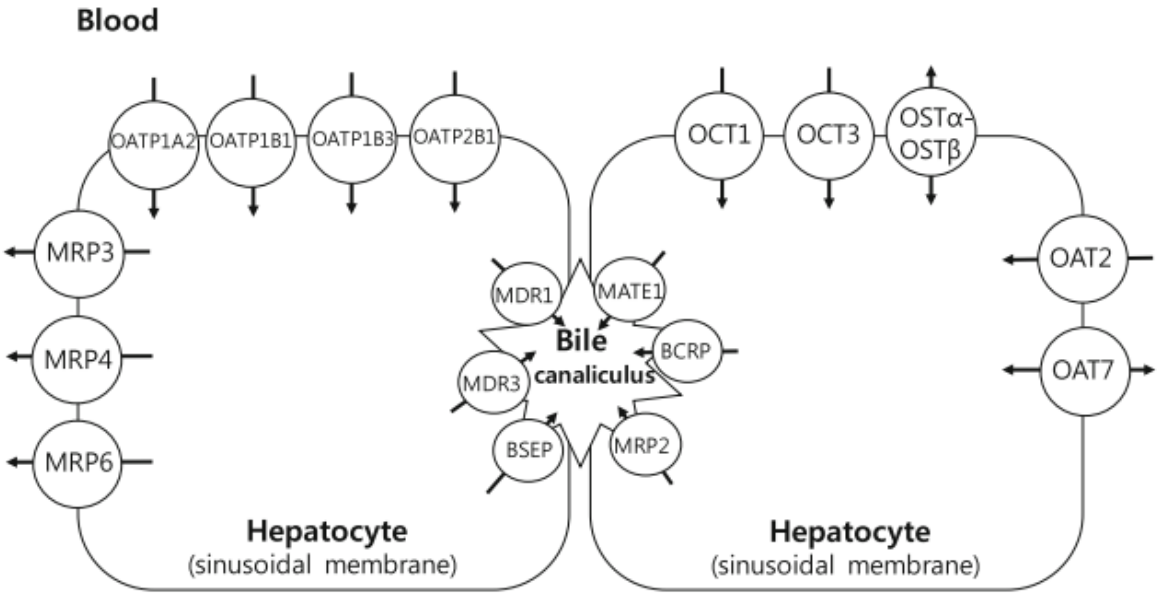

Figure 1.3. Major SLC and ABC transporters involved in hepatic drug transport and excretion in polarized hepatocytes (from Shin *et al*., 2015).

1.2.3. Kidney

Another toxicologically relevant excretion pathway is renal elimination. Kidney plays essential role in the homeostasis of the organism through control of renal secretion and reabsorption of numerous metabolized and non-metabolized xenobiotics and endogenous metabolites. Categorization of renal transporters is based on their preferences for organic anions or cations (Ullrich, 1993) and their localization at the basolateral and brush-border membranes (Pritchard and Miller, 1996). Members of the SLC superfamily are located on both sides of kidney proximal tubule cells and are responsible for

the uptake of substrates from the blood on the basolateral membrane and excretion into urine in the brush-border membrane (Fig. 1.4). Uptake of organic anions is mediated by members of organic anion transporters, OAT1, OAT2 and OAT3, together with OATP4C1, whereas OCT2 mediates transport of organic cation across basolateral membrane of kidney proximal tubule (Giacomini *et al*., 2010). On the opposite, brush-border membranes, SLCO and SLC22 family members are responsible for excretion and reabsorption of organic anions and cations, together with members of ABC superfamily, as presented on Figure 1.4. There are also two members of the SLC47 family, MATE1 and MATE2-K, which function as H^+/organic cation antiporters and mediate transport of tetraethylammonium, MPP+, cimetidine, cephalexin and oxaliplatin (Tanihara *et al*., 2007).

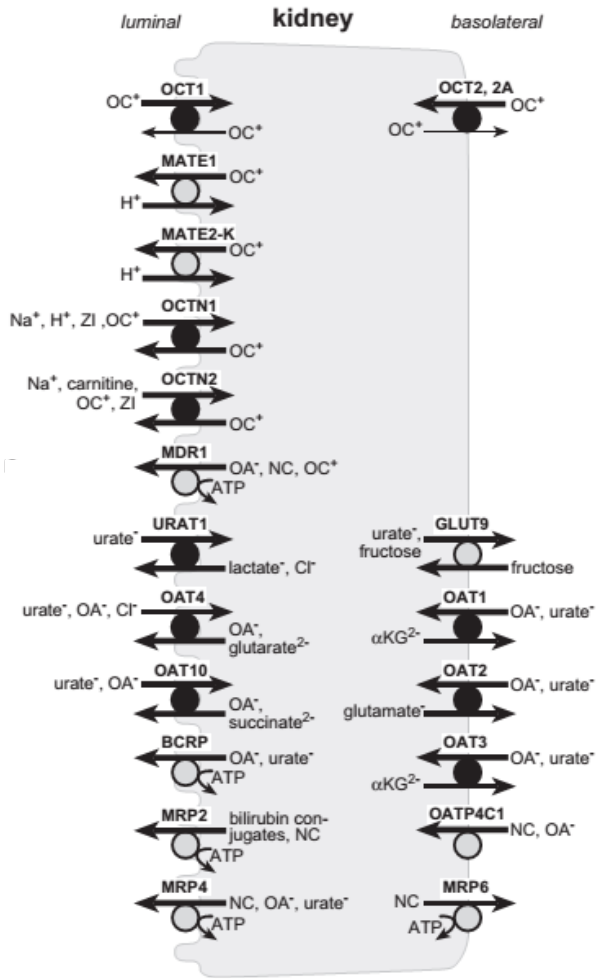

Figure 1.4. Localization of human drug and urate transporters in renal proximal tubule cells. OC^+ organic cation, NC non-charged compound, OA^- organic anion, ZI zwitterion (from Koepsell, 2013).

1.2.4. Blood – brain barrier

As it was mentioned in previous explanations related to significance of membrane transporters in blood – tissue barrier, members of both SLC and ABC superfamilies play important roles in disposition of endo- and xenobiotics in blood – brain barrier (Fig. 1.5). Membrane transporters expressed in/on the membranes of blood-brain barrier have potentially more significant role in physiological processes. However, they also have a crucial role in ADME processes and are important for understanding of pharmacodynamic and pharmacokinetic properties of substances (Giacomini *et al*., 2010).

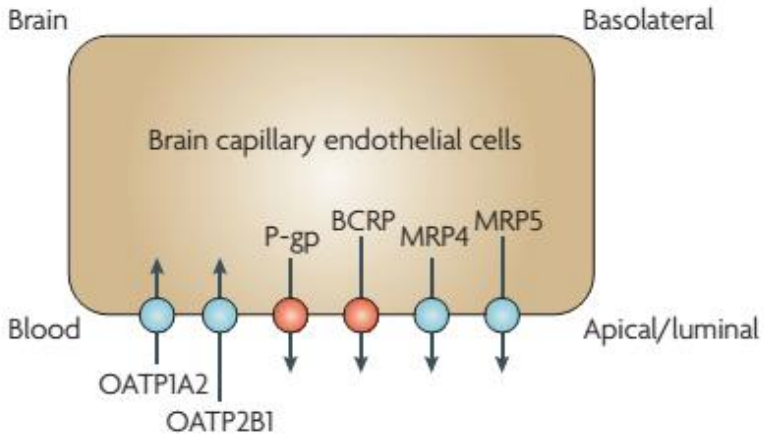

Figure 1.5. Plasma membrane transporter localization on apical/luminal membrane of blood – brain barrier (from Giacomini *et al*., 2010).

1.3. SLC22 family of membrane transporters

The solute carrier (SLC) superfamily of proteins currently encompasses 398 proteins, organized within 52 families (Schlessinger *et al*., 2013). This large number of functionally diverse proteins makes the SLC superfamily the largest known protein family. Members of SLC families are membrane transporters responsible for the uptake and extrusion of enormous variety of organic and inorganic substrates, from glutamate and neutral amino acids, transported by SLC1 (Kanai and Hediger, 2004) to riboflavin, transported by SLC52 (Yonezawa and Inui, 2013). The nomenclature of SLC members is proposed by HUGO gene nomenclature committee (http://www.genenames.org) and it is based on functional, rather than evolutional properties, with focus on their amino acid homology, substrate preferences and transport mechanism. Members of each SLC family have 20 – 25% amino acid identity among each other, whereas members of different SLC families have close to or below 1% identity (Heidiger et al., 2004). The SLC22 family members are members of major facilitator superfamily (MFS) clan, which

encompasses all SLCs, together with other membrane proteins and it is one of the largest clans of membrane transporters found in humans (Höglund *et al*., 2010).

Human SLC22 family consists of 23 functionally characterized membrane transporters, divided in three substrate-specific subfamilies: organic cation transporters (OCTs) (Fig. 1.6A), organic zwitterion/cation transporters (OCTNs) and organic anion transporters (OATs) (Fig. 1.6B). Members of SLC22 family act as uniporters, which induce facilitated diffusion (OCTs and OCTNs), anion exchangers (OATs) and Na^+/zwitterion cotransporters (Koepsell, 2013). Regardless of the maximal amino acid sequence homology of 25%, all members of SLC22 family have similar secondary and tertiary protein structures (Fig. 1.6). They are monomeric polypeptides consisted of 12 transmembrane α-helices, which form transmembrane domains and are incorporated in plasma membranes of the cell. Order and steric arrangement of transmembrane helices define polyspecific active site clefts of the transporters (Koepsell *et al*., 2007).

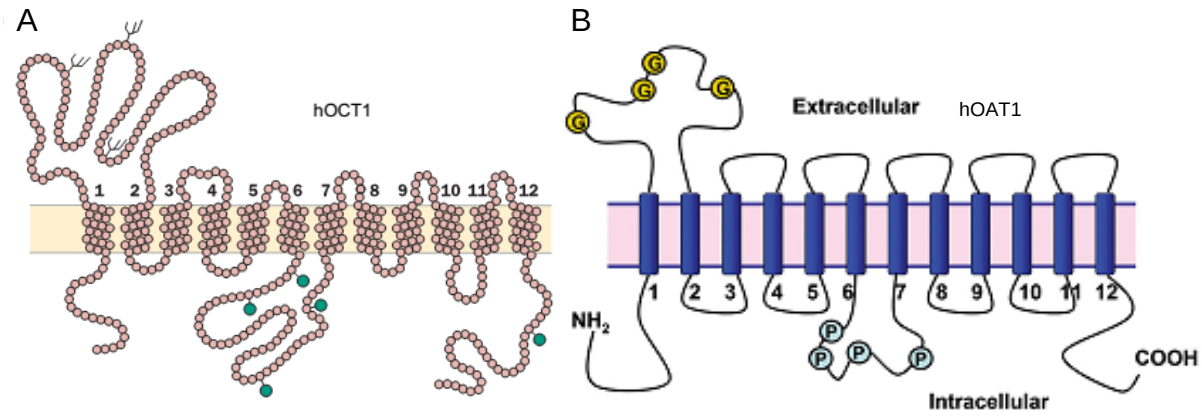

Figure 1.6. Comparison of A) Predicted topology of the OCT1 organic cation transporters in humans with predicted N-glycosylation sites on the large extracellular loop (ψ) and predicted phosphorylation sites (green) in intracellular loop; from Koepsell, 2004); B) Predicted topology of human OAT1 organic anion transporter with predicted N-glycosylation sites (G) and phosphorylation sites in intracellular loop (P) (from Nigam *et al*., 2015).

SLC22 transporters mediate small intestinal absorption and hepatic and renal elimination of drugs, toxins and deleterious endogenous compounds and participate in homeostatic processes in brain (Koepsell, 2013). Included endogenous substrates of SLC22 carriers are monoamine neurotransmitters, cyclic nucleotides, steroid hormones, prostaglandins, and urate, whereas important xenobiotic substrates emphasize polyspecific nature of these transporters with specificities raging from

antimalarial, antiviral drugs, antibiotics, nonsteroidal anti-inflammatory drugs to toxins such as ethidium bromide and aflatoxin B1 (Koepsell, 2013).

Ten members of organic anion transporter (OAT) family constitute almost half of all SLC22 transporters (Fig. 1.7). OATs are ubiquitously expressed in almost all barrier epithelia throughout the organism, with OAT1 – 3 expressed on the basolateral membrane and OAT4 expressed on the luminal membrane of renal proximal tubules, where they play crucial roles in excretion of broad and overlapping set of deleterious compounds as well as in anion homeostasis maintenance by regulating the reabsorption of excreted anions (Nigam *et al*., 2015). OAT2, OAT5 and OAT7 are mainly expressed in liver, where they mediate hepatic excretion of endogenous substrates such as glutamate, glutarate, urate, L-ascorbate, cyclic nucleotides, prostaglandin E2 and F2, estrone-3-sulfate, dehydroepiandrosterone and α-ketoglutarate, along with transport of xenobiotics such as salicylate, erythromycin, tetracycline, ranidine, 5-fluorouracil, methothrexate, taxol, aflatoxin B1 and other drugs and toxins (Nigam *et al*., 2015).

There are two representatives of organic zwitterion/cation transporters (OCTNs) within SLC22 family (Fig. 1.7). Expression of OCTN1 on luminal membranes of renal proximal tubules contributes in excretion and reabsorption of zwitterions and organic cations. Some of OCTN1 substrates are tetraethylammonium (TEA), acetylcholine (Pochini *et al*., 2012), quinidine, pyrilamine, verapamil (Tamai, 2012), and the anticancer drugs mitoxantrone and doxorubicin (Koepsell *et al*., 2007; Okabe *et al*., 2008). OCTN1 contributes in erythroid differentiation through intestinal absorption of antioxidant ergothioneine and reabsorption of ergothioneine in proximal tubules (Nakamura *et al*., 2008). Apart from OCTN1 localization in luminal membranes, it is also localized in mitochondrial membranes (Koepsell *et al*., 2007). On the other hand, second OCTN member, OCTN2, as pivotal transporter of L-carnitine contributes to mitochondrial uptake of fatty acids by L-carnitine-acyl cotransporter (Koepsell, 2013). OCTN2 plays a role in intestinal absorption and renal reabsorption of L-carnitine. It is crucial transporter of L-carnitine in numerous tissues such as adipocytes, skeletal muscle cells (Furuichi *et al*., 2010), colonic epithelial cells and across the blood–retinal barrier (Koepsell *et al*., 2007; Tachikawa *et al.*, 2010).

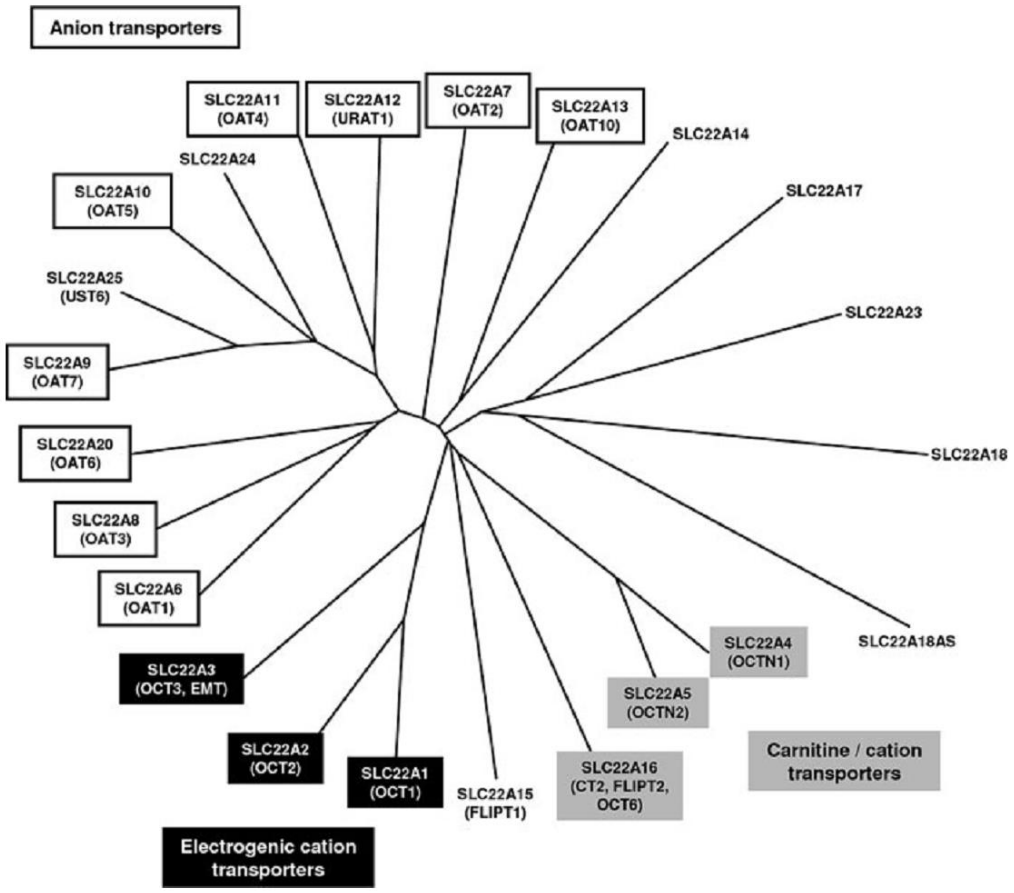

Figure 1.7. Phylogenetic tree of the 23 transporters of the human SLC22 family. Electrogenic cation transporters are marked by black boxes, transporters for organic cations and carnitine by gray boxes, and transporters for organic anions by white boxes. Transporters whose function is as yet unknown are unmarked (from Nies *et al*., 2011).

1.4. Organic cation transporters

Members of human SLC22 family responsible for plasma membrane transport of numerous organic cations are organic cation transporters (OCTs), with three representatives, OCT1 – 3. The first member, OCT1, was initially identified in human (Zhang *et al*., 1997a), following by identification of orthologs in rat, mouse and rabbit (Terashita *et al.*, 1998; Green *et al.*, 1999). Further investigation showed the presence of OCT orthologs in all vertebrate genomes, with considerable diversities in functional isoforms, such as active isoform of rat OCT1 missing the first two transmembrane domains and the large extracellular loop (Zhang *et al*., 1997b) or active isoform of human OCT2 (OCT2B) missing the last three TMDs (Urakami *et al*., 2002). Human OCT coding genes are localized within a cluster on chromosome 6.q26-7 (Koehler *et al*., 1997). Each of the three genes comprises 11 exons and 10 introns (Hayer *et al*., 1999).

1.4.1. Tissue Distribution and Membrane Localization

1.4.1.1. OCT1 (SLC22A1)

Human *OCT1* exhibits the strongest expression in the liver (Gorboulev *et al*., 1997) whereas in rodents, *Oct1* is strongly expressed in liver, kidney and small intestine. *OCT1* is also found in epithelial cells and neurons (Koepsell *et al*., 2003). Tissue expression analysis of both human and rodent *OCT1/Oct1* also revealed their presence in many other organs and tumor cells and basophilic granulocytes (Gorboulev *et al*., 1997). Human and rat *OCT1/Oct1* is located at the sinusoidal membrane of the hepatocytes (Meyer-Wentrup *et al*., 1998) and basolateral membrane of epithelial cells in the S1 and S2 segments of proximal tubules (Sugawara-Yokoo *et al*., 2000), whereas mouse *Oct1* ortholog is located at the basolateral membrane of enterocytes (Chen *et al*., 2001). Contrary to the localization in renal, hepatic and intestinal cells, in human and rodent trachea and bronchi *OCT1* is located in the luminal membrane of epithelial cells (Lips *et al*., 2005; Kummer *et al*., 2006).

1.4.1.2. OCT2 (SLC22A2)

Comparing with *OCT1*, *OCT2* shows more restricted expression pattern. Human *OCT2* is most strongly expressed in the kidney (Okuda *et al*., 1996), within all three segments of proximal tubules (Motohashi *et al*., 2002) whereas rat *Oct2* is located in the S2 and S3 segments (Karbach *et al.,* 2000). There has also been reported expression and localization of *OCT2* in other organs including basolateral membranes of small intestine (Gorboulev *et al*., 1997), the luminal membrane of epithelial cells in trachea and bronchi (Lips *et al*., 2005) and brain (Busch *et al*., 1998). Expression of *Oct2* in rat brain showed the localization in the apical membrane in epithelial cells of choroid plexus (Sweet *et al*., 2001).

1.4.1.3. OCT3 (SLC22A3)

The tissue expression pattern of human *OCT3* is more ubiquitous comparing with previous two members. Contrary to *OCT1* and *OCT2*, *OCT3* is not only expressed in epithelial cells of toxicologically crucial tissues and neurons, but also in muscle cells and glia cells (Inazu *et al.,* 2003; Zhang *et al*., 2008). The highest expression of human *OCT3* is determined in skeletal muscle, sinusoidal membrane of hepatocytes, basolateral membrane of the trophoblast in placenta (Sata *et al*., 2005), luminal membranes of bronchial epithelial cells and small intestinal enterocytes, heart, brain and in some cancer cell lines (Lips *et al*., 2005; Müller *et al*., 2005; Nies *et al*., 2011). Additionally, rodent *Oct3* is expressed in Sertoli cells, basophile granulocytes (Slitt *et al*., 2002; Alnouti *et al*., 2006) and in hippocampus, medial hypothalamus, and ependym of the third ventricle (Gasser *et al*., 2006; Vialou *et al*., 2004).

1.4.2. Functional Properties of OCT1-3

As it can be seen from tissue expression patterns and localizations of organic cation transporters, their role in physiological and toxicological processes is diverse and essential. The reported overlapping of tissue expression also contributes to their transport characteristics, which are similar in numerous investigated species. The first characteristic of OCT1-3 is a variety of transported organic cations with widely differing molecular structures, as well as numerous additional inhibitors which are not transported by OCTs, but their interaction is reported. The relative molecular mass of most OCT substrates is below 400 $gmol^{-1}$, which belongs to type I of organic cations, with the smallest reported diameter below 4 Å (Schmitt and Koepsell, 2005). Second common functional characteristic of OCTs is electrogenic mechanism of substrate translocation. Electrogenic transport of organic cations is reported for human OCT1 and OCT2 (Dresser *et al*., 1999) and rat Octs (Arndt *et al*., 2001). Third specific characteristic of OCTs is that they operate the transport of cationic substrates autonomously of Na^+ gradient, and are also independent of H^+ gradients when the effect of proton gradients on the membrane potential is excluded (Keller *et al*., 2005). Fourth characteristic of OCTs is the ability of bidirectional translocation of organic cations across the plasma membrane, which is reported for human and rodent OCTs (Nagel *et al*., 1997) (Fig. 1.8).

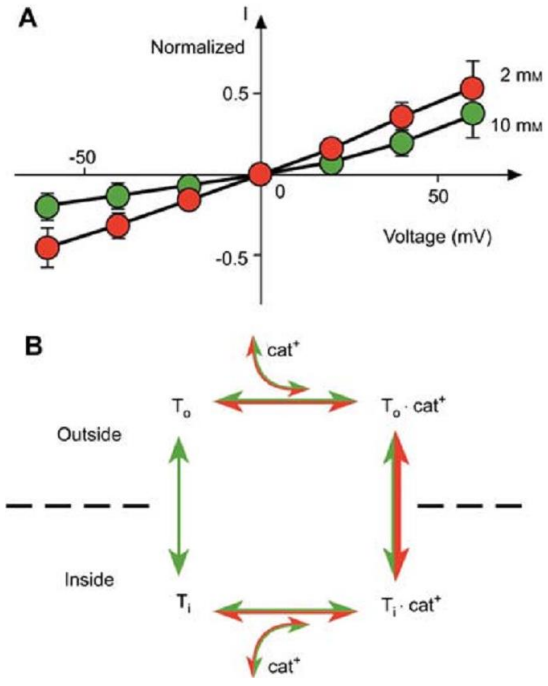

Figure 1.8. Illustration of symmetrical electrogenic transport mechanism of choline by rat Oct2. A) Dose response of two choline concentrations (2 mM and 10 mM) with voltage – current relationship graph in giant patches of *X. laevis* oocytes in inside-out orientation, B) Model of a simple cation translocation by rat Oct2, with the individual reaction steps involved in electrogenic cation uniport (green arrows)

and electroneutral cation/cation exchange (red arrows). T_o and T_i represent transporter conformations with the cation-binding site oriented inside and outside the cell, respectively. cat^+ is monovalent organic cation (from Koepsell, 2011).

Substrate specificities of the OCT/Oct transporters range from mostly organic cations and weak bases that are positively charged at physiological pH, with some exceptions in non-charged compounds. OCTs/Octs translocate endogenous compounds, drugs, xenobiotics, and model cationic compounds, such as 1-methyl-4-phenylpyridinium (MPP+), which displays high uptake rates and similar K_m affinity constants among mammalian species (Gorboulev *et al*., 1997). There has also been reported a variety of cations which inhibit OCT transport but are not transported by OCTs. Some of reported OCT inhibitors are positively charged tetrapentylammonium, decynium 22 and disprocynium, non-charged molecules such as corticosterone, deoxycorticosterone, and b-estradiol, as well as certain anions, probenecid and α-ketogluatarate (Zhang *et al*., 1997a). Substrate and inhibitor preferences of OCTs/Octs largely overlap. However, the differences in substrate and inhibitor specificities between individual subtypes and between identical subtypes of different species have been reported (Koepsell *et al*., 2003), which show that some cations transported by one OCT/Oct transporter are non-transported inhibitors of another transporter (Dresser *et al*., 2000). Reported overlapping of substrate/inhibitor affinities of individual OCTs/Octs indicates the complexity of substrate/inhibitor binding versus substrate transport. Different types of interaction between OCTs/Octs and their substrates and inhibitors, which deviate from classical types of inhibition, have been observed and point to complexity of interaction of OCT/Oct active sites and their substrates or non-transported inhibitors (Schmitt and Koepsell, 2005).

1.4.3. Substrate and Inhibitor Specificities of OCTs

Cationic compounds transported by human OCT1 comprise of the model cations MPP+, tetraethylammonium (TEA), tetrapropylammonium (TPA), tetrabutylammonium (TBA), N-methylquinine and N-(4.4-azo-n-pentyl)-21-deoxyajmalinium, the endogenous compounds acetylcholine, choline, and agmatine, and the xenobiotics such as quinidine, quinine, acyclovir, ganciclovir and metformin (Koepsell, 2013). Human OCT1 shows the highest affinities for MPP+ (K_m = 15 – 32 µM) and TBA (30 µM) (Suhre *et al*., 2005). There have also been reported higher affinities of OCT1 for non-transported inhibitors, such as phencyclidine, diphenylhydramine and ranitidine, comparing with OCT2 and OCT3 (Amphoux *et al*., 2006; Tahara *et al*., 2005), whereas some reported substrates of human OCT2 and OCT3, such as epinephrine, norepinephrine, and histamine, are not

transported by OCT1. The most potent non-transported inhibitors of human OCT1 are atropine (K_i = 1.2 µM) and prazosin (K_i = 1.8 µM) (Hayer-Zillgen *et al*., 2002).

Human OCT2 transport of cationic substrates has been determined for much more compounds than with OCT1 and OCT3 due to better established electrogenic transport assays in *X. laevis* oocytes, which resulted with higher cation induced currents (Koepsell, 2007). Certain portion of human OCT2 substrates overlaps with OCT1. The examples of such substrates are MPP+, TEA, quinine, and metformin with similar K_m values (Koepsell *et al*., 2003). Human OCT2 also translocates acetylcholine with an approximately 4-fold higher affinity than OCT1 (Koepsell *et al*., 2003). Additional cationic substrates of OCT2 are endogenous compounds such as choline, dopamine, norepinephrine, epinephrine, serotonin, histamine, agmatine (Gründemann *et al*., 2003) and xenobiotics such as glutamate receptor antagonists amantadine and memantine, histamine H2 receptor antagonists cimetidine, famotidine and ranitidine, cytostatic cisplatin, and antihypertensive drug debrisoquine (Koepsell, 2013).

Contrary to similar reported affinities for MPP+ transport by human OCT1, OCT2 and OCT3, a much higher K_m of 47 µM value was determined for translocation of TEA by OCT3 compared to OCT1 and OCT2 (Otsuka *et al*., 2005). However, lower inhibition constants of human OCT3 compared to OCT1 and OCT2 was noticed for amantadine, memantine, phenylcyclidine, clonidine, diphenylhydramine, atropine, procainamide and cocaine (Amphoux *et al*., 2006). Disprocynium 24, decynium 22 and corticosterone showed highest inhibition of OCT3 with K_i values of 0.015 µM, 0.1 µM and 0.12 µM, respectively (Hayer-Zillgen *et al*., 2002).

1.4.4. Regulation

In order to determine more detailed role of OCT function in physiological as well as in pharmacological and toxicological sense, their short and long term regulation must be elucidated. It has been shown that the regulation of organic cation transporters is very complex and can happen at all levels of protein expression. It can appear at the transcriptional level, as message stability, translational and numerous posttranslational modifications. Regulation may be different for subtypes and orthologues of transporters and may vary for an individual transporter in different tissues.

1.4.4.1. Short Term Regulation of OCTs/Octs

Short term regulation of OCT1, OCT2 and OCT3 was studied *in vitro* on various cell lines and studies showed some important differences in short term regulation among human OCTs, as well as between

human and other mammalian orthologs (Ciarimboli *et al*., 2004). Studies of human OCTs regulation by protein kinase A (PKA) revealed the inhibition of uptake of the fluorescent organic cation 4-(4-(dimethylamino)styryl)- N-methylpyridinium iodide (ASP+) mediated by OCT1 and OCT2, whereas PKA did not alter the MPP+ uptake by OCT3 (Cetinkaya *et al*., 2003). Contrary to PKA uptake inhibition, cation uptake by human OCTs is stimulated by the Ca^{2+}/calmodulin (CaM) pathway (Cetinkaya *et al*., 2003). Surprisingly, the *in vivo* regulation of human OCTs did not always match the determined *in vitro* regulation in HEK293 or CHO cell lines, especially in the regulation of ASP+ uptake by OCT2 and OCT3 in basolateral membranes of renal proximal tubules (Ciarimboli *et al*., 2004; Martel *et al*., 2001). The short term regulation of human OCTs may also interact with OCT substrate specificities, changing the substrate affinities. Inhibition of CaM pathway by calmidazolium decreased the affinity for TEA 6-fold for OCT1 and 10-fold for OCT2 (Cetinkaya *et al*., 2003). Additional short term regulation of human OCT3 was reported by proteins containing PDZ (PSD95, Dlg, ZO1) domains, which indicate the role of OCTs in signaling functions in the cell (Kato *et al*., 2004). *In vitro* studies with HEK293 cells stably transfected with rat *Oct1* gene, confirmed the ASP+ transport stimulation by activators of PKC, PKA, and tyrosine kinase (Mehrens *et al*., 2000). Additional mutagenesis studies confirmed the interaction of PKC with rat Oct1 through ASP+ uptake by rat Oct1, which was diminished when individual serine and threonine residues in putative PKC phosphorylation sites were replaced by alanine. The alterations of PKC phosphorylation sites also affected the affinities of TEA and TPA, which resulted with inhibition of ASP+ uptake (Ciarimboli *et al.,* 2005).

1.4.4.2. Long Term Regulations of OCT1-3

Long term regulation of OCTs/Octs is focused on gender differences among the transporters. Expression of OCT2/Oct2 is gender dependent and regulated by steroid hormones, which is confirmed with observed TEA uptake in renal cortical slices of male rats. TEA uptake is greater in renal cortical slices of male rats, comparing with female, which is also confirmed on mRNA and protein levels (Urakami *et al*., 1999). Regulation by steroid hormones was confirmed by administering of testosterone to female rats which resulted in increased renal expression of Oct2, whereas application of estradiol to male rats decreased the renal expression of Oct2 (Urakami *et al*., 2000). Testosterone mediated transcriptional upregulation of rat Oct1 is controlled by androgen receptor which was confirmed by identification of two testosterone dependent androgen receptor promoters within *Oct2* promoter region (Asaka *et al*., 2006). However, the steroid hormone regulation of Oct2 is species dependent and may not correlate with protein expression and activities. The example is renal expression of rabbit Oct2, where higher expression of male Oct2 was observed, without any significant difference in protein expression of TEA uptake (Groves *et al*., 2006). Transcription of human *OCT1* is

activated by hepatocyte nuclear factor-4a (HNF-4a), by two HNF-4a response elements within *OCT1* promoter (Saborowski *et al*., 2006). HNF-4a mediated transcription is inhibited by the bile acid chenodeoxycholic acid (Saborowski *et al*., 2006). On the other hand, mouse *Oct1* transcription is regulated by peroxisome proliferator agonist receptor (PPAR) response element and upregulation is activated by PPAR agonists, clofibrate and ciglitazone (Nie *et al*., 2005). Certain pathological and drug disruptions resulted with alteration in the expression of OCTs/Octs. In the case of chronic renal failure, the expression of rat Oct2 is decreased in kidney (Ji *et al*., 2002). Decrease in renal expression of OCTs/Octs is also observed in diabetes (Grover *et al*., 2002), while methamphetamine treatment decreased the expression of Oct3 in rat brain, suggesting a drug-induced downregulation (Kitaichi *et al*., 2003; Zhu *et al*., 2010).

1.4.5. *Oct* gene knockout studies

In general, gene knockout studies on *Oct1*, *Oct2*, and *Oct*3 showed no effect on mouse fertility and no visible physiological disruptions (Jonker *et al*., 2003). The studies with *Oct1* knockout mice and injected substrates showed decreased concentrations of TEA, MPP+ and metformin in liver and small intestine (Jonker *et al*., 2001). The biliary excretion of TEA decreased, whereas the renal excretion was increased, which indicates crucial role of Oct1 in biliary excretion of TEA as a good Oct1 substrate, and compensatory renal excretion. On the other hand, disruption of *Oct2* did not affect biliary and renal excretions of TEA (Jonker *et al*., 2003). Oct1 and Oct2 double knockout mice revealed that renal excretion of TEA in mice is mainly mediated by Oct1 and Oct2 (Jonker *et al*., 2003). Studies with Oct1 and Oct2 double knockout mice also implied to minor role of Oct3 in liver and kidney excretion, whereas Oct3 showed the important role in heart. Pharmacokinetic studies in Oct3 knockout mice with MPP+ as model substrate showed significant decrease in concentration of MPP+ in mouse heart, regardless to expression of Oct1 and Oct2 in mouse heart, as well as good transport of MPP+ by all three members of mouse Octs, confirming Oct3 as most important cation transporter in mouse heart (Zwart *et al*., 2001). The studies with pregnant Oct3 knockout mice confirmed important role in embryonic uptake of MPP+, without effect on the passage of MPP+ over maternofetal barrier (Vialou *et al*., 2004).

1.4.6. Mutations and polymorphisms of OCT1-3

Studies on recorded polymorphisms of human OCT genes contributed to a more detailed understanding of roles and functions of OCTs. Observed 18 single nucleotide polymorphisms (SNPs) of *OCT1* result in substitutions or deletions of single amino acid (Kerb *et al*., 2002). Reduced transport

activities were observed as a result of six mutations (Arg61Cys, Cys88Arg, Gly220Val, Pro341Leu, Gly401Ser, and Gly465Arg), whereas mutation Ser14Phe resulted with increase in transport activity (Shu *et al*., 2003). OCT2 analysis revealed 10 functionally active variants that caused amino acid changes, with no significant functional difference compared to wild type OCT2 (Fujita *et al*., 2006). Contrary to OCT1 and OCT2, no OCT3 mutations have been reported that lead to exchange in amino acids.

1.4.7. Structure – function relationships

Site directed mutagenesis of rat OCT1 revealed seven amino acid residues involved in cation binding (Fig. 1.9): tryptophan 218, tyrosine 222 and threonine 226 on the predicted fourth transmembrane domain (TMD); alanine 443, leucine 447 and glutamine 448 in the tenth TMD (Gorboulev *et al*., 2005); and aspartate 475 in the middle of the eleventh TMD (Gorboulev *et al*., 1999).

Mutagenesis experiments confirmed that Asp475 is located within or in close proximity of the substrate binding site of rat Oct1, which is more defined as substrate binding region because it possesses several, only partially overlapping interaction domains for different substrates. Mentioned conclusions were confirmed by Asp475Glu mutation which resulted in reduction to 2 – 4% of TEA and choline maximal transport rate, after expression in *X. laevis* oocytes and 11% for MPP+, respectively. On the other hand, the affinity for TEA showed 8–15-fold increase, whereas the K_m value for MPP+ remained unchanged (Gorboulev *et al*., 1999). Three additional amino acid residues – Trp218, Tyr222 and Thr226 on the TMD4 – lay within the substrate binding region of rOct1. Mutations of these residues caused an increase in affinities for individual substrates and in some cases changes in V_{max} values (Popp *et al*., 2005). Amino acid residues Arg440, Leu447 and Gln448 on TMD10 are also identified as interacting residues within or close to substrate binding region of rat Oct1. These conclusions are based on 30 – 40-fold increase in corticosterone affinity after mutations: Ala443Ile, Leu447Phe and Gln448Glu (Volk *et al.*, 2009). Second proof of localization and importance of mentioned amino acid residues are mutations Leu447Phe and Gln448Glu, resulting in a significant increase in affinity for MPP+, whereas Ala443Ile, Leu447Phe and Gln448Glu caused a decrease of the K_m value for TEA (Popp *et al*., 2005). Presented data on corticosterone interactions with different amino acid residues also confirm previous conclusions about the presence of the substrate binding region instead of substrate binding site(s) (Volk *et al.*, 2009).

The findings of site directed mutagenesis studies are also confirmed by homology modeling analysis, based on known crystal structures of two bacterial proteins of the MFS superfamily, lactose permease (LacY) and glycerol-3-phosphate transporter (GlpT) from *E. coli.* Crystal structures of these two MFS

proteins showed great similarity with obtained OCT model, with large cleft formed by eight transmembrane α-helices (Popp *et al*., 2005). The most importantly, the model confirmed that the seven amino acids, determined by site directed mutagenesis lay at a similar depth within this cleft.

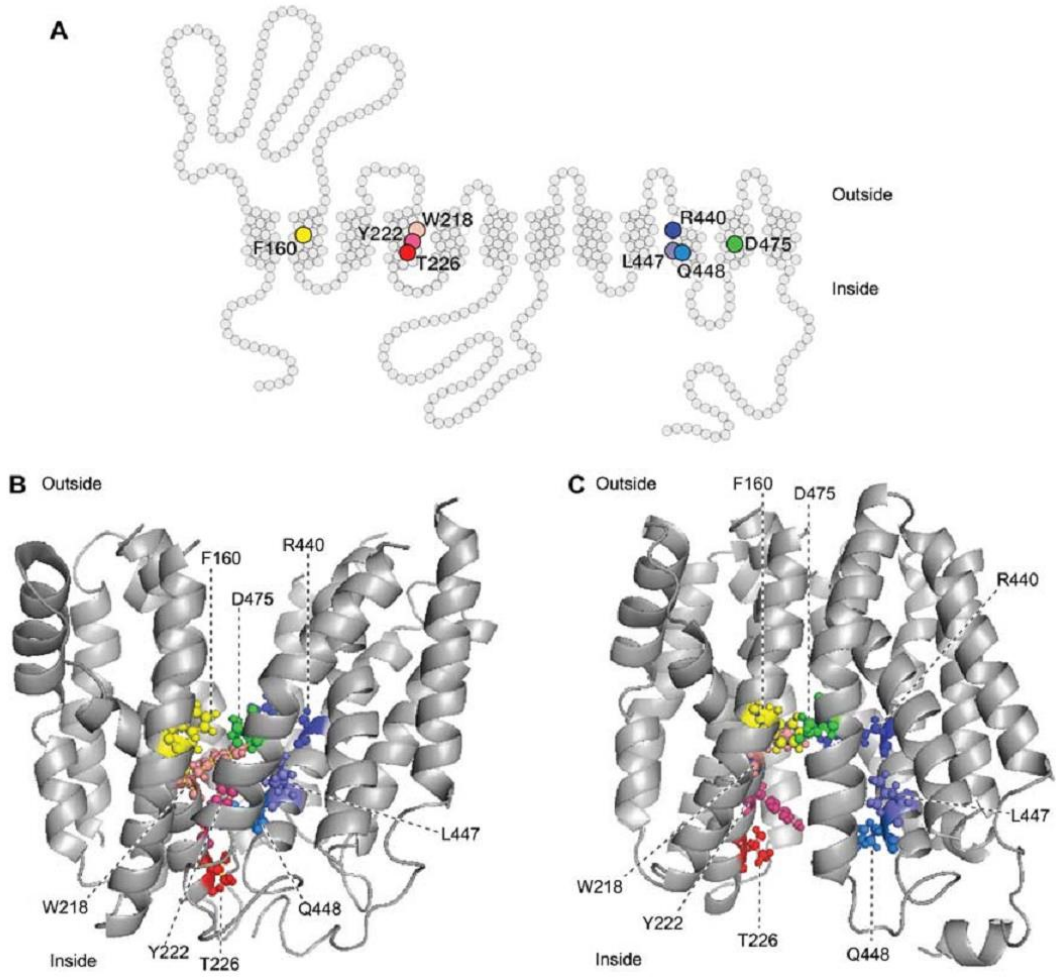

Figure 1.9. Structure models of rat Oct1 with amino acids that are crucial for substrate affinity. A) Predicted membrane topology of rat Oct1; B) Modeled tertiary structure of rat Oct1 in the outward-facing conformation (side view); C) Modeled tertiary structure of the inward-facing conformation (side view) (from Koepsell, 2011).

The model of rat Oct2 was also confirmed by observation of cysteine 474 accessibility from the aqueous phase (Pelis *et al*., 2006). Additional confirmation of substrate binding region was determined with comparison of substrate binding region in the model with the sizes of model substrates, suggesting that more than one compound can bind to the region at the same time. Studies with non-transported inhibitors, TBA and corticosterone, and their interaction with binding region of rat Oct2 from extracellular and intracellular side, enabled a more detail characterization of substrate binding

region of OCTs/Octs (Volk *et al*., 2009). Mutual interaction of cationic substrates and non-transported inhibitors of OCTs/Octs confirmed their overlapping interaction with key amino acid residues within binding region. These findings were basis of the study which confirmed that same region interacts with substrates and inhibitors from both sides of the cell. Corticosterone and TBA affect the OCT transport of choline from both sides of the membrane, with significantly higher affinity for TBA from the outside compared to the inside, whereas corticosterone had a higher affinity from the inside compared to the outside. This confirmed the complexity of OCTs substrate binding region that changes between an outwardly directed and an inwardly directed orientation during the transport cycle and exhibits similar but not identical substrate specificity from both sides (Fig. 1.9). During the change in orientation of substrate binding region, the conformational changes occur, which affect binding of transported substrates and non-transported inhibitors. Considering possible conformational changes it can be expected that individual substrates and inhibitors may interact with changing substrate binding regions in many different ways and also in different manner on the inside or outside of the cell (Koepsell, 2011).

1.5. The Slc family in teleost fish

Teleost fish represent the largest and most diverse group of vertebrates, with approximately 30,000 species, which is roughly half of all living vertebrate species (Nelson, 2006). Due to vast number of diverse teleost species, their diversity is exhibited not only through their morphologies, but through their genomes as well (Volff, 2005). Hundreds of duplicate gene pairs were generated by the whole-genome duplication (tetraploidization/rediploidization) which occurred during the early evolution of the ray-finned fish (Actinopterygian) lineage. Newly duplicated genes gave the basis for emergence of great number of new diverse genes through 300 – 450 million years of teleost evolution. The quantity and enormous diversity of teleost genes was further supported by frequent gene – linkage duplications, due to much higher chromosomal rearrangements than in other vertebrates. Another significant difference which gave teleost fishes such superiority in gene number and diversity is the number of conserved non-coding elements, whose diversification started before the whole genome duplication and resulted in enormous variability of teleost fish genomes. This characteristic of teleost fishes is one of the reasons why they are such attractive research model organisms which can be used as a very useful research tool in addressing many biological questions included those related to the evolution of gene functions and/or of their regulatory control (Kassahn *et al*., 2009; Sato *et al*. 2009).

Teleost fish genes coding for *Slc* transporters have been described in the last two decades, and preliminarily classified in *Slc* -like form in 50 families and at least 338 genes (Verri *et al*., 2012). Despite

the partial completeness of the annotations and the limited amount of submitted sequence information in public databases, *Slc* transporters have been identified in 49 teleost fish species (Romano *et al*., 2014). As expected, several *Slc* genes were found in duplicates due to the whole genome duplication and previously mentioned evolutionary processes. The highest number of genes is found in zebrafish (304 genes) and considerably lower number in *Salmo salar* (Atlantic salmon) with 53 genes, *Oncorhynchus mykiss* (rainbow trout) with 22, *Takifugu rubripes* (torafugu) with 16, *Takifugu obscurus* (mefugu) with 11, and *Anguilla japonica* (Japanese eel) with 10, followed by *Slc* genes from various teleost fish species (Verri *et al*., 2012).

Among all identified teleost *Slc* genes, less than 50 Slc proteins have been functionally characterized by expression in suitable heterologous expression systems, again with dominance in zebrafish Slc transporters. In most of teleost Slc transporter characterizations, the research was focused on role of Slc transporters in basic processes connected to fish as aquatic organism, such as absorption and excretion of salts, anionic and cationic organic nutrients and xenobiotic as well as inorganic compounds, especially metals. The biggest portion of teleost Slc transporter research is done on zebrafish as model organism. Previous studies determined functions of several Slc transporters in zebrafish such as 13 members of Slc4 with roles in bicarbonate transport in ionocytes of zebrafish skin and gills (Hwang, 2009), as well as Na^+ - HCO_3^- cotransport in zebrafish kidneys (Shmukler *et al*., 2005). Slc8a1 is a sodium – calcium exchanger, whose disruptions are connected with cardiac fibrillation in zebrafish, whereas Slc8a1b is found in gill and it is responsible for calcium excretion in mitochondrion-rich cells (Ebart *et al*., 2005; Liao *et al*., 2007). Slc9 is localized within proximal tubules of zebrafish kidneys and together with 8 isoforms it is characterized as Na^+ uptake transporter (Ivanis *et al*., 2008). Slc12a2 is identified and characterized as sodium – potassium – chloride co-transporter, required for control of otic vesicle and swim bladder volumes in zebrafish embryos (Abbas *et al*., 2009). Another Slc transporter with crucial role in development of zebrafish embryos is Slc20a1 which is characterized as Na^+/PO_4 co-transporter (Nichane *et al*., 2006). Member of zebrafish Slco (Slc21), Oatp1d1, was characterized in detail as crucial pH gradient – dependent transporter, responsible for biliary elimination of steroid hormones and various xenobiotic compounds (Popovic *et a*l., 2013). The research also identified 14 zebrafish *Slc22* genes within five subfamilies (Table 1.1). Slc26 transporter is localized in skin and gill ionocytes, where it functions as anion transporter, responsible for transport of Cl^-, HCO_3^-, OH^-, SO_4^{2-}, formate, oxalate and iodide (Bayaa *et al*., 2009). As far as transporters form zebrafish Slc22 family are concerned, the data are very scarce, with only information about identified 14 members within five subfamilies and basic expression patterns which showed ubiquitous expression of *Slc22* members in zebrafish tissues, with emphasis on Oat and Oct transporters, which showed expression in toxicologically relevant tissues, such as liver, kidney, intestine and gills (Popovic, 2014). The

disproportion in research between zebrafish and other teleost species points to significance and numerous advantages of zebrafish as a model organism in various fields of biology and biomedicine.

Table 1.1. List of representatives of zebrafish SLC22 family (from Popovic, 2014).

	Oat								Oct			Octn			Oct6	Orctl	
Species	1	2	3	4	5	6	7	Urat	1	2	3	1	2	3		3	4
H. sapiens	1	1	1	1	1	1	1	1	1	1	1	1	1	-	1	1	1
M. musculus	1	1	1	-	-	1	-	1	1	1	1	1	1	1	1	1	1
G. gallus	-	1	-	-	-	-	-	-	1	1	1	1	1	-	-	1	1
A. carolinensis	1	1	1	-	-	-	-	-	1	1	1	1	1	-	1	1	-
X. laevis	1	-	1	-	-	-	-	-	1	-	-	1	1	-	1	-	-
D. rerio	1	5	1	-	-	-	-	-	1	1	-	1	1	-	1	1	1
G. morhua	1	2	1	-	-	-	-	-	1	1	-	1	1	-	1	-	-
T. rubripes	1	2	1	-	-	-	-	-	1	-	-	1	1	-	1	1	-
T. nigroviridis	1	4	-	-	-	-	-	-	1	1	-	2	-	-	1	3	1
G. aculeatus	1	2	1	-	-	-	-	-	1	1	-	1	1	-	1	-	-
O. latipes	1	1	1	-	-	-	-	-	-	-	-	1	1	-	1	1	1
C. intestinalis	-	-	-	-	-	-	-	-	-	-	-		1		2	-	-

1.6. Zebrafish as model organism

Zebrafish (*Danio rerio* Hamilton, 1822) is one of approximately 3600 members of Cyprinidae family, within class of Actinopterygii. The natural habitats of zebrafish are tropical rivers of northern India, northern Pakistan, Nepal, and Bhutan. From initial use as aquarium pet fish, in the last three decades zebrafish emerged as one of the most popular and widely used model organisms in numerous research fields such as developmental and behavioral biology, biomedicine, pharmacology as well as (eco)toxicology (Fig. 1.10). Zebrafish as model organism possesses certain advantages in comparison with both widely used invertebrate models such as fruit fly (*Drosophila melanogaster*) and *Chenorabditis elegans*, together with mouse (*Mus musculus*) and other rodents as most popular vertebrate models. Similarly as invertebrate models, zebrafish possesses the ability of rapid and massive reproduction. This represents advantage when comparing with laborious and time demanding reproduction of mammalian model organisms. However, zebrafish unifies the advantages of both model organism groups. Their large and rapidly developing embryos are transparent, which is ideal for the research directed to development of classical vertebrate organ systems, something which cannot be accomplished in invertebrate models. During the rapid embryonic development in the first 24 hours post fertilization, all major organs form and within 72 hours the fish hatch and start feeding. Sexual maturation is achieved after 3 – 4 months and new adult zebrafish can generate new offspring. A single female can lay up to 200 eggs per week.

Additional advantage of zebrafish as model organism is its genetics. The teleost specific whole genome duplication (WGD) provided the evolutionary driving force in generating enormous number of newly functional genes, whose research can provide new understanding of human gene changes connected with numerous diseases. However, it has to be emphasized that only 25% of genes generated by WGD survived in today's zebrafish genome (Ravi and Venkatesh, 2008). Fully sequenced zebrafish genome is organized in 25 chromosomes and their genome consists of about 15 billion base-pairs, compared with mammalian genome sizes of about 30 billion base-pairs. The knowledge on the full zebrafish genome provided the basis for genetic investigation in the field of comparative genomics. All mentioned advantages make zebrafish potentially ideal research model in the study of human diseases including cancer, blood disorders and cardiovascular diseases, muscle diseases, infections and inflammation as well as for the study of vertebrate embryonic development (Xu and Zon, 2010).

Figure 1.10. Picture of adult zebrafish together with picture of differently colored zebrafish tissues and transparent embryos (adapted from http://www.uniprot.org/taxonomy/7955).

In addition, zebrafish permits efficient screens of phenotypic changes in response to genetic alterations, allowing the use of zebrafish in monitoring and modelling of cell behavior underlying vertebrate development and organ formation, unique features not offered by other vertebrate models (Barut and Zon, 2000; Davis, 2004; Lieschke and Currie, 2007). The availability of thousands of existing mutants and transgenic lines is also a vital resource, readily offered to researchers by e.g., recently founded European Zebrafish Resource Center (EZRC) at Karlsruhe Institute of Technology (KIT), Germany (http://www.itg.kit.edu/ezrc), or the Zebrafish International Resource Center (ZIRC) at University of Oregon, US (http://zebrafish.org/zirc/home/guide.php). Furthermore, numerous protocols for molecular biological methods, toxicological tests on a large scale, and functional genomics tools are established for zebrafish (Embry *et al*., 2010; Tiefenbach et al., 2010; Huang *et al*, 2011).

Considering research on membrane transporters, many cellular studies have identified the compounds that transporters are able to transport *in vitro*. However, in addition to detailed molecular/cellular

characterization, the functional importance of each transporter needs to be verified *in vivo*, in which the demonstration of function in knockout mice used to be the gold standard. However, several aspects of murine biology limit its routine use in large-scale genetic screening. On the other hand, sophisticated mutagenesis and screening strategies on a large scale, along with the cost-benefit ratio that is not possible to match using other vertebrate systems, have promoted zebrafish as a highly valuable alternative (Lieschke and Currie, 2007). As a consequence, the pharmaceutical industry and environmental science are strongly interested in using zebrafish for drug/pollutant screens and the whole animal toxicology studies.

Therefore, a better understanding of the presence, role and (eco)toxicological significance of polyspecific uptake and efflux transporters should represent a high priority research goal for many research fields that increasingly use zebrafish as a model. Currently, the knowledge on related membrane transporters in zebrafish is limited, and the major research objectives of this study are set to significantly overcome the described deficiencies related to OCT transporters.

1.7. Summary and aims

In summary, since OCT/Oct transporters in humans and other mammals play crucial role in ADME processes, as well as in physiological maintenance of organic cation homeostasis, the main goal of this work was to provide the first insight in potential role of organic cation transporters in zebrafish as an important model organism. More specific goals of our study were:

To perform a complete phylogenetic analysis of SLC22 families in zebrafish which would enable to:
determine the number of genes within each group,
position zebrafish genes against their co-orthologs in other vertebrate species, and
assign protein names to the unannotated zebrafish transporters.

To perform conserved synteny analysis in order to:
determine chromosome locations of Oct genes,
determine level of gene order preservation among zebrafish, human and other fish OCT/Oct genes.

To obtain the tissue expression profile of *Slc21* and *Slc22* genes in zebrafish, leading to:
determination of the mRNA expression in liver, kidney, intestine, gills, brain and gonads of zebrafish,
determination of gender differences in expression patterns, and

identification of dominantly expressed genes in tissues that are key determinants of xenobiotic elimination (intestine, liver, kidney and gills).

To perform functional and structural studies directed to:
functional characterization of zebrafish Oct transporters and identification of novel fluorescent substrates and Oct interactors among various endo- and xenobiotic compounds,
molecular characterization of a selected zebrafish and human Oct/OCT transporter with homology modeling, using 3D models and molecular docking studies in order to identify crucial amino acid residues and give more detailed characterization of Oct/OCT substrate binding region.

2. Materials and Methods

2.1. Materials

All fluorescent dyes were purchased from Sigma-Aldrich (Taufkirchen, Germany) except ethidium bromide, which was purchased from Serva Electrophoresis GmbH (Heidelberg, Germany). The other used chemicals were purchased from Sigma-Aldrich (Taufkirchen, Germany) or Carl Roth GMBH (Karlsruhe, Germany).

Plasmids used in this study are listed in Table 2.1., enzymes are listed in Table 2.2., commercial kits in Table 2.3. and antibodies used for Western blotting analysis and immunocytochemistry in Table 2.4. Primers used for cloning of full length amplicons/genes and for the quantitative PCR analysis are listed in Table 2.5. and 2.6., respectively.

For the purpose of multiplication, we used DH5α *E. coli* competent cells (Life Technologies, CA, USA). These cells were grown on agar plates (Sigma-Aldrich, Taufkirchen, Germany) or in liquid Luria-Bretani medium (Becton, Dickinson and Company, Sparks, USA), supplemented with 100 μg/mL of ampicilin (Sigma-Aldrich, Taufkirchen, Germany).

Human Embryonic Kidney cells (HEK293) (ATCC, CRL-1573) were used in all experiments for purpose of heterologous expression. This cell line was selected due to short duplication time (<24 h) and high transfection efficiency (Tom *et al*., 2008). The cells were cultivated in DMEM-FBS medium, which is Dulbecco's modified Eagle medium (DMEM) with high glucose (Life technologies, CA, USA) and 10% fetal bovine serum (FBS) (Lonza, Basel, Switzerland) at 37°C and 5% CO_2 maintained atmosphere. Transient transfection of HEK293 cells was achieved using branched polyethyleneimine (PEI) transfection reagent (Sigma-Aldrich, Taufkirchen, Germany) in 48-well plates. The transfection was achieved using PEI's ability to encapsulate negatively charged plasmid DNA into positive particles, which interact with negatively charged cell surface and enter the cell through endocytosis (Boussif *et al*., 1995).

In order to determine protein concentrations we performed Bradford assay (Bradford, 1976). For that purpose we made Bradford reagent, which is made by dissolving 100 mg Coomassie Brilliant Blue G250 (Sigma-Aldrich, Taufkirchen, Germany) in 50 mL of absolute ethanol (Kemika, Zagreb). Afterwards, 100 mL of phosphorous acid was added to ethanol solution. Finally, 850 mL of mQ water was added to the mixture and filtered through membrane filter (pore diameter 0.2 μm) (TPP Techno Plastic Products AG, Switzerland).

Western blot analysis was perforemed using Mini-PROTEAN 3 Cell electrophoresis chamber (Bio-Rad Laboratories, CA, USA) for polyacrylamide gel electrophoresis, together with Multiphor ll Electrophoresis System (Pharmacia LKB Biotechnology, Uppsala, Sweden) for semidry transfer to

polyvinylidene difluoride membrane (Millipore, MA, US). Protein size was estimated by use of protein marker (ThermoFischer Scientific, MA, USA).

Together with antibodies listed in Table 2.4., for the immunofluorescence localization we used 4',6-diamidino-2-phenylindole (DAPI) (Sigma-Aldrich, Taufkirchen, Germany) in order to stain nuclei. Finally, prepared samples on coverslips were mounted on microscope slides using Fluoromount medium (Sigma-Aldrich, Taufkirchen, Germany).

Table 2.1. Plasmids used in the study.

Plasmid	Description	Producer
pGEM - T	Amp^R, T7 promoter, *E. coli* expression	Promega, WI, USA
pJET 1.2	Amp^R, T7 promoter, *E. coli* expression	Life Technologies, CA, USA
pcDNA 3	Amp^R, CMV promoter, mammalian cells expression	Life Technologies, CA, USA
pcDNA 3.1-His(+)	Amp^R, CMV promoter, mammalian cells expression	Life Technologies, CA, USA
pcDNA/LacZ	Amp^R, CMV promoter, β-galactosidase expression	Life Technologies, CA, USA
pEGFP-N	Kan/Neo^R, SV40 promoter, mammalian cells expression	Takara, Shiga, Japan

Table 2.2. Enzymes and markers used in the study.

Enzyme/Marker	Producer
Taq DNA polymerase	Life Technologies, CA, USA
Phusion proof reading polymerase	Thermoscientific, MA, USA
Reverse transcriptase	Life Technologies, CA, USA
FastDigest restriction enzymes: KpnI, NotI, XbaI, XhoI	Life Technologies, CA, USA
Dnase I	Life Technologies, CA, USA
T4 DNA ligase	Life Technologies, CA, USA
GeneRuler DNA ladder mix	Thermoscientific, MA, USA
Precision plus protein ladder	Bio-Rad Laboratories, CA, USA

Table 2.3. Commercial kits used in the study.

Commercial kit	Producer
Rneasy Mini Kit	Qiagen, Hilden, Germany
MinElute Gel Exctraction Kit	Qiagen, Hilden, Germany
QIAquick PCR Purification Kit	Qiagen, Hilden, Germany
QIAprep Spin Miniprep Kit	Qiagen, Hilden, Germany
Plasmid MIDI Kit	Qiagen, Hilden, Germany
High Capacity cDNA Reverse Transcription Kit	Life Technologies, CA, USA
pGEM-T Vector System I	Promega, WI, USA

Table 2.4. Antibodies used in the study.

Antibody	Host	Producer	Cat. No.
Mouse IgG_{2b}-6xHis monoclonal primary antibody	mouse	Bio-Rad Laboratories, CA, USA	620-0203
Mouse IgG_1-Xpress monoclonal primary antibody	mouse	Life Technologies, CA, USA	R910-25
Mouse IgG_{2b}-Na, K-ATPase monoclonal primary antibody	mouse	SantaCruz Biotechnology, CA, USA	sc-48345
Mouse IgG-HRP secondary antibody	goat	Bio-Rad Laboratories, Ca, USA	170-6516
Mouse IgG-FITC secondary antibody	goat	SantaCruz Biotechnology, CA, USA	sc-2010
Mouse IgG-Cy3 secondary antibody	goat	SantaCruz Biotechnology, CA, USA	sc-166894

Table 2.5. Primers used for cloning of zebrafish *Oct1* and human *OCT1* and *2* genes. Part of the primer sequences that were introduced for digestion with specific restriction enzymes are shown in blue. Primers were purchased from Life Technologies (Carlsbad, CA, USA).

Gene name		Primer sequence 5' -> 3'
DrOct1	F	TTAGCGGCCGCAAGCTTTCATGACCACTTTCGAAGAGATT
	R	TTAGGTACCTCTAGACTTCAAACCGCTGTAACGTCTTT
DrOct2	F	TTAGCGGCCGCAAGCTTTCATGTCTAACTTTGACGAACTT
	R	TTAGGTACCTCTAGACTTCACTTTTGGGATGTTTTCT
HsOCT1	F	TTAGGATCCTATGCCCACCGTGGATGAC
	R	TCTAGACTCGAGTCAGGTGCCCGAGGGTT
HsOCT2	F	TTAGGATCCTATGCCCACCACCGTGGA
	R	TCTAGACTCGAGTTAGTTCAATGGAATGTCTAGTTTC

Table 2.6. Primers used in the quantitative Real time PCR. Primers were purchased from Life Technologies (Carlsbad, CA, USA).

Gene name		Primer sequence 5' -> 3'	T_a	Final conc. (nM)	Efficiency (%)
DrOct1	F	GTTATGTCCCGTACGTTTTAC	58	300	99
	R	TGAATGTGGGCAGAGTCATG	60	300	
DrOct2	F	GAGTCACAGGGATTCTGGT	60	300	99
	R	ACCATCCAACCGCCCTTCA	60	300	
Ef1α	F	CCTGGGAGTGAAACAGCTGATC	60	300	96
	R	GCTGACTTCCTTGGTGATTTCC	60	300	

Table 2.7. Buffers used in the study.

Buffer	Composition	pH
Phosphate-buffered saline	1.37 M NaCl, 27 mM KCl, 100 mM Na_2HPO_4, 18 mM KH_2PO_4	7.4
Transport buffer	145 mM NaCl, 3 mM KCl, 1 mM $CaCl_2$, 0.5 mM $MgCl_2$, 5 mM D-glucose and 5 mM hydroxyethyl piperazineethanesulfonic acid (HEPES)	7.4
RIPA buffer	150 mM NaCl, 1 mM EDTA, 25 mM Tris, 0.8% NP-40	-
Blocking solution	5% low fat milk, 50 mM Tris, 150 mM NaCl, 0.05% Tween 20	-

2.2. Methods

2.2.1. Phylogenetic analysis and membrane topology

Using blastx algorithm, nucleotide and protein sequences were retrieved from the following NCBI (http://www.ncbi.nlm.nih.gov/) and ENSEMBL (http://www.ensembl.org/index.html) databases, respectively. Following species were included in the phylogenetic analysis: mammals – human (*Homo sapiens*) and mouse (*Mus musculus*); bird – chicken (*Gallus gallus*); reptile – anole lizard (*Anolis carolinensis*), amphibian – frog *Xenopus laevis*; actinopterygian or ray-finned fishes – zebrafish (*Danio rerio*), pufferfishes – Japanese pufferfish (*Takifugu rubripes*) and green spotted pufferfish (*Tetraodon nigroviridis*), Atlantic cod (*Gadus morhua*), stickleback (*Gastrosteus aculeatus*) and medaka (*Oryzas latipes*) and tunicate sea squirt (*Ciona intestinalis*).

Sequences were considered to be part of the *SLC22/Slc22* family if there was blastx hit with threshold value of e = 10^{-3} False positive results were excluded based on the phylogenetic analysis. Sequences were aligned with MUSCLE algorithm (Edgar, 2004) and phylogenetic tree was constructed using Maximum Likelihood method in PhyML 3.0.1 software (Guindon and Gascuel, 2003). Confidence of nodes was estimated by approximate likelihood ratio test (aLRT) (Anisimova and Gascuel, 2006). Based on the phylogenetic relationships, all previously unclassified genes were provisionally annotated. Names were given in accordance with the new nomenclature adopted by the HUGO Gene Nomenclature Committee (Hagenbuch and Meier, 2004).

TMDs were predicted using HMMTOP algorithm version 2.0. (Tusnady and Simon, 2001), followed by prediction correction according to the multiple alignments with human SLC22 proteins. BioEdit Software version 7.0. was used for sequence editing and alignment display (Hall, 1999), while sequence identities were calculated in DNAstar Software (version 7.0.0). Potential N-glycosylation sites were predicted using the NetNGlyc 1.0 server (http://www.cbs.dtu.dk/services/NetNGlyc/).

Orthology predictions using syntenic relationships between zebrafish and human genes of interest were made using Genomicus (http://www.genomicus.biologie.ens.fr/genomicus), a conserved synteny browser synchronized with genomes from the Ensembl database (Louis *et al*., 2013).

2.2.2. Tissue-specific gene expression analysis

Adult zebrafish of both genders were purchased from a local supplier and sacrificed for the collection of tissues. In order to obtain sufficient amount of material for RNA isolation, six tissues (brain, gills, liver, intestine and gonads) from five specimens of the same gender were pooled together, with one pool representing one sample. Three independent pools were collected. In the case of RNA isolation from kidney, 14 specimens were pooled together due to small size of zebrafish kidneys. In that way, 3-5 samples for each tissue were collected to conduct tissue- and gender-specific expression analysis. After isolation, tissues were stored in RNA later for long time storage at -20˚C. For RNA isolation, tissues were homogenized using a rotor-stator homogenizer at 10,000 rpm for 20 s. Total RNA isolation from each tissue was carried out with RNeasy Mini Kit (Qiagen, Hilden, Germany), RNA was quantified using Bio-Spec Nano spectrophotometer (Shimadzu Corporation, Kyoto, Japan), and the integrity of RNA was determined by gel electrophoresis. Genomic DNA digestion was carried out using RNase-free DNase Set (Qiagen, Hilden, Germany). Purified total RNA was reversely transcribed (1 μg of total RNA) using High Capacity cDNA Reverse Transcription Kit with RNase Inhibitor (Applied Biosystems, Foster City, CA, USA).

The primers were designed using Primer express 3.0 Software (Applied Biosystems, CA, USA) and adjusted manually if necessary. Target amplicons of 90-120 bp were amplified and cloned using the pGEM-T Vector System I (Promega, Medison, WI, USA). Plasmids were purified by QIAprep Spin Miniprep Kit (Qiagen, Hilden, Germany), and amplicons were verified by sequencing at the Ruđer Bošković Institute DNA Service (Zagreb, Croatia). Primer efficiencies were determined for each gene using the recombinant plasmid as a template (Table 2.6.). Primer concentrations were optimized combining three primer concentrations: 300, 600 and 900 nM. The concentrations resulting in the highest fluorescence signal at the lowest Ct number were chosen as optimal. Quantification of the *Oct* genes was performed using the qRT-PCR relative quantification method (Qgene method) and normalized to the housekeeping gene *ef1α* (elongation factor 1α), as previously described (Muller *et al.*, 2002; Loncar *et al.*, 2010). The relative quantification method is described with equation:

$$MNE = ((E_{ref}) \hat{} Ct_{ref,mean}) / ((E_{target}) \hat{} Ct_{target,\ mean})$$

where, MNE stands for mean normalized expression; E_{ref} is housekeeping gene efficiency; E_{target} is target gene efficiency; Ct_{ref}, mean is mean Ct value for the housekeeping gene; and Ct_{target}, mean stands

for mean Ct value of the target gene. Data are presented as gene of interest expression relative to the housekeeping gene expression multiplied by the factor of 10,000. Elongation factor (EF1α) was chosen as a housekeeping gene given the fact that its expression was similar across all analysed tissues. Expression was considered to be high for MNE > $600*10^5$ (Ct < 22), moderate for MNE $20*10^5$ - 600*105 (Ct = 23-26) and low for MNE < $20*10^5$ (Ct >27).

qRT-PCR was performed using the ABI PRISM 7000 Sequence Detection System using Power SYBR Green PCR Master Mix (Applied Biosystems, Foster City, CA, USA). qRT-PCR reaction mix was prepared to a final volume of 10 µl containing: 5 µl of SYBER Green master mix, 0.5 µl of each primer (of optimal concentration), 1 µl of template (10 ng/sample) and 3 µl of Ultrapure Dnase/Rnase free distilled water (Molecular Bioproducts, San Diego, CA, USA). After the initial denaturation at 95˚C for 10 min, 40 cycles of amplification were carried out with denaturation at 95˚C for 15 sec, annealing and elongation at 60˚C for 1 min, altogether followed by the melting curve analysis. Data were analysed with ABI PRISM Sequence Detection Software 1.4 (Applied Biosystems, Foster City, CA, USA) and GraphPad Prism Software version 5.00.

2.2.3. Cloning and heterologous expression

In order to amplify full-length zebrafish and human *Oct* genes, specific primers were designed based on known sequences of zebrafish *Oct1* and *Oct2* genes and human *Oct* genes. Genes were amplified from human and zebrafish cDNA by polymerase chain reaction (PCR) using high fidelity Phusion DNA polymerase (Thermo Scientific, MA, USA), using specific forward and reverse primers, with introduced cloning sites for NotI and HindII restriction enzymes on zebrafish *Oct1* and *Oct2* forward primers and BamHI oh human *OCT1* and *OCT2* forward primes. Restriction sites for KpnI and XbaI restriction enzymes were used on zebrafish *Oct1* and *2* reverse primers, and XhoI and XbaI on human *OCT1* and *2* reverse primers, respectively. Amplified DNA fragments were separated using agarose gel electrophoresis and specific gene bands were purified with commercially available kit (Table 2.3). Since Phusion DNA polymerase produces amplicons with blunt ends, we performed blunt-end ligation of the amplicons with previously prepared linearized pJET 2.0 vector. pJET/*Oct1* and *Oct2* constructs were transformed into DH5α *E. coli* competent cells (Invitrogen, Carlsbad, CA, USA). The presence of ampicilin resistance gen in pJET vector allowed the growth of transformed DH5α cells on ampicillin-selective agar plates, overnight at 37˚C. Grown bacterial colonies were screened for presence of inserted *Oct* genes using PCR with Taq DNA polymerase and specific primers of each gene. In order to obtain sufficient amount of plasmid, transformed cells were grown in liquid cultures with ampicilin-selective Luria-Bretani medium. Recombinant plasmid with inserted gene was purified using

commercial plasmid isolation kit (Table 2.3). Minimum of three positive clones were verified by DNA sequencing at the Ruđer Bošković Institute DNA Service (Zagreb, Croatia). Sequenced genes of each clone were compared to the reported gene sequences from the NCBI and ENSEMBL databases. If sequence of one clone differed from the sequences of two other clones in one or more base pairs, the sequences of two identical clones were considered to be valid and one of these two clones was chosen for further investigation.

After the sequence confirmation, each gene was cloned into the pcDNA3.1 and pcDNA3.1/His, with gene promoter suitable for high-level heterologous expression in the mammalian cell lines. Zebrafish *Oct* genes were also cloned into the vectors for expression and visualization of a protein of interest fused to green fluorescent protein (EGFP). The cloning was performed using primer-inserted restriction sites, which allowed the digestion of *Oct*/pJET vector constructs with restriction enzymes and excision of inserted genes. Excised inserts were separated with agarose gel electrophoresis and purified with commercial gel extraction kit. Destination vectors, pcDNA3.1, pcDNA3.1/His and pEGFP-N1, were also digested using the same combination of restriction enzymes and linearized vectors were purified using commercial PCR purification kit. Sticky ends of purified gene inserts and linearized vectors were ligated using T4 DNA ligase (Table 2.2). The ligation mixtures were used for transformation of DH5α competent cells and cultivation on ampicillin selection plates. Positive transformants were screened using PCR and multiplied by cultivation of liquid cultures. For purpose of heterologous expression, the greater volumes of liquid cultures were cultivated and plasmid purification MIDI kit was used (Table 2.3).

Transient transfection method was based on previously described method by Tom *et al*., 2008 with some modifications. In order to reach 90% confluence, HEK293 cells were seeded in the 48-well plates 48 hours prior to transfection at cell density of $2.1*10^5$ cells/cm^2, with final volume of 0.25 mL per well. The transfection mixture consisted of recombinant plasmid with inserted gene and PEI reagent in the 1:1 ratio with the final concentration of 0.375 µg/well for 48-well plate. PEI and plasmid solutions were prepared in phosphate buffered saline buffer (PBS) at 37°C. Solutions were mixed and briefly vortexed (3 x 3 s) and incubated at room temperature for 15 minutes. After the incubation, 25 µL of plasmid/PEI mixture was added to each well with 225 µL of DMEM medium without FBS and incubated for 4 hours at 37°C and 5% CO_2. Four hours later, the medium with transfection mixture was replaced with new DMEM-FCS. The transfected cells were left to grow in standard conditions for 24 hours and after that period the cells were ready for transfection efficiency evaluation and conduction of transport assays. In order to evaluate transfection efficiency, separate cells were transfected with pcDNA3.1/His/LacZ plasmid and transfection efficiency was evaluated 24 h after transfection with the LacZ staining protocol (Sambrook *et al*., 1989). The assay is based on the ability of enzyme β-galactosidase, coded by *LacZ* gene, to catalyze X-gal (5-bromo-4-chloro-3-indolyl-β-D-galactopyranoside) into the blue

product 5,5'-dibromo-4,4'-dichloro-indigo. Adherent HEK293 cells transfected with pcDNA3.1/His/LacZ were washed twice with PBS, followed by fixation in 0.5% glutaraldehyde (in PBS), and 2 – 24 h incubation (at 37°C) in the X-gal solution (1 mM X-gal, 40 mM ferricyanide, 40 mM ferrocyanide, 2 mM MgCl2 in PBS).

2.2.4. Transport assays

Transfected cells that showed more than 70% of transfection efficiency were used in transport assays (Fig. 2.1). DMEM-FCS was removed from cells grown in 48 well plates and cells were preincubated in 200 µL of the transport medium for 10 min at 37°C. To assess transport and dose responses of fluorescent substrates, 50 µL of five times concentrated fluorescent substrates were added to the preincubation medium and incubated 5 to 15 minutes at 37°C, depending on the substrate used. After the incubation, the cells were washed two times with 250 µL of pre-chilled transport medium and lysed with 0.1% of sodium dodecyl sulphate (SDS) for 30 minutes. Lysed cells were transferred to the 96-well black plates and the fluorescence was measured with the micro plate reader (Infinite 2000, Tecan, Salzburg, Austria). The transport rates were determined by subtracting the measured fluorescence of transfected cells with the fluorescence of non-transfected control cells and by normalization of the obtained fluorescence unit calibration curves for each substrate and protein content. Calibration curves for fluorescent dyes were generated in the 0.1% SDS and in the cell matrix dissolved in the 0.1% SDS. Total protein concentration was measured using Bradford assay (Bradford, 1976). Using the calibration curves and total protein content, uptake of the fluorescent substrates was expressed as nM of substrates per mg of protein.

After the determination of transport kinetics for fluorescent dyes, they were used in the inhibition assays. Inhibition measurements were based on co-exposure of transfected cells and non-transfected control with determined model substrate and potential interactor. The cells were preincubated for 10 minutes in transport medium, and for 40 seconds with test compounds, followed by 5 to 15 minutes incubation with model substrate with concentration that showed to be in the linear slope segment of determined dose response curve. The interaction was screened for one or two concentrations of tested compound, and for the interactors that showed uptake inhibition above 50%, inhibition constants (K_i) were determined. Compounds with K_i values in nanomolar and low micromolar range (<5 µM) were considered to be very strong interactors, compounds with K_i of 5 - 20 µM were designated as strong interactors, whereas K_i of 20 – 100 µM indicated moderate interaction and K_i above 100 µM, weak interaction.

In order to distinguish the nature of interaction with tested compounds, changes in K_m and V_{max} values for model substrates were determined in the presence of a target compound at the concentration equal to the K_i value of a compound, at varying concentrations of model substrates (6 – 8 points) and after 5 – 15 minutes of incubation, which was within the linear range of the model substrate transport rate.

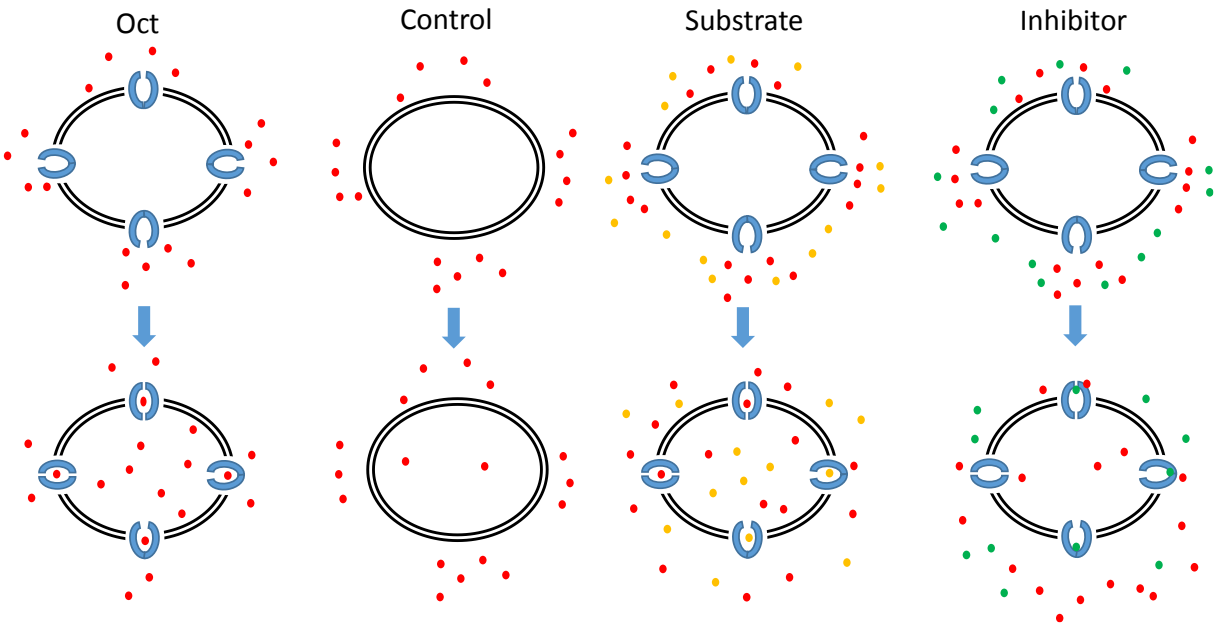

Figure 2.1. Schematic representation of transport assay based on the uptake of fluorescent substrate by transporter overexpressing cells.

2.2.5. Western blot analysis

Cells were collected from 2 wells of a 6-well microplate 24 h after transfection and lysed in RIPA buffer (NaCl 150 mM, EDTA 1 mM, Tris 25 mM, NP-40 0.8%) with protease inhibitors cocktail AEBSF (Sigma-Aldrich, Taufkirchen, Germany) for 30 min on ice. After the lysis, cells were subjected through 3 freeze/thaw cycles, briefly sonicated and centrifuged at 1,000 *g* for 10 min at 4°C. Protein concentration in total cell lysate (TCL) was measured using Bradford assay (Bradford, 1976). Twenty micrograms of protein per lane was separated by electrophoresis in 1% sodium dodecyl sulphate polyacrylamide gel. The proteins were then transferred to the polyvinylidene difluoride membrane (Millipore, MA, US) by semidry blotting. Blocking was performed in blocking solution. Subsequently, membranes were washed and incubated for 1 h with anti-Xpress, or 2 h with anti-His antibody (1:5000). Goat anti-mouse IgG-HRP (1:3000) was used as secondary antibody (Bio-Rad Laboratories, CA, USA).

The proteins were visualized by chemiluminescence (Abcam, Cambridge, UK). Protein size was estimated by use of protein marker (ThermoFischer Scientific, MA, USA).

2.2.5. Immunocytochemistry

For immunofluorescence localization of proteins expressed by transiently transfected plasmids, HEK293 cells were grown on glass coverslips in 24-well culture plates. Fixation of transiently transfected cells was performed with 4% paraformaldehyde in PBS during 30 min incubation. Cells were washed three times in 100 mM glycin/PBS, permeabilized with methanol for 15 min and blocked in 5% low fat milk for 30 min with gentle agitation at room temperature. Subsequently, coverslips were transferred on microscope slides and incubated with Xpress antibody (1:100) in blocking solution for 1 h at 37°C in humidity chamber, washed and incubated with secondary FITC antibody (fluorescein isothyocyanate) (1:100) in blocking solution for 1 h at 37°C. When double staining was performed after incubation with FITC, blocking was done in 5% low fat milk for 30 min with gentle agitation, followed by incubation with Na,K-ATPase anti-mouse primary antibody for 2 hours (1:150), washing, and 1 hour incubation with Cy3-conjugated anti-mouse IgG-HRP (Cyanine3) as a secondary antibody (1:200). Nuclei were stained with DAPI for 45 min at 37°C in 300 nM DAPI/PBS. After mounting the samples in Fluoromount medium, immunofluorescence was detected using confocal microscope Leica TCS SP2 AOBS (Leica Microsystems, Wetzlar, Germany).

2.2.6. Modeling the tertiary structure of organic cation transporters

Homology modeling was used to predict three-dimensional structures of organic cation transporters (hOCT1, hOCT2, and drOct1). Accelrys Discovery Studio's protocol Build Homology Models was used to build homology models of organic cation transporters based on an alignment of the model sequence and the template structure. Build Homology Models protocol uses MODELER (Sali and Blunell, 1999) automodel to build homology models. To model the three-dimensional structure of hOCT1 and hOCT2, the tertiary structure of lactose permease LacY from *E. coli* (ID code 1PV6) (Abramson *et al*., 2003) was used as the template structure, an approach previously reported by Popp *et al*. (2005). In accordance with their approach, the large loops of hOCT1 and hOCT2 were excluded from the modeling since LacY lacks a corresponding structure (loop between TMHs 1 and 2) or shows low structural similarity (loop between TMHs 6 and 7). To build homology models of hOCT1 and hOCT2, the input sequence alignment between the model sequences of hOCT1 or hOCT2 and the LacY template structure was used as reported by Popp *et al*. (2005). For the input sequence alignment between hOCT1 and LacY, 11.8% of the amino acids were identical and 32.8% of the amino acids were similar, whereas for the

input sequence alignment between hOCT2 and LacY, 9.5% of the amino acids were identical and 32.7% of the amino acids were similar. To model the three-dimensional structure of drOct1, the homology model of hOCT1 was used as the template structure. The input sequence alignment between the model sequence of drOct1 and the hOCT1 template structure was obtained were 45.8% of the amino acids were identical and 68.2% of the amino acids were similar. Rest of the parameters in the Parameters Explorer of Build Homology Models protocol were set as follows. Cut Overhangs was set to True to cut terminal residues of the input model sequence that were not aligned with the templates. Number of Models was set to 5 to define how many models to create from an initial structure with Optimization Level set to Low to specify the amount of molecular dynamics with simulated annealing to perform. To build refinement models on detected loop regions, i.e. model sequence segments of at least 5 residues length which are not aligned with the templates, Refine Loops was set to True. Build Homology Models protocol uses the DOPE (Discrete Optimized Protein Energy) (Shen and Sali, 2006) method to refine loops. Refine Loops Number of Models was set to 5 to specify the number of models to be created by loop optimization and Refine Loops Optimization Level was set to Low to specify the number of models to be created by loop optimization. Refine Loops Use DOPE Method was set to High Resolution to use the DOPE-HR method, a method very similar to the DOPE method but obtained at higher resolution. After running Build Homology Models protocol, from the generated output models, Best Model Structure Superimposed to Templates was chosen for docking study.

2.2.7. Molecular Docking

Ligands to be docked in the homology models of hOCT1, hOCT2, and drOct1 were created with ChemBio3D Ultra 12.0 and minimized using the MMFF94 force field implemented in ChemBio3D Ultra 12.0.

Accelrys Discovery Studio's protocol Dock Ligands (CDOCKER) was used for the docking study. CDOCKER is a grid based molecular docking method that employs CHARMm force field (Brooks *et al*, 2004). Best Model Structure Superimposed to Templates of homology models of hOCT1, hOCT2, and drOct1 generated by Build Homology Models protocol were used as the rigid receptors while the ligands were allowed to flex during the refinement. Binding site within the homology models was defined by a sphere (r = 13.5 Å) surrounding the amino acids that have been located within the substrate binding site by mutagenesis experiments (Koepsell, 2011). The following steps were included in the CDOCKER protocol. First, a set of 20 random ligand conformations for each test compound were generated using high-temperature molecular dynamics (MD). Number of steps in high-temperature MD was set to 1000 and target temperature used to generate random starting conformations was set

to 1000 K. In the following step 20 random orientations for each of the conformations from dynamics were produced by translating the center of the ligand to a specified location within the receptor active site, and performing a series of random rotations. Softened energies were calculated and the orientations were kept if the energy was less than a specified threshold value of 300 vdW. This process continued until either the desired number of low-energy orientations were found, or the maximum number of bad orientations has been tried. The maximum number of bad orientations was set to 800. In the next step each orientation was subjected to simulated annealing molecular dynamics. The temperature was heated up to 700 K then cooled to 310 K. Numbers of heating and cooling phase steps during simulated annealing were set to 2000 and 5000, respectively. For the simulated annealing refinement grid extension (8.0 Å) was used. In the subsequent step a final minimization of each refined pose of the ligand in the rigid receptor is performed using full potential. In the end, for each final pose, the CHARMm energy (interaction energy plus ligand strain) and the interaction energy alone are calculated. The poses are sorted by CHARMm energy and the 30 top scored (most negative, thus favorable to binding) poses are retained.

2.2.7.1. Score Ligand Poses

The binding affinities of docked ligands in the poses generated by Dock Ligands (CDOCKER) protocol were estimated using the scoring functions as implemented in the Accelrys Discovery Studio's protocol Score Ligand Poses. The following scoring functions were calculated. LigScore1_Dreiding and LigScore2_Dreiding (Krammer *et al*., 2005) are fast, simple scoring functions for predicting receptor-ligand binding affinities which are computed in units of pKI (-logKI). PLP1 (Gelhaar *et al*., 1995) and PLP2 (Gelhaar *et al*., 1999) are fast, simple, docking functions that have been shown to correlate well with protein-ligand binding affinities. PLP scores are measured in arbitrary units. Higher PLP scores indicate stronger receptor-ligand binding (larger pKI values). Jain (Jain, 1996) is an empirical scoring function developed through an evaluation of the structures and binding affinities of a series of protein-ligand complexes. The Jain score is a sum of five interaction terms. These terms describe: lipophilic interactions, polar attractive interactions, polar repulsive interactions, solvation of the protein and ligand and an entropy term for the ligand. The PMF (Muegge, 1999) and PMF04 (Muegge, 2006) scoring functions were developed based on statistical analysis of the 3D structures of protein-ligand complexes. They were found to correlate well with protein-ligand binding free energies while being fast and simple to calculate. The PMF04 score is an updated version of the original PMF score. The PMF scores are reported in arbitrary units with the sign reversed. A higher score indicates a stronger receptor-ligand binding affinity.

2.2.7.2. Consensus Score

To identify the poses of docked ligands that score high in more than one scoring function, the Accelrys Discovery Studio's protocol Consensus Score was used. The Consensus Score protocol calculates the consensus scores of a series of docked ligands for which other scores have been previously computed. For each selected scoring function, the ligands are listed by score in descending order. The consensus score for a ligand is an integer between zero (none of the scores are in the top ranking percentile) and the total number of scores (all of the scores are in the top ranking percentile) listed in Input Properties. Thus, in the Parameters Explorer of Consensus Score protocol, the following parameters were set. In Input Properties score properties –PLP2, -PMF, -PMF04, Jain, -CDOCKER_ENERGY, -CDOCKER_INTERACTION_ENERGY, LigScore2_Dreiding, and LigScore1_Dreiding were chosen to calculate the consensus score. Consensus Percentage was set to 20 to specify the percentage of top molecules to include in the consensus. Use Best Pose only was set to False.

2.2.7.3. Minimization

The poses of docked ligands with highest consensus score were minimized using Accelrys Discovery Studio's protocol Minimization. Smart Minimizer algorithm was used to perform the minimization. The applied algorithm performs 1000 steps of Steepest Decent with a RMS gradient tolerance of 3, followed by Conjugate Gradient minimization with the values of Max Steps and RMS Gradient set to 500 and 0.01, respectively. Generalized Born with Molecular Volume (GBMV) implicit solvent model (Feig and Brooks, 2004) was used in the calculation with the effective Born radii calculated by numerical integration of molecular volume. (Nina *et al*., 1997). The non-polar surface area was used to approximate the non-polar component of the solvation energy. Implicit solvent dielectric constant was set to 80. Distance cutoff value used for counting non-bonded interaction pairs was set to 14.0 Å.

2.2.8. Data analysis

All assays were performed in 2 - 4 independent experiments run in triplicates. Data represents mean ± standard errors (SE) or standard deviations (SD). All calculations were performed using GraphPad Prism 6 for Windows as described below. The kinetic parameters, K_m and V_m values were calculated using the Michaelis-Menten equation,

$$V = \frac{V_m \times [S]}{S + K_m}$$

where V is velocity (nanomoles of substrate per milligram of proteins per minute), V_m is maximal velocity, [S] is substrate concentration and K_m is the Michaelis Menten constant. The uptake into vector-transfected HEK293 cells was subtracted to obtain transporter-specific uptake. For the purpose of K_i calculations data were fitted to the sigmoidal four parameters dose–response model (variable slope):

$$V = V_{min} + \frac{(V_{max} - V_{min})}{1 + 10^{((\log Ki - A)h))}}$$

where V is response, V_{min} represents minimum of response, V_{max} represents maximum of response, h is Hill slope parameter, K_i is the concentration of inhibitor that corresponds to 50% of maximal effect and A is concentration of tested compound.

3. Results

3.1. Gene identification and phylogenetic analysis

In order to elucidate phylogenetic relationships of zebrafish *Oct* genes within the *Slc22* family, we constructed a phylogenetic tree. We have previously identified fourteen genes inside the zebrafish Slc22 family (Popovic *et al*., 2014). Two of them, *Slc22a1* and *Slc22a2*, belong to subgroup of organic cation transporters (*Oct1* and *Oct2*). The subgroup of human organic cation transporters is comprised of OCT1, 2 and 3 co-orthologs, whereas in zebrafish there are only two *Oct* members. OCT1/Oct1 and OCT2/Oct2 are conserved within all analyzed vertebrate species from fish to mammals, with the exception of only one ortholog present in *X. laevis* genome, whereas OCT3/Oct3 orthologs are present only in higher vertebrates from reptiles to humans (Fig. 3.1).

Phylogenetic analysis revealed specific clustering of vertebrate *SLC22/Slc22* genes. Zebrafish *Oct*s clustered with other vertebrate *OCTs/Octs*, and with *OCTN/Octn* and *OCT6/Oct6* gene groups of other vertebrates. Contrary to the observed gene clustering of organic cation transporter group within *SLC22/Slc22* family, zebrafish and other vertebrate members of *SLC22A13/Slc22a13* and *SLC22A14/Slc22a14* group, Organic Cation Transporter-Like 3 (*ORCTL3/Orctl3*) and Organic Cation Transporter-Like 4 (*ORCTL4/Orctl4*), clustered closer together with Organic Anion Transporters (*OAT*s/*Oat*s), indicating closer phylogenetic relationship with transporters of organic anions than expected relationship with organic cation transporters. However, *C. intestinalis* orthologs, *Orctl1* and *Orctl2*, clustered more closely with *OCTN/Octn* group (Fig. 3.1).

OCTN/Octn group is well conserved from fish to mammals with two members in each tetrapod species: OCTN1/Octn1 and OCTN2/Octn2. Two co-orthologs of these human genes are found in all vertebrates, including zebrafish, with the exception of presence of third *Octn* member in *T. nigroviridis* (Fig. 3.1). OCT6/Oct6 co-orthologs are found in all vertebrate species analyzed. Altogether, zebrafish Oct/Octn group includes 5 transporters provisionally annotated as DrOct1, DrOct2, DrOctn1, DrOctn2 and DrOct6. Amino acid sequence identity within Octn group is 44-52%, whereas OCT6/Oct6 orthologs share 39-59% identity among vertebrates, and 70 - 74% among fish proteins. Two Oct6 proteins from *C. intestinalis* are 23-32% identical to vertebrate OCT6/Oct6 proteins.

Accession codes and annotations of protein sequences for chordate SLC22/Slc22 family members are given in the Supplemental material (Table S1).

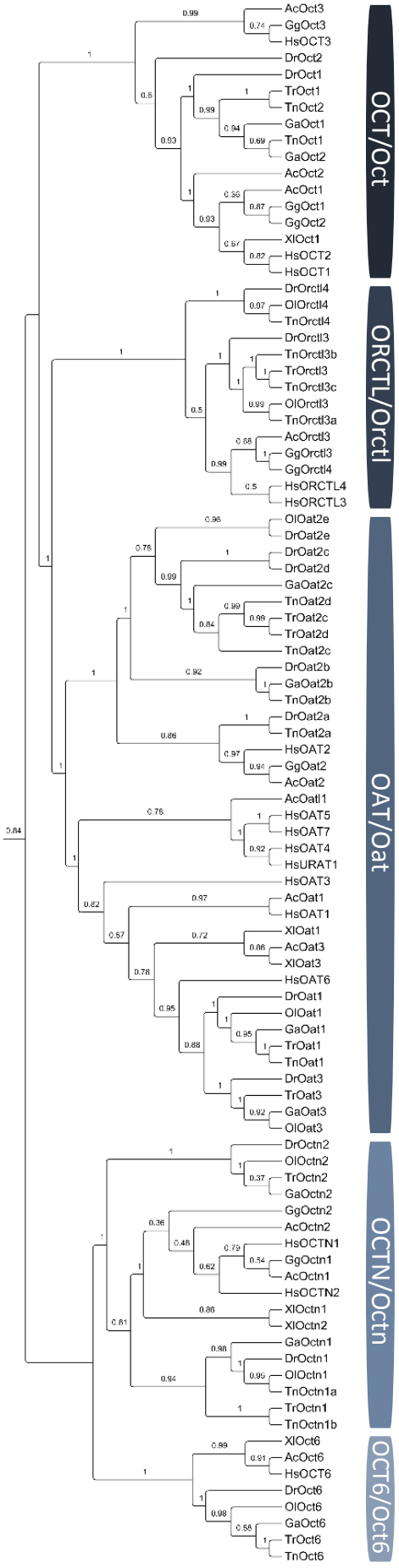

Figure 3.1. Phylogenetic tree of vertebrate SLC22/Slc22 family. Species abbreviations: Hs, *Homo sapiens*; Gg, *Gallus gallus*; Ac, *Anolis carolinensis*; Xl, *Xenopus laevis*; Dr, *Danio rerio*; Ga, *Gastrosteus aculeatus*; Ol, *Oryzes latipes*; Tn, *Tetraodon nigroviridis*; Tr, *Takifugu rubripes*.

3.2. Synteny analysis

The analysis of gene block conservation and changes during evolution provided an insight into syntenic relationships among fish and human *OCT/Oct* genes. Synteny analysis was performed on human, zebrafish, *Tetraodon nigroviridis* and stickleback (*Gasterosteus aculeatus*) genomes. Human *OCT* genes are organized as a cluster of three genes, following one another without inserted genes among them. The human *OCT* gene cluster is located on chromosome 6, between 160.54 and 160.77 megabase pair (Mbp), with forward orientation of OCT1 and OCT3, whereas OCT2 is oriented in reverse direction (Fig. 3.2). Genetic neighborhood of the human *OCT* gene cluster is represented with seven neighboring genes. Three genes are located upstream from the *OCT* cluster. The *IGF2R* gene is located next to the cluster with same reverse orientation as *OCT2*. Further upstream, there are two neighboring genes which showed to be important for determination of syntenic relationship with zebrafish *Oct2*. Genes *FUCA2* and *TXLNB* lay on 143.82 and 139.56 Mbp, respectively, and they are oriented equally as *OCT2* gene in the cluster and contrary to neighboring *IGF2R*. Two more neighboring genes are located upstream of the cluster, *RFX6* and *VGLL2*, laying in forward orientation on 116.87 and 117.26 Mbp, respectively. Two neighboring genes, *PLG* and *GPR31*, located downstream of the *OCT* cluster were shown to be important for determination of syntenic relationship between human *OCT* cluster and zebrafish *Oct1*, together with Oct genes from *T. nigroviridis* and stickleback (Fig. 3.2).

Syntenic analysis revealed location of zebrafish *Oct1* ortholog on chromosome 20, and it showed conserved synteny with human *OCT* cluster (Fig. 3.2). Neighboring genes of zebrafish *Oct1* matched the neighboring genes of the human ortholog cluster. *Igf2r* gene on zebrafish chromosome 20 is located upstream at 42.59 Mbp, next to *Oct1* gene, in same forward orientation as human IGF2R. *Rfx6* and *Vgll2* genes showed similar locations, upstream of *Oct1* gene in respect to location of human *VGLL2* and *RFX6* on the same side of the human *OCT* cluster. Gene *Plg*, which is located downstream next to Oct1 at 42.72 Mbp, showed opposite reverse orientation in comparison with human *PLG* (Fig. 3.2).

Another zebrafish ortholog *Oct2* is located on chromosome 17. Synteny analysis of *Oct2* showed conserved syntenic relationship with human *OCT* cluster, which was confirmed by analysis of only two neighboring gene locations (Fig. 3.2). Analysis revealed locations of two neighboring genes, *Txlnbb* and *Fuca2*, downstream and in the same reverse orientation as zebrafish *Oct2*, whereas human orthologs of these genes are located upstream of human *OCT* cluster in the same orientation (Fig. 3.2).

Results of *T. nigroviridis* genome and synteny analysis revealed syntenic relationships between human and *T. nigroviridis* OCT/Oct genes (Fig. 3.2). Neighboring genes of *T. nigroviridis Oct2* cluster of four

splice variants matched the genetic neighborhood of human *OCT* cluster. *Gpr31* and *Igf2r* genes on *T. nigroviridis* chromosome 14, at the location downstream of *Oct2* cluster, showed opposite localization and orientation in comparison with human orthologs. Upstream of *Oct2* cluster there are three genes, *Plg, Vgll2a* and *Rfx6*, that showed same forward orientations as human orthologs, whereas *Plg* showed differences from human ortholog which is located downstream of *OCT* cluster. Different location in respect to human and *T. nigroviridis OCT/Oct* cluster was also reported for *Igf2r* gene, which is located downstream of *T. nigroviridis Oct* cluster, whereas human *IGF2R* ortholog is located upstream of *OCT* cluster. *Gpr31* gene is located downstream of *T. nigroviridis* Oct cluster, same as human ortholog but in opposite forward orientation (Fig. 3.2).

Conserved syntenic relationship with human *OCT* cluster was also confirmed in analysis of stickleback *Oct* and neighboring gene localizations. The results showed similar relationships with human *OCT* gene cluster as reported for *T. nigroviridis Oct* genes, with crucial difference in number of *Oct2* splice variants in stickleback, which showed only two splice variants. Forward oriented *Vgll2a* and *Plg* genes are located upstream of reverse oriented Oct cluster, which matches previously reported differences in *PLG/Plg* localizations between human and analyzed fish genomes. The same difference is reported for *Igf2r* gene, located on the opposite downstream side of the human ortholog (Fig. 3.2). On the other hand, *Gpr31* has the same location as human ortholog, downstream of *OCT/Oct* cluster, with opposite orientation than human ortholog (Fig. 3.2).

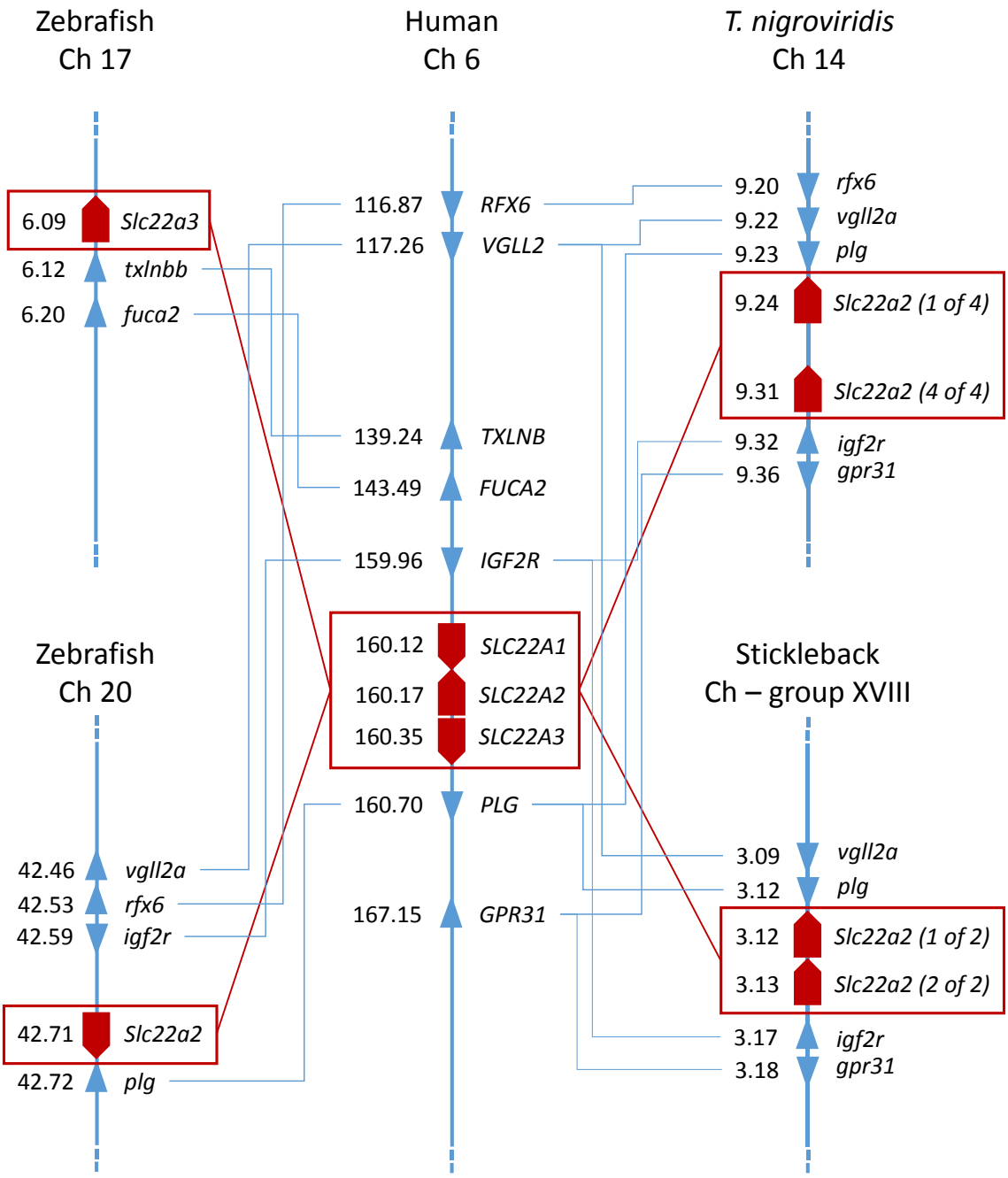

Figure 3.2. Conserved synteny analysis of human, zebrafish, *T. nigroviridis* and stickleback OCT/Oct genes. Numbers next to the gene names represent megabase pair (Mbp) of particular gene location on the chromosome.

3.3. Cell localization and topology analysis

Using TMHMM online server for secondary structure protein predictions, we determined characteristic transmembrane formations of zebrafish Octs, with characteristic extra- and intracellular loops. Analysis of Oct1 showed that Oct1 forms twelve transmembrane α-helices (Fig. 3.3). The first and the

second transmembrane helix of Oct1 are divided with long extracellular loop of 105 amino acids. Next five transmembrane helices are positioned tightly next to each other up to the large intracellular loop of 62 amino acids, located between sixth and seventh transmembrane helix. After the intracellular loop, the rest of six transmembrane helices are positioned without gaps in between. All observed transmembrane helices have the same length of 22 amino acids, except for the ninth transmembrane helix which is 18 amino acids long. Concerning protein membrane topology, the N- and C-terminus of the Oct1 are located on the cytoplasmic side of the cell, and the transmembrane helices are organized so that they form transmembrane pore with the active site within the pore.

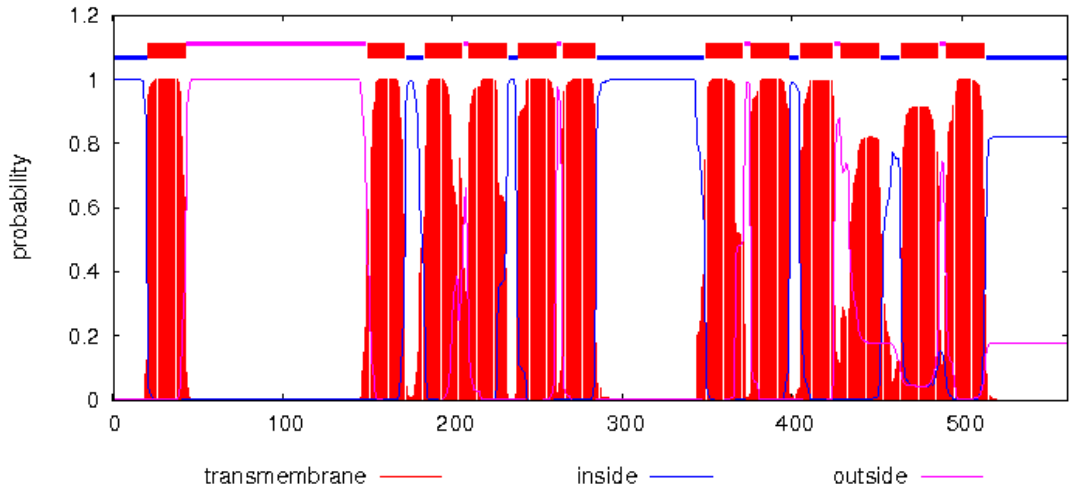

Figure 3.3. Graphic representation of zebrafish Oct1 (DrOct1) secondary structure analysis. On the top of probability graph is a schematic presentation of DrOct1 secondary structure with red rectangles representing 12 identified transmembrane α-helices (TMH). The pink line represents large extracellular loop between TMH1 and 2. The blue line represents big intracellular loop between TMH6 and 7, and it also indicates that both N- and C-terminal regions are localized inside the cell.

Analysis of Oct2 revealed the differences between these two proteins. The major differences are in the number of transmembrane helices, with nine transmembrane helices of Oct2. The difference is also in the topology of the protein within the membrane, with the N-terminal end in the cytosolic part of the cell, whereas C-terminal end is located in the extracellular space (Fig. 3.4). Similarities are preserved in the form of large extracellular loop between the first and second transmembrane helix and slightly smaller intracellular loop between the sixth and seventh transmembrane helix. In contrast to Oct1, the transmembrane helices of Oct2 are more divergent in a sense of their length. Helices 1, 3, 4, 7, 8, 9 are 22 amino acids in length, whereas the helices 2 and 5 are 17 amino acids long and the helix 6 is 19 amino acids long.

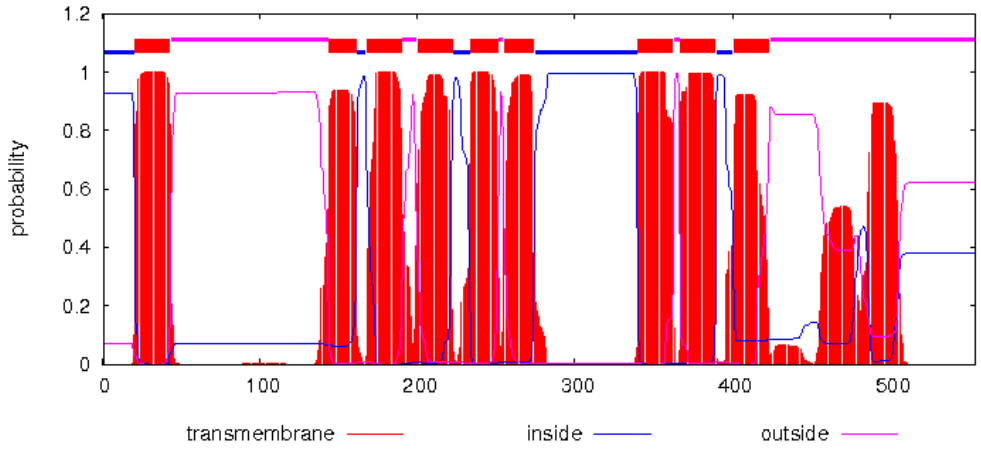

Figure 3.4. Graphic representation of zebrafish Oct2 (DrOct2) secondary structure analysis. On the top of probability graph is schematic representation of DrOct2 secondary structure with only 9 TMH and large extra- and intracellular loops. Due to lack of 3 TMH, DrOct2 C-terminal region is located outside of the cell.

3.4. Secondary structure and specific motifs

Multiple alignment of amino acid sequences of human and zebrafish OCTs/Octs revealed some crucial similarities and differences. The OCTs/Octs are comprised of 554 – 562 amino acids, with amino acid sequence identity of 41 – 47% among human and zebrafish proteins, whereas the sequence similarity was higher, from 62 to 67%. Amino acid sequence identity among three human OCT members was 49 – 70%, which was higher than 45% identity among zebrafish Oct1 and Oct2. Conserved domain analysis showed specific motifs within OCT/Oct sequences that belonged to amphiphilic solute facilitator (ASF) domain and major facilitator superfamily (MFS) domain, respectively (Fig. 3.5). The ASF domain was identified in all five analyzed proteins and is located at the end of large extracellular loop, just before the second transmembrane domain, as well as at the end of intracellular loop and between transmembrane domain 10 and 11 (Fig. 3.5). Characteristic MFS motif $GX_3GX_4GX_3$DRFGRR is found in all five examined proteins, within transmembrane domain 2 and between transmembrane domain 2 and 3, together with characteristic MSF motifs between transmembrane domain 4 and 5 and at the beginning of large intracellular loop (Fig. 3.5). Multiple sequence alignment of the examined proteins also revealed the sequence similarities within the regions of previously identified transmembrane domains, whereas the sequences are more different in the regions between the transmembrane domains, especially within large extra- and intracellular loops. Greater differences are also observed near C-terminal regions of the proteins (Fig. 3.5).

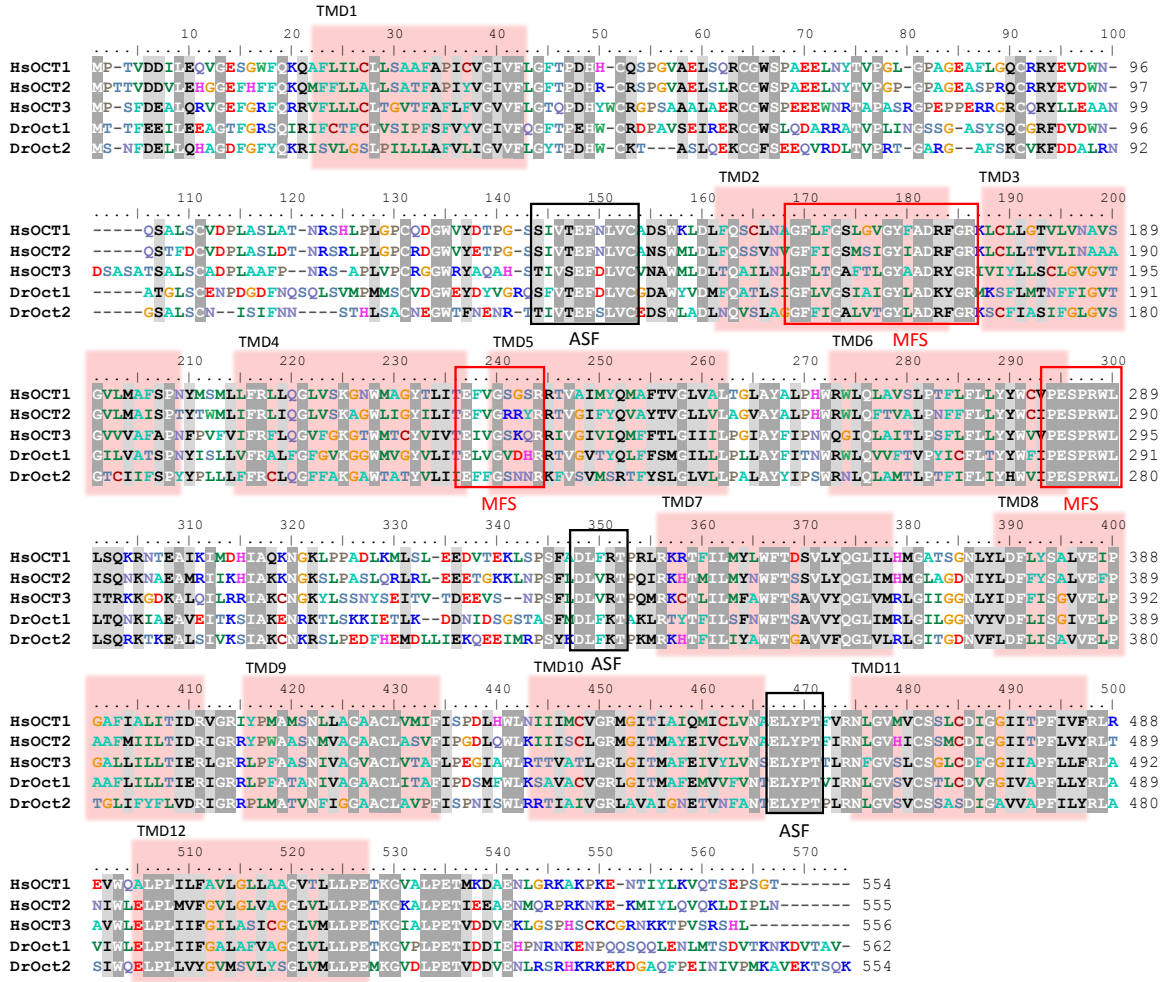

Figure 3.5. Amino acid sequence alignments of human and zebrafish OCT/Oct proteins. Conserved parts of sequences are shaded. Characteristic MFS motif is framed in red and ASF motif is framed in black.

3.4.1. N-glycosylation sites

The NetNGlyc 1.0 online server analysis of zebrafish Oct proteins revealed potential N-glycosylation sites within large extracellular loops of both transporters (Fig. 3.6). The analysis identified three potential N-glycosylation sites on Oct1 extracellular loop, with characteristic motif and positions: 78NGSS, 96NATG, 110NQSQ. Contrary to Oct1, the N-glycosylation analysis of Oct2 revealed total of seven N-glycosylation sites, with five of them within large extracellular loop as in Oct1, whereas the other two sites are located on the extracellular C-terminal end of the transporter. Seven identified N-glycosylation motifs are: 92NGSA, 99NISI, 104NNST, 105NSTH, 121NRTT, 418NISW and 438NETV.

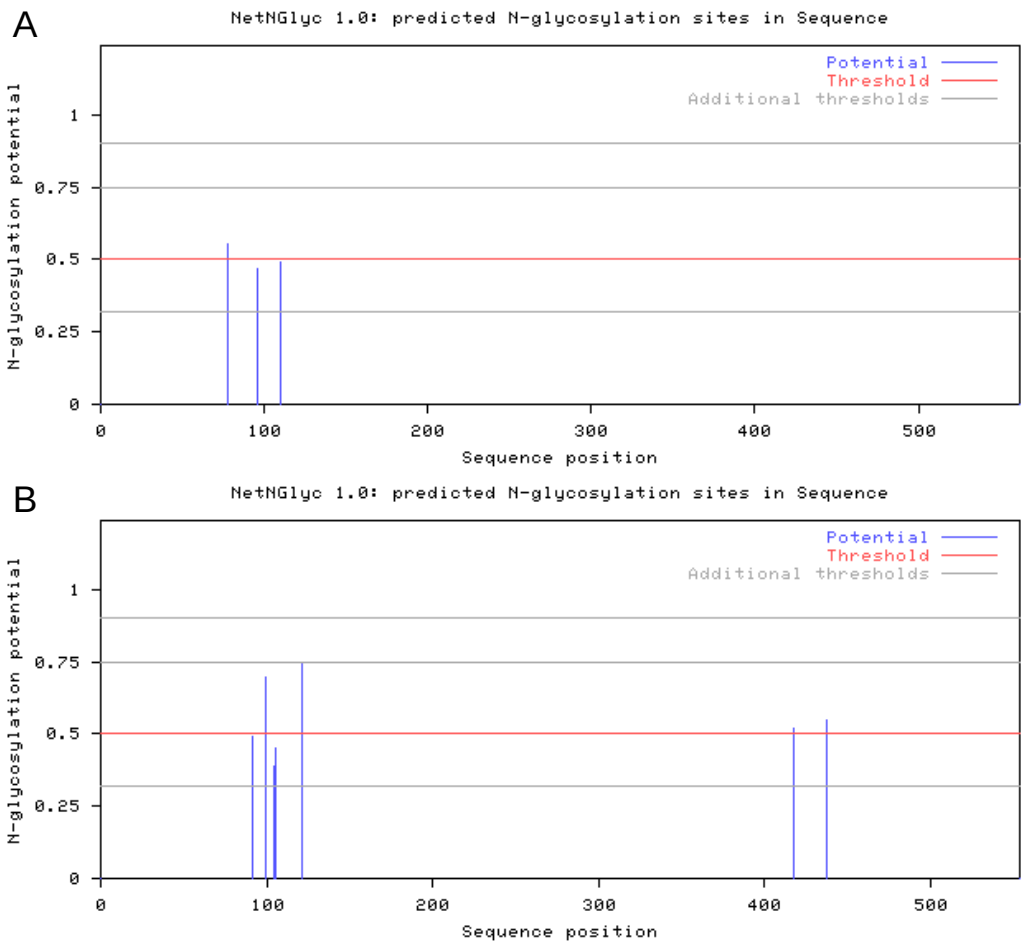

Figure 3.6. Graphic display of the NetGlyc 1.0 N-glycosylation analysis of zebrafish Oct1 (A) and Oct2 (B).

3.5. Tissue expression profiles

qRT-PCR analysis revealed tissue expression patterns of two zebrafish *Oct* genes (Fig. 3.7). The highest observed expression of *Oct1* was in kidney, with clear expression differences among genders. Almost 3-fold higher expression of *Oct1* was observed in female kidneys than in male. Taken together, the *Oct1* gene in female and male kidneys, with almost 45000 MNE*10^5 and 15000 MNE*10^5 (Ct value below 21), respectively, showed the highest expression among all *Slc22* genes in all observed zebrafish tissues. *Oct1* expression in female kidney was almost 15-fold higher than in male liver and almost 45-fold higher than in testes. High expression of *Oct1* was observed in zebrafish liver, with dominant expression in male liver. The expression of *Oct1* in male liver of almost 3000 MNE*10^5 was approximately 10-fold higher than expression in female liver (Fig. 3.7). *Oct1* showed high expression in zebrafish testes, with distinct gender differences, revealing almost non-existent expression in

zebrafish ovaries. Moderate expression of *Oct1* was also observed in brain, with dominance in male tissues.

In comparison with *Oct1, Oct2* showed considerably lower expression in all analyzed zebrafish tissues. The highest expression of *Oct2* was observed in zebrafish testes, with great differences among genders, revealing a pattern of gender dependent expression similar to *Oct1* in gonads. However, the highest reported *Oct2* expression in zebrafish testes was almost 25-fold lower than most dominant expression of *Oct1* in female kidney, and in similar range in gonads. The next notable expression of *Oct2* was observed in kidneys with evident gender variation. *Oct2* expression was more dominant in male tissues, which was almost 19-fold lower than *Oct1* in male kidneys and almost 53-fold lower than in *Oct1* in female kidneys. The expression of *Oct2* in other analyzed tissues was in lower range of moderate expression, starting from intestine and followed by liver, gills, brain and lowest observed expression in ovaries.

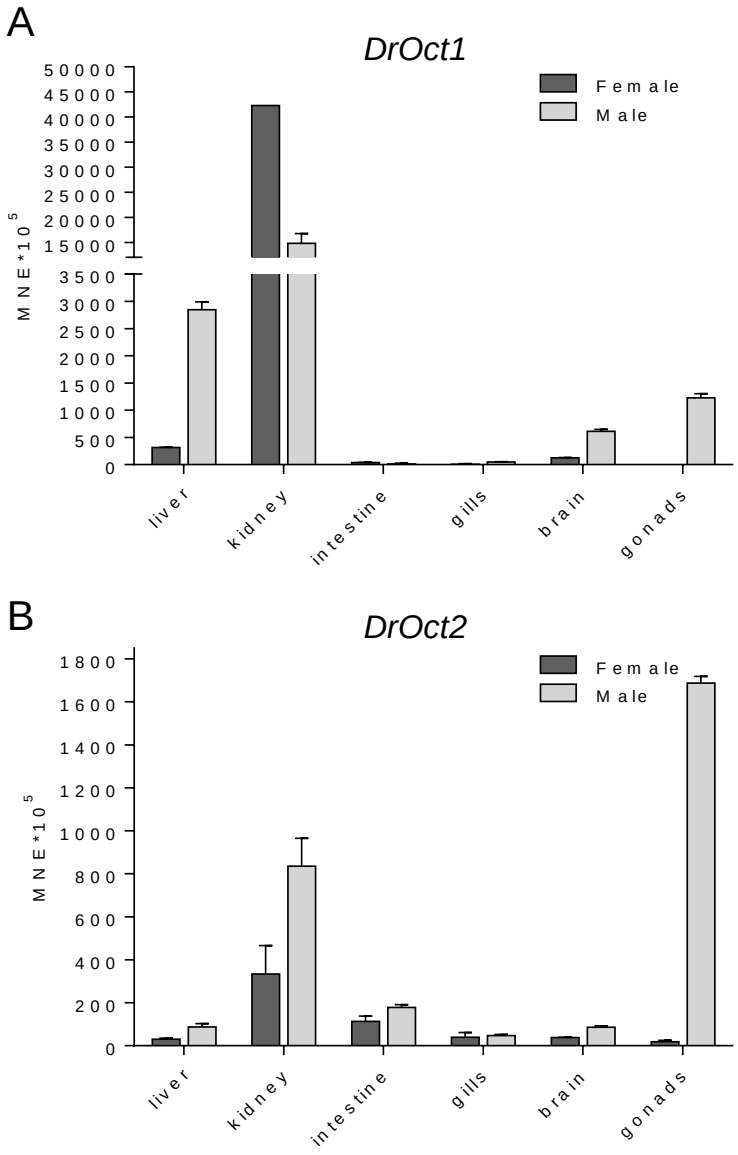

Figure 3.7. qRT-PCR analysis of *Oct* genes in adult male and female zebrafish: A) DrOct1, B) DrOct2. Data represent MNE (mean normalized expression) ± SD normalized to the Ef1α.

3.6. Protein identification and cell localization

In order to identify expressed zebrafish Oct proteins, we performed Western blot analysis. The analysis was based on the expression of specific tags, fused together with the Oct proteins in the heterologous expression system. Immunofluorescence analysis determined the localization of zebrafish organic cation transporters within the cells and revealed some critical differences between Oct1 and Oct2. The analysis showed clear localization of Oct1 within the cell membranes. This was confirmed by co-localization of green colored Oct and red colored Na/K ATPase, which is naturally localized in the cell membranes. As the result of co-localization the signals of two dyes were combined and subsequently

produced an orange signal, which confirmed the localization of zebrafish Oct1 within the cell membrane (Fig. 3.8A). However, the red color of cell membranes in the system transfected with zebrafish *Oct2* gene indicated the presence of only naturally constituted Na/K ATPase. The green coloring below the cell membranes and in the cytoplasm of transfected HEK293 cells confirmed the lack of cell membrane localization of Oct2, which was serious indicator that Oct2 may not be active in the used expression system (Fig. 3.8B).

3.7. Functional characterization of zebrafish Oct1

3.7.1. Substrates

Initial tests of cationic fluorescent dyes which could be used as substrates for functional characterization of zebrafish Octs revealed five potential fluorescent substrates of Oct1. However, Oct2 showed no activity with any of tested substrates, which confirmed initial data, implying that Oct2 may not be active in the used heterologous expression system due to previously reported lack of localization in the cell membranes of HEK293 cells.

We identified five fluorescent dyes that showed accumulation in *Oct1* transfected HEK293 cells, thus revealing the interaction with Oct1 as potential substrates. Time and dose-response assays confirmed the tested dyes as substrates of Oct1, whose transport followed the classical Michaelis-Menten kinetics. First confirmed fluorescent substrate was 4-(4-(dimethylamino)styryl)-N-methylpyridinium iodide (ASP+), a fluorescent dye with excitation wavelength of 460 nm and emission wavelength of 600 nm. Time response measurements of accumulation of ASP+ in the Oct1 expressing cells showed the saturable uptake after 10 min of accumulation (Fig. 3.9A). The dose-response assay confirmed classic Michaelis-Menten transport kinetics and revealed high affinity of Oct1 for ASP+ with K_m value of 25.97 ± 1.7 µM, with V_{max} of 992.5 ± 25.6 pmol/mg protein/min (Fig. 3.9B).

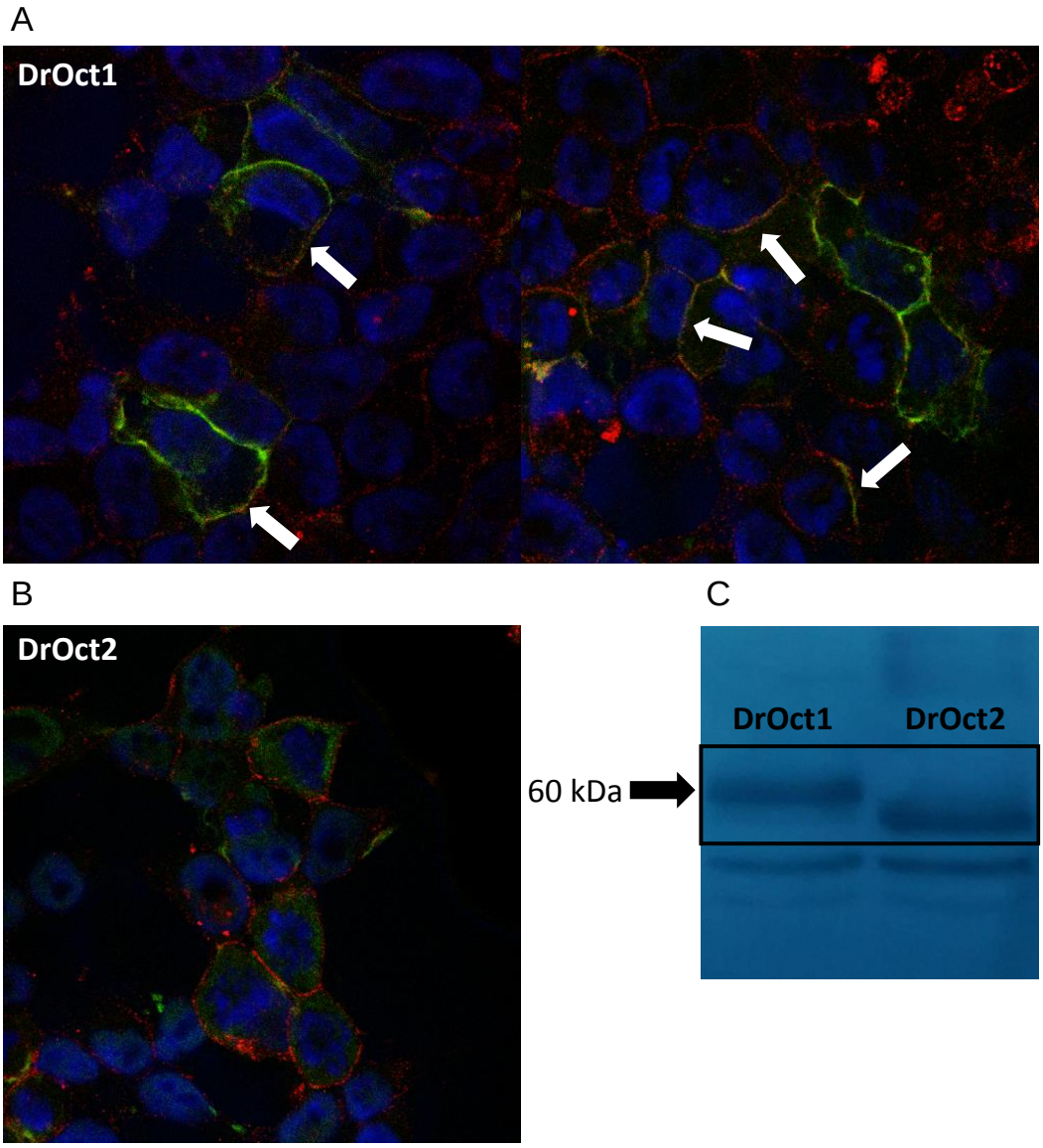

Figure 3.8. Cell localization of zebrafish Oct1 (A) and Oct2 (B) tagged with N-terminal Xpress tag. Immunocytochemistry was performed with fluorescein conjugated secondary antibody (FITC) that binds to the primary Xpress antibody and stains the protein in green. Nuclei are dyed in blue with DAPI, and plasma membranes are stained in red after binding of primary antibody Na,K-ATPase and Cy3-conjugated IgG secondary antibody (all anti-mouse). The membrane color turns to orange (white arrows) because of the overlap of green and red. Cytosolic forms are seen as green areas in the cytoplasm. White arrows mark co-localization of Na,K-ATPase and Oct1 in cell membranes (orange). (C) Western blot analysis of zebrafish Oct1 and Oct2 confirming the expression in transiently transfected HEK293 cells with approximate size of 60 kDa.

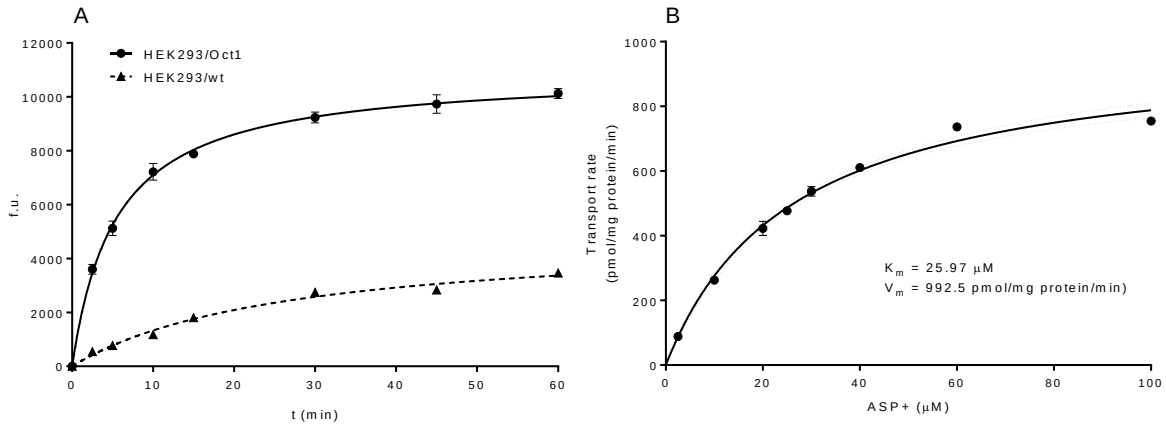

Figure 3.9. Michaelis-Menten kinetics of zebrafish Oct1 mediated uptake of fluorescent dye ASP+. A) Time dependent uptake of ASP+ by HEK293 cell overexpressing Oct1 and by wild type HEK293 cells. ASP+ accumulation is expressed as increase in fluorescence (fluorescence units – f.u.) over time (min). B) Dose-response of Oct1 ASP+ uptake expressed as transport rate (pmol/mg protein/min) over ASP+ concentration (µM) after 5 min incubation with ASP+.

Rhodamine 123 also showed accumulation in Oct1 expressing cells, which confirmed the rhodamine 123 as the second possible model Oct1 fluorescent substrate. Rhodamine 123 is a cationic fluorescent dye that gives fluorescent signal at excitation wavelength of 510 nm and emission wavelength of 530 nm. Time dependent accumulation of rhodamine 123 in Oct1 expressing cells showed that the transport of rhodamine 123 by Oct1 reaches the saturation point after 30 min of accumulation (Fig. 3.10A), whereas the transport in non-transfected cells was much lower in the same time period, confirming the role of Oct1 as transporter of rhodamine 123. The dose-response assay of rhodamine 123 revealed very low K_m in nanomolar range of 103.7 ± 14.9 nM and low V_m of 13 ± 0.6 pmol/mg protein/min (Fig. 3.10B).

Berberine is a cationic fluorescent dye, with excitation wavelength of 355 nm and emission wavelength of 540 nm. The accumulation assays with transfected and non-transfected cells revealed berberine as another fluorescent substrate of Oct1. Time dependent accumulation of berberine showed that the transport of berberine by Oct1 reaches the saturation at 30 min of accumulation (Fig. 3.11A), with clear difference between transfected and non-transfected cells, which showed lower accumulation of berberine in the same time period. Dose-response assay showed that Oct1 transports berberine with high affinity of 3.96 ± 0.74 µM and with V_m of 43.49 ± 2.17 pmol/mg protein/min (Fig. 3.11B).

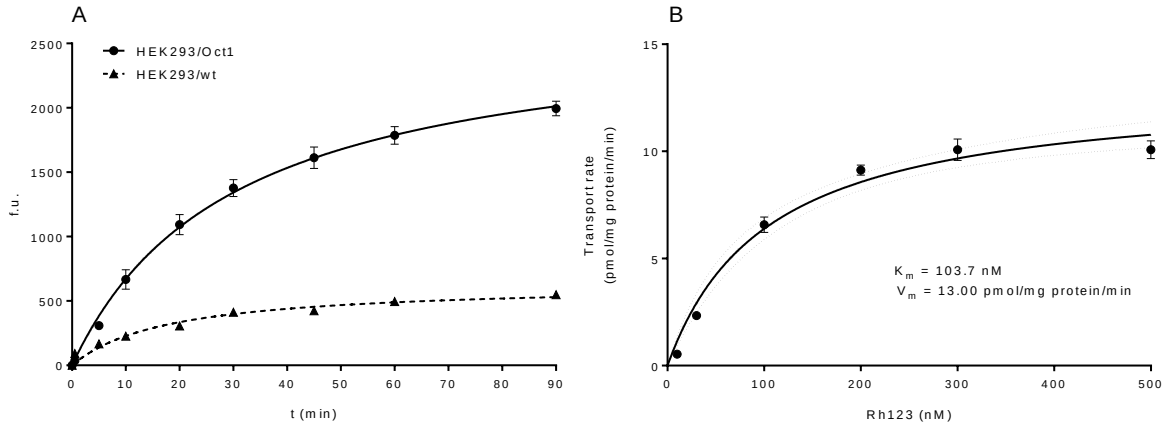

Figure 3.10. Michaelis-Menten kinetics of zebrafish Oct1 mediated uptake of fluorescent dye rhodamine 123 (Rh123). A) Time dependent uptake of Rh123 by HEK293 cell overexpressing Oct1 and by wild type HEK293 cells. Rh123 accumulation is expressed as increase in fluorescence (fluorescence units – f.u.) over time (min). B) Dose-response of Oct1 Rh123 uptake expressed as transport rate (pmol/mg protein/min) over Rh123 concentration (nM) after 10 min incubation with Rh123.

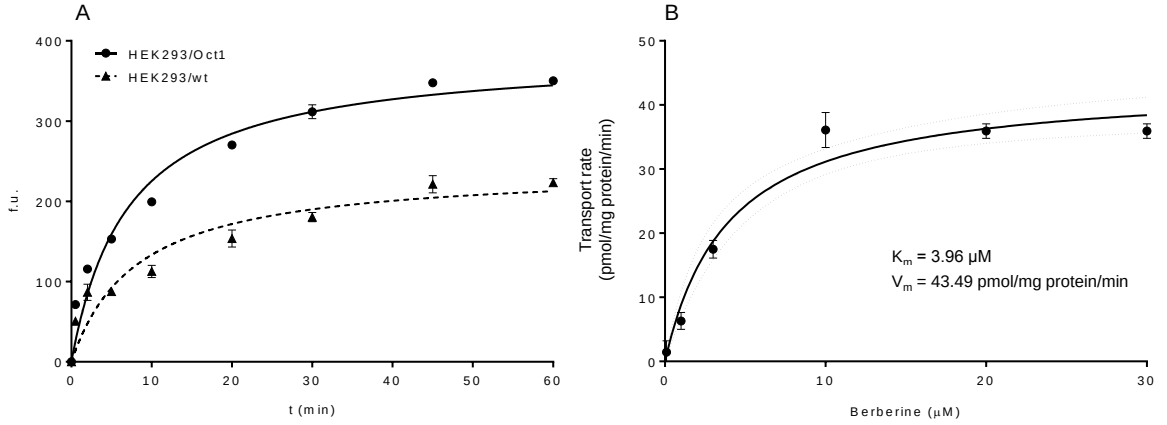

Figure 3.11. Michaelis-Menten kinetics of zebrafish Oct1 mediated uptake of fluorescent dye berberine. A) Time dependent uptake of berberine by HEK293 cell overexpressing Oct1 and by wild type HEK293 cells. Berberine accumulation is expressed as increase in fluorescence (fluorescence units – f.u.) over time (min). B) Dose-response of Oct1 berberine uptake expressed as transport rate (pmol/mg protein/min) over berberine concentration (µM) after 10 min incubation with berberine.

Our further search for model Oct1 fluorescent substrates revealed DAPI as a new potential substrate. DAPI is a neutrally charged compound, which strongly interacts with A-T rich regions on DNA. DAPI bound to DNA has the excitation maximum at a wavelength of 358 nm and emission maximum at 461 nm. This property of DAPI to reach its fluorescence maximum when bound to the DNA inside of the cell, allowed the conduction of transport measurements of DAPI with Oct1 in real time. Transport

measurement revealed very short saturation time of 1.5 min, with great difference in accumulation between the cells overexpressing Oct1 and non-transfected cells (Fig. 3.12A). Dose-response kinetics in real time showed that Oct1 transports DAPI with high affinity of 0.78 ± 0.18 µM and low V_m of 6.87 ± 0.3 pmol/mg protein/min (Fig. 3.12B).

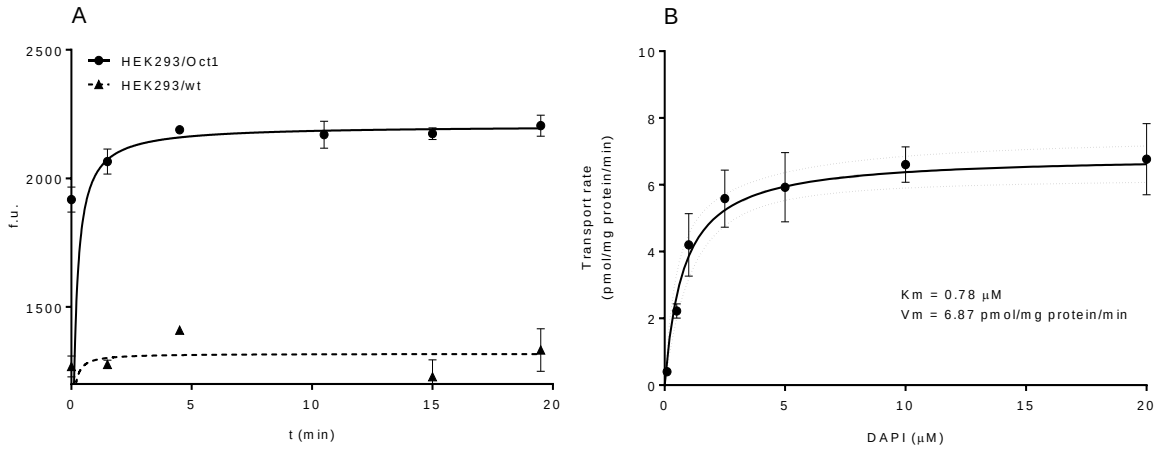

Figure 3.12. Michaelis-Menten kinetics of zebrafish Oct1 mediated uptake of fluorescent dye DAPI. A) Time dependent uptake of DAPI by HEK293 cell overexpressing Oct1 and by wild type HEK293 cells. DAPI accumulation is expressed as increase in fluorescence (fluorescence units – f.u.) and it was measured in real time in time periods of 1 min for total of 20 min. B) Dose-response of Oct1 DAPI uptake expressed as transport rate (pmol/mg protein/min) over berberine concentration (µM) after 1.5 min incubation with DAPI.

Similar Oct1 transport properties were determined with ethidium bromide (EtBr). Since ethidium bromide expresses the fluorescence maximum following the interaction with DNA, we were able to perform transport measurements in real time. Ethidium bromide reaches its excitation maximum at wavelength of 535 nm and emission maximum at 590 nm. Kinetic measurements revealed great difference between Oct1 transfected and non-transfected cells, with saturation time of 15 min (Fig. 3.13A). Dose-response assay determined low K_m value of 96.93 ± 10.82 nM together with low V_m value of 5.34 ± 0.13 pmol/mg protein/min (Fig. 3.13B).

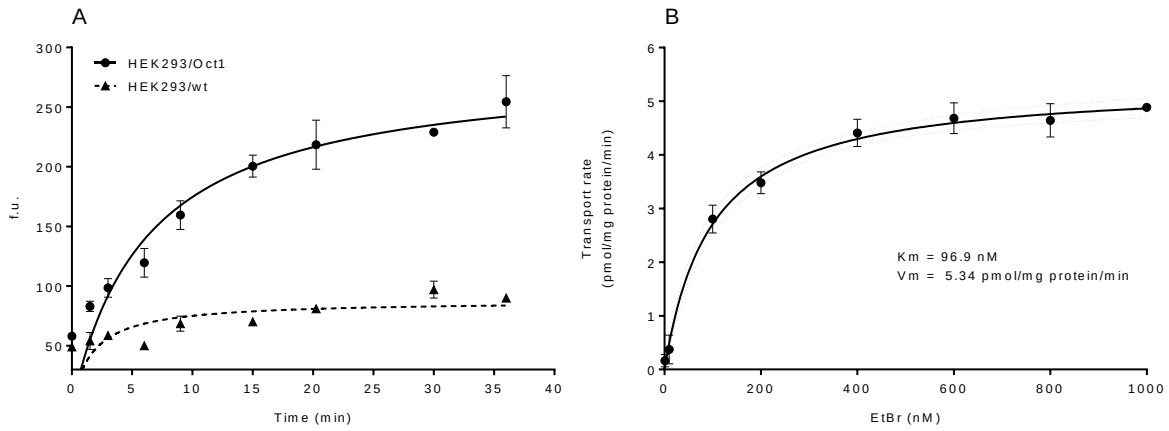

Figure 3.13. Michaelis-Menten kinetics of zebrafish Oct1 mediated uptake of fluorescent dye EtBr. A) Time dependent uptake of EtBr by HEK293 cell overexpressing Oct1 and by wild type HEK293 cells. EtBr accumulation is expressed as increase in fluorescence (fluorescence units – f.u.) and it was measured in real time in time periods of 1 min for total of 35 min. B) Dose-response of Oct1 EtBr uptake expressed as transport rate (pmol/mg protein/min) over EtBr concentration (nM) after 10 min incubation with EtBr.

3.8. Inhibition tests

3.8.1. The interaction screen assay

In order to determine interaction of Oct1 with various compounds of interest, we performed inhibition assays based on co-exposure of Oct1 overexpressing cells with potential interactor and fluorescent dye as a model substrate. Based on the difference in the accumulation of fluorescent substrate in transfected and non-transfected, control cells, we were able to see the effect these compounds have on Oct1 transport. In the initial phase of investigation, the inhibition screen was made with a wide range of xeno- and endobiotic compounds known as interactors of mammalian OCT/Oct members. The initial screen was performed using single concentration of over fifty potential interacting compounds that were expected to have effect on Oct1 transport of fluorescent substrates.

The interaction screen assay revealed interactions with a wide range of physiological compounds, confirming polyspecific properties of Oct1 interactions (Fig. 3.14). Oct1 showed major interactions with steroid hormones. The most potent interaction was observed with androstenedione, which resulted in only 1% of the ASP+ uptake that remained in co-exposure with 100 µM androstenedione. Progesterone also strongly inhibited Oct1 transport of ASP+ and showed only 2.7% uptake in comparison with control (100%). Additional four steroid hormones showed interactions that resulted with less than 50% of ASP+ uptake. The co-exposure of Oct1 overexpressing cells with corticosterone, testosterone, 19-methyltestosterone and β – estradiol resulted with 19.4%, 13.9%, 19.6% and 37.55%

of ASP+ uptake, respectively. Steroid hormones whose interaction with Oct1 resulted in a moderate ASP+ uptake that ranged around 50% were 5a-androstan-17b-ol-3-one (dihydrotestosterone) with 55.6%, and medroxyprogesterone with 57.1% of ASP+ uptake. The tested steroid hormones that caused minor changes in ASP+ uptake by Oct1 were cortisol, 19 – norethindrone, pregnenolon and prostaglandine E2 with 78%, 74%, 73% and 88% of ASP+ uptake, respectively. The interaction tests with other groups of physiological compounds, ranging from physiologic metabolites to neurotransmitters, revealed lower interactions with Oct1 in comparison to steroid hormones (Fig. 3.14). However, co-exposure with acetylcholine and tyramine resulted with moderate inhibition of ASP+ with 56% and 52% of ASP+ uptake, respectively.

Figure 3.14. Interaction of zebrafish Oct1 with steroid hormones and other physiological compounds known as interactors of mammalian OCT/Oct members. Data are expressed as percentage (%) of ASP+ uptake after co-incubation with each interactor (100 μM) relative to ASP+ uptake in the absence of interactor which is set to 100% (Control).

A broad range of xenobiotic compounds, ranging from toxic model cations and pharmaceuticals to toxins and other xenobiotics, were tested for the interaction with Oct1 (Fig. 3.15). The model cation MPP+ showed very potent interaction with Oct1, which resulted with only 4.7% remaining uptake of

ASP+. Other model cations from the family of quaternary ammonium cations also showed high interactions with Oct1, with the highest determined interactions with tetrapentylammonium and tetrabutylammonium, which resulted with the remaining ASP+ uptake of less than 1% in co-exposure with TPA and 15.4% with TBA. Other xenobiotic compounds that showed interaction with Oct1 were prazosin which caused decrease of ASP+ uptake to 0.6%, and mitoxantrone and cimetidine which caused moderate inhibition of ASP+ uptake of 25% and 34%, respectively. The rest of tested xenobiotics showed lower inhibition of ASP+ uptake. However, the majority of these compounds showed inhibition in the range from 50 to 70%, indicating lower interaction which could be investigated in more detail only with higher concentrations of interacting compounds (Fig. 3.15).

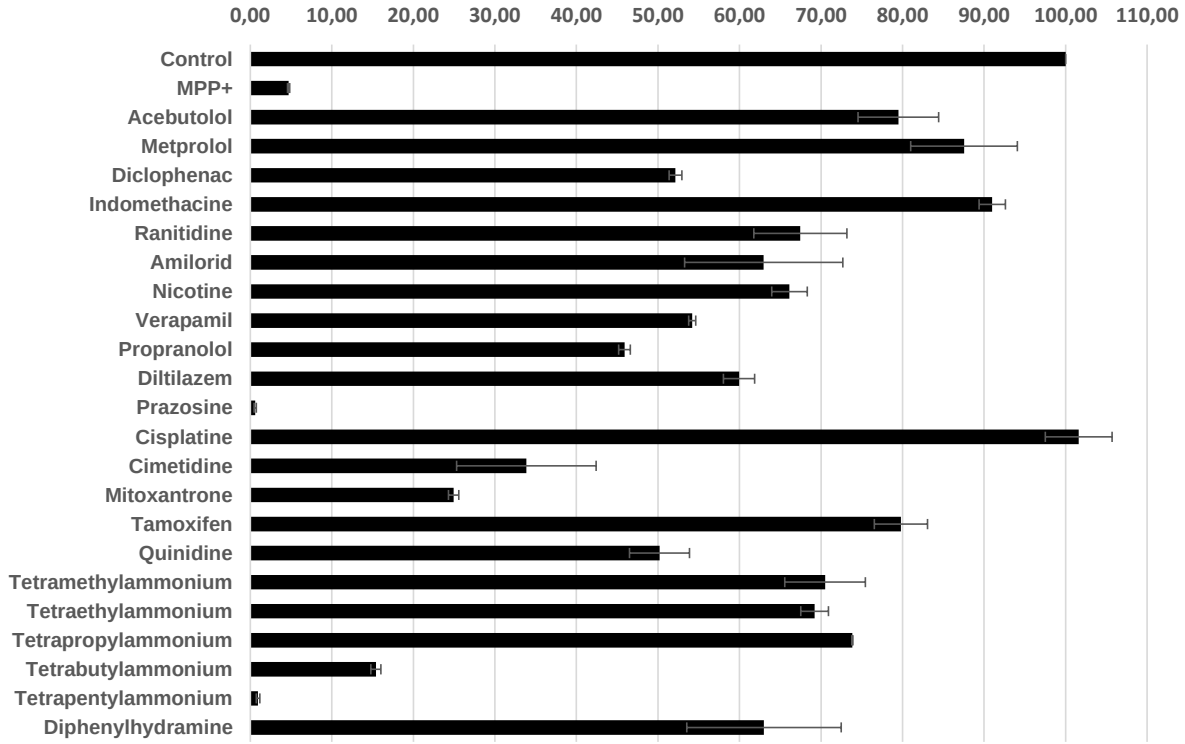

Figure 3.15. Interaction of zebrafish Oct1 with a series of pharmaceuticals and quaternary ammonium cations. Data are expressed as percentage (%) of ASP+ uptake after co-incubation with each interactor (100 µM) relative to ASP+ uptake in the absence of interactor which is set to 100% (Control).

We also investigated the Oct1 interactions with organotin group of compounds, which showed to be important environmental contaminants, especially in the aquatic environment. Tested organotin compounds showed high level of Oct1 interaction. The most potent organotin compounds were dibutyltin chloride, tripropyltin chloride, tributyltin chloride and triphenyltin chloride (Fig. 3.16). Co-

exposure of Oct1 cells with these four organotin compounds resulted in strong inhibition of ASP+ uptake, especially in co-exposure with tripropyltin and tributyltin chloride, resulting in 1.4% and 2.6% of ASP+ uptake, respectively.

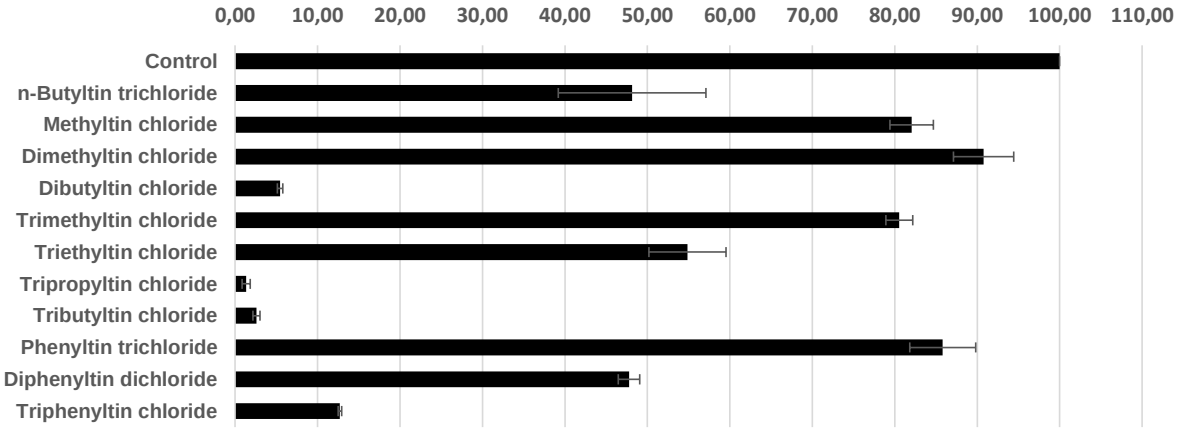

Figure 3.16. Interaction of zebrafish Oct1 with organotin compounds. Data are expressed as percentage (%) of ASP+ uptake after co-incubation with each interactor (100 µM) relative to ASP+ uptake in the absence of interactor which is set to 100% (Control).

3.8.2. Dose-response assays

After the initial interaction screen with various groups of endo- and xenobiotics, further investigation was performed in order to fully characterize interaction kinetics of Oct1 with compounds of interest. In order to elucidate the concentration range in which tested compounds interact with ASP+ transport by Oct1, the dose-response experiments were performed. Using dose-response assays, we were able to obtain inhibition constants of each tested compound. The dose-response assays were also performed with other identified fluorescent substrates in order to obtain more inhibition constants, which would help in the determination of the types of interactions between Oct1 and tested compounds.

3.8.2.1. Oct1 interaction with physiological compounds

The Oct1 interaction screen elucidated that the first major group of endogenous compounds includes steroid hormones. The initial screen indicated strong interactions of Oct1 with non-conjugated steroids from the group of 21-carbon progestenes, progesterone with high affinity (K_i = 1.99 µM) (Fig. 3.17). Oct1 showed very weak interactions with the other progesten member pregnenolon, with only 26.5% inhibition of ASP+ uptake in the initial interaction screen (Fig. 3.14).

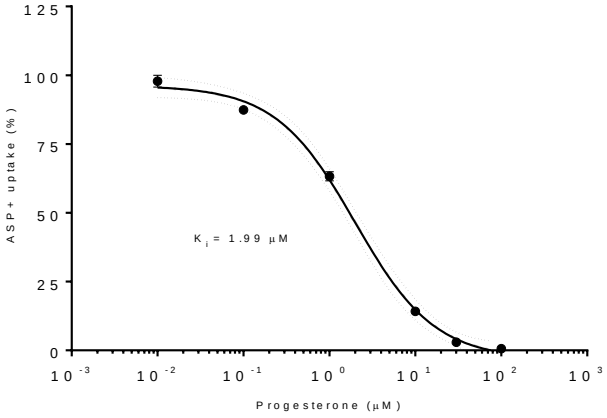

Figure 3.17. Concentration dependent inhibition of Oct1 mediated ASP+ uptake by steroid hormone progesterone. Data are expressed as percentage (%) of ASP+ uptake over logarithm of interactor concentrations (µM) after 5 min of co-exposure. Each data point represents mean ± SD from triplicate determinations.

Following high inhibition with progesterone, the second potent group of Oct1 steroid interactors were 19-carbon androgens, with the highest interaction determined with androstenedione (K_i = 5.13 µM) and testosterone (K_i = 13.19 µM) (Fig. 3.18).

Structurally similar testosterone conjugate, 19-methyltestosterone showed weaker interaction with Oct1 with K_i value of 54.06 µM (Fig. 3.19A). Initial interaction screen revealed interaction of Oct1 with one more member of androgen steroid hormones, dihydrotestosterone. Dose-response assay with potent androgen hormone, dihydrotestosterone determined K_i value of 53.62 µM (Fig. 3.19B).

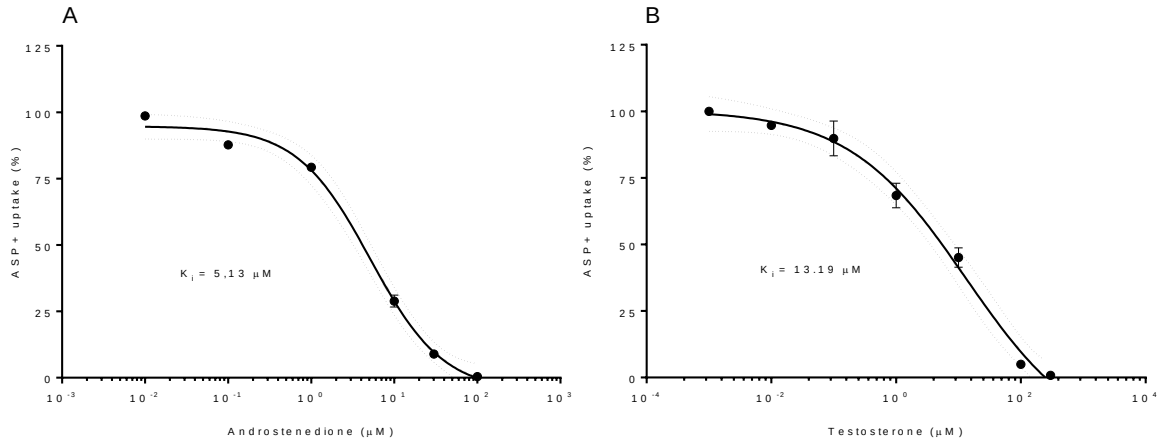

Figure 3.18. Concentration dependent inhibition of Oct1 mediated ASP+ uptake by steroid hormones: A) androstenedione, B) testosterone. Data are expressed as percentage (%) of ASP+ uptake over

logarithm of interactor concentrations (µM) after 5 min of co-exposure. Each data point represents mean ± SD from triplicate determinations.

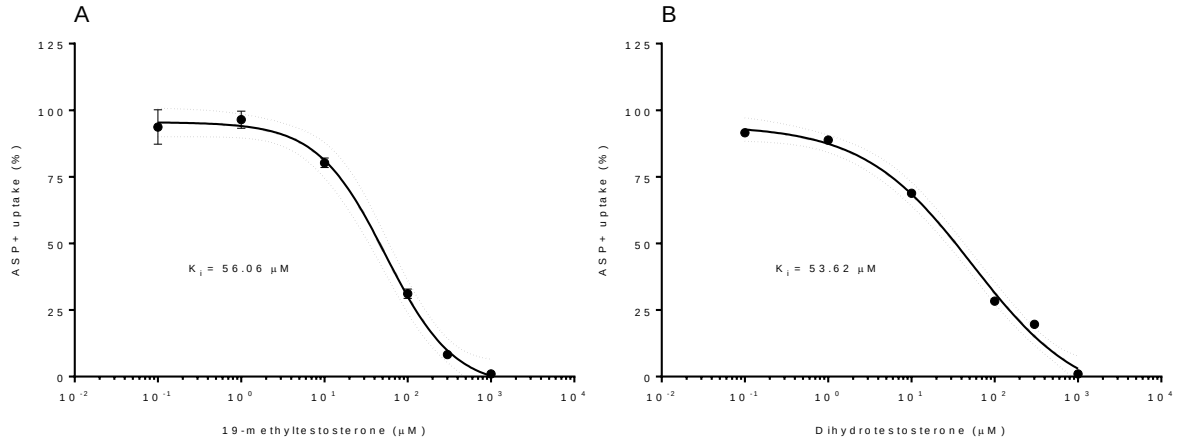

Figure 3.19. Concentration dependent inhibition of Oct1 mediated ASP+ uptake by steroid hormones: A) 19-methyltestosterone, B) dihydrotestosterone. Data are expressed as percentage (%) of ASP+ uptake over logarithm of interactor concentrations (µM) after 5 min of co-exposure. Each data point represents mean ± SD from triplicate determinations.

The next group of steroid hormones that showed considerably high interaction with Oct1 were 21-carbon glucocorticoids, especially corticosterone with K_i of 16.53 µM (Fig. 3.20A), whereas member of glucocorticoid group, cortisol showed weaker interaction, which resulted with only 21.85% inhibition of ASP+ uptake in the initial interaction screen (Fig. 3.14). One member of 18-carbon estrogen group, β-estradiol also showed high interaction with Oct1 with K_i value of 44.35 µM (Fig. 3.20B).

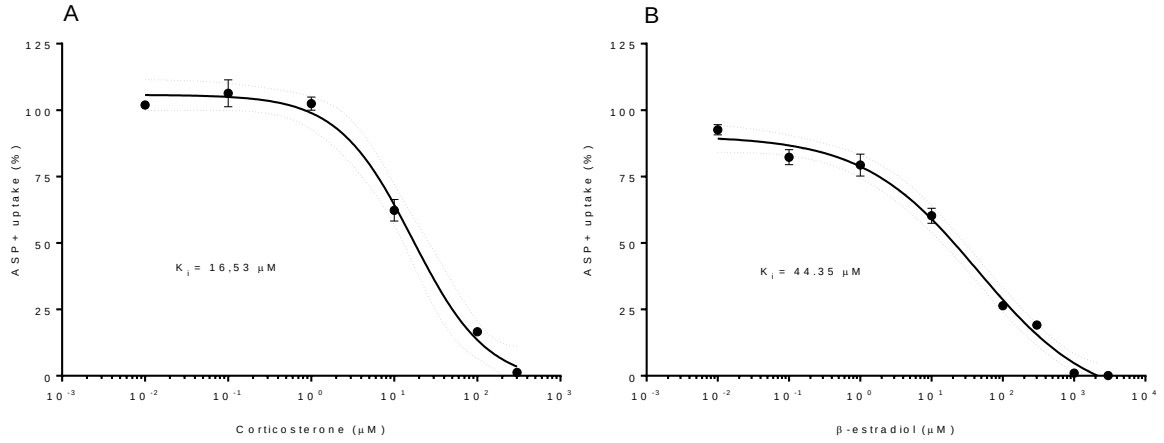

Figure 3.20. Concentration dependent inhibition of Oct1 mediated ASP+ uptake by steroid hormones: A) corticosterone, B) β-estradiol. Data are expressed as percentage (%) of ASP+ uptake over logarithm of interactor concentrations (µM) after 5 min of co-exposure. Each data point represents mean ± SD from triplicate determinations.

Endogenous compounds outside the group of steroid hormones that showed interaction with Oct1 were neurotransmitter acetylcholine and tyrosine metabolite tyramine. These physiological compounds showed much lower interaction with Oct1 in comparison with investigated steroid hormones, with dose-responses resulting in high inhibition constants of 710.8 µM for acetylcholine and 1.02 mM for tyramine, respectively (Fig. 3.21).

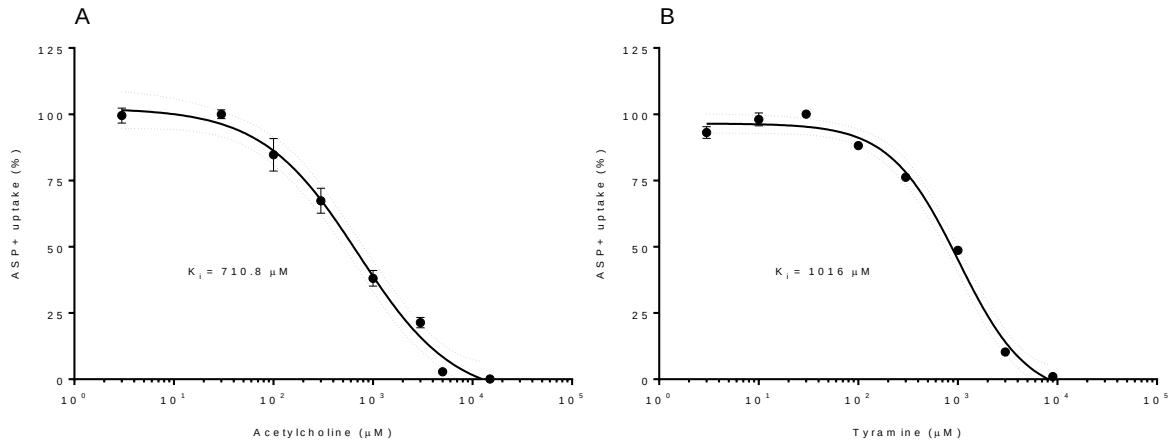

Figure 3.21. Concentration dependent inhibition of Oct1 mediated ASP+ uptake by: A) acetylcholine, B) tyramine. Data are expressed as percentage (%) of ASP+ uptake over logarithm of interactor concentrations (µM) after 5 min of co-exposure. Each data point represents mean ± SD from triplicate determinations.

3.8.2.2. Oct1 interaction with xenobiotics

Based on the initial interaction screen with Oct1, we proceeded with detailed investigation of interactions between Oct1 and various xenobiotics, using ASP+ as model fluorescent substrate. Dose response assays revealed the most potent interaction of Oct1 with the group of organotin compounds, indicating important role of Oct1 in determination of the effect these environmental contaminants may have on zebrafish and other aquatic organisms. Oct1 showed the highest interaction with dibutyltin chloride, with K_i value of 0.4 µM, following with tributyltin and tripropyltin chloride with K_i values of 3.9 µM and 13.37 µM, respectively (Fig. 3.22). Other members of organotin compounds showed the less potential interaction with Oct1 than previously mentioned compounds. Triethyltin chloride inhibited ASP+ transport with determined K_i of 206.3 µM and triphenyltin chloride with K_i of 450.2 µM.

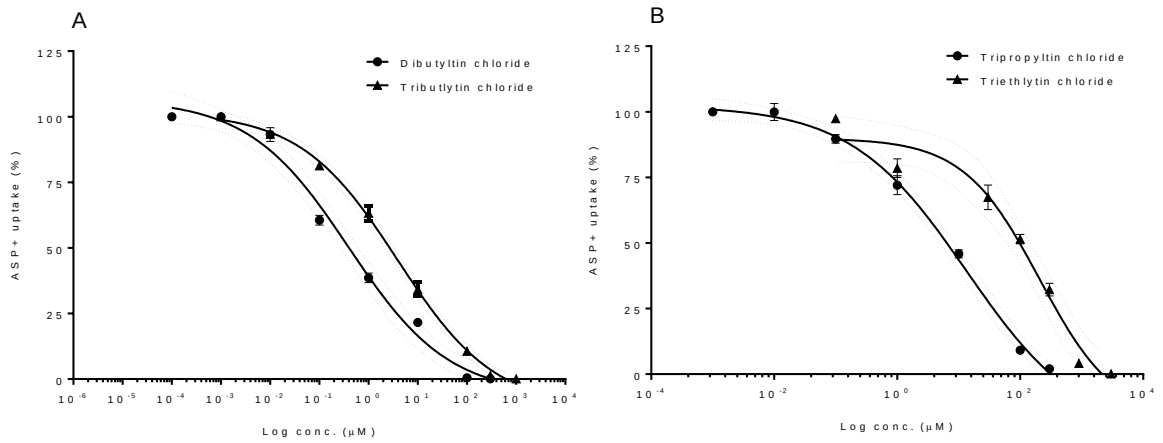

Figure 3.22. Concentration dependent inhibition of Oct1 mediated ASP+ uptake by organotin compounds: A) dibutyltin chloride and tributyltin, B) tripropyltin chloride and triethyltin chloride. Data are expressed as percentage (%) of ASP+ uptake over logarithm of interactor concentrations (µM) after 5 min of co-exposure. Each data point represents mean ± SD from triplicate determinations.

Dose-response assays also revealed high affinity interactions of Oct1 with various pharmaceuticals. Antimalarial drug pyrimethamine and sympatholytic drug prazosin showed potent interactions with K_i values of 0.9 µM and 2.48 µM, respectively (Fig. 3.23A). The members of quaternary ammonium cation family showed high interactions with Oct1, especially tetrapentylammonium with low K_i value of 8.35 µM and tetrabutylammonium 28.05 µM (Fig. 3.23B), whereas tetraethylammonium inhibited ASP+ transport with higher K_i of 820.5 µM and inhibition with tetramethylammonium was in even higher millimolar range (K_i > 10 mM). The inhibition constants of quaternary ammonium salts, obtained from dose-response assays were in correlation with initial interaction screen, where percentage of ASP+ uptake inhibition decreased going from tetrapentylammonium to the members with shorter sidechains (Fig. 3.23B).

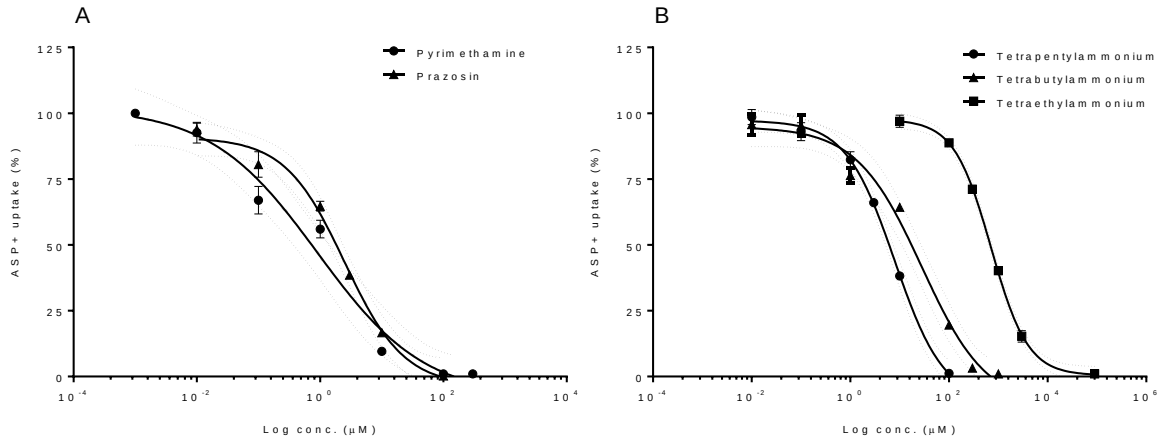

Figure 3.23. Concentration dependent inhibition of Oct1 mediated ASP+ uptake by: A) pyrimethamine and prazosin, B) quaternary ammonium salts – tetraethylammonium, tetrabutylammonium and tetrapentylammonium. Data are expressed as percentage (%) of ASP+ uptake over logarithm of interactor concentrations (μM) after 5 min of co-exposure. Each data point represents mean ± SD from triplicate determinations.

Interaction analysis also confirmed the inhibition of ASP+ uptake by zebrafish Oct1 with MPP+, as previously determined model cation and substrate of other mammalian OCTs/Octs which inhibited ASP+ uptake with K_i value of 22.29 μM (Fig. 3.24A). We determined interactions with the pharmaceuticals from the family of antiarrhythmic drugs, verapamil, propranolol and quinidine with K_i values of 13.74, 119.4, and 139.5 μM, respectively. Antineoplastic drugs, mitoxantrone and tamoxifen inhibited ASP+ uptake by Oct1 with K_i values of 54.33 and 85.27 μM, respectively (Fig. 3.24D). We also confirmed interactions of Oct1 with antidepressant imipramine with K_i value of 62.91 μM, antihypertensive drug diltiazem from the group of calcium channel blockers, with K_i value of 61.89 μM, and antiulcer drug cimetidine with high K_i value of 522.2 μM. The interaction with the members of tyrosine kinase inhibitors was also reported. Vandetanib inhibited ASP+ uptake with low K_i value of 3.74 μM, whereas dasatinib inhibition resulted with higher K_i value of 29.1 μM (Fig. 3.24E).

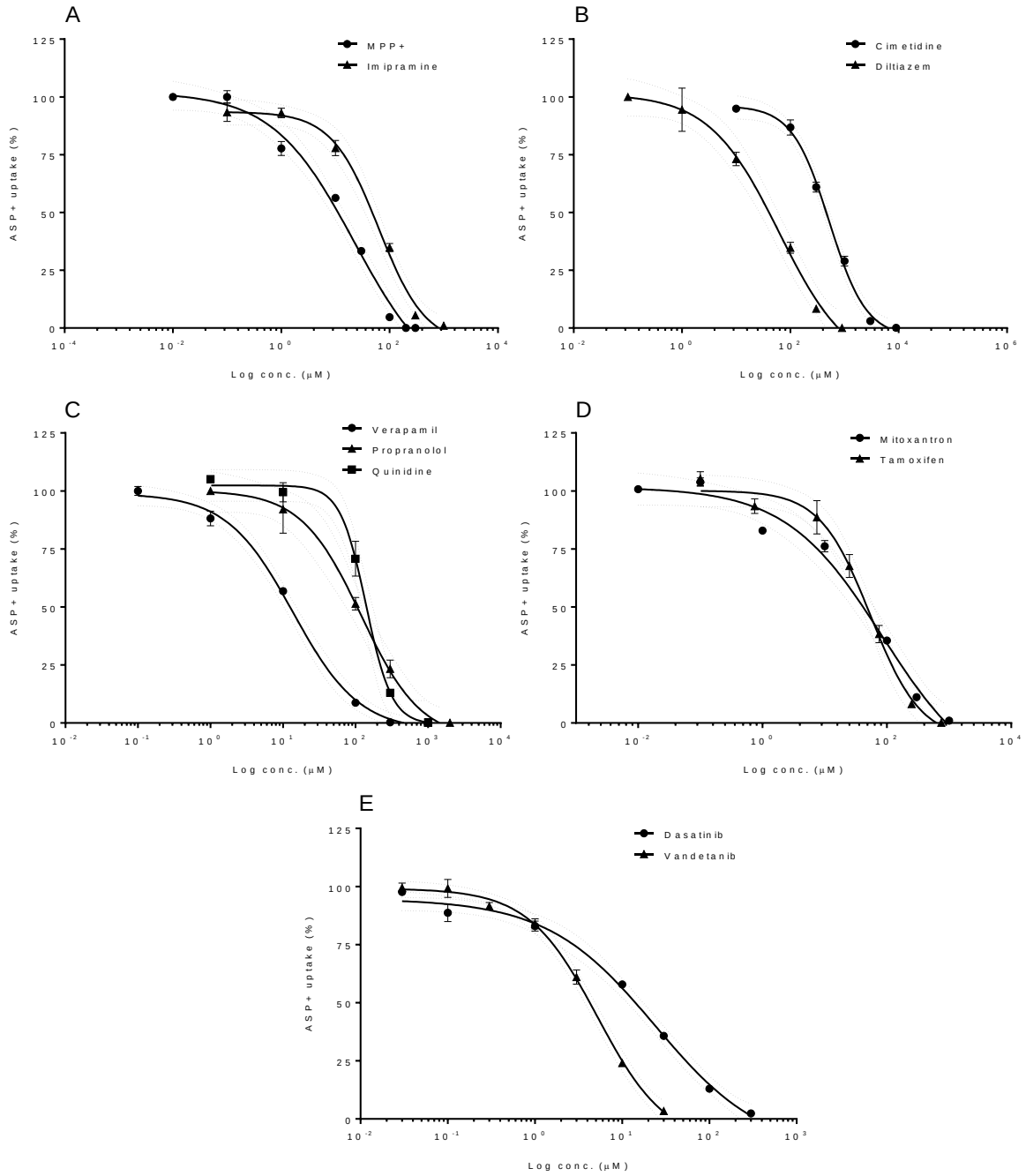

Figure 3.24. Concentration dependent inhibition of Oct1 mediated ASP+ uptake by: A) MPP+ and imipramine, B) cimetidine and diltiazem, C) verapamil, propranolol and quinidine, D) mitoxantrone and tamoxifen, E) dasatinib and vandetanib. Data are expressed as percentage (%) of ASP+ uptake over logarithm of interactor concentrations (µM) after 5 min of co-exposure. Each data point represents mean ± SD from triplicate determinations.

3.8.3. Interaction analysis with other fluorescent substrates

After the detailed interaction analysis of zebrafish Oct1 with ASP+ as model fluorescent substrate and a broad range of endo- and xenobiotic compounds, we performed additional interaction analyses with other identified fluorescent substrates and specific physiological compounds and xenobiotics that showed high interaction in previous analysis. The goal of additional interaction tests with other fluorescent dyes was to determine similarities and differences in inhibition constants in order to perform more detailed characterization of the Oct1 transport mechanism. We selected group of known interactors and performed the dose response assays with all five fluorescent substrates. The obtained inhibition constants were used in correlation test in order to elucidate the mode of interaction between tested group of interactors and model substrates, which would give more information about the possible presence of only one versus more active sites that are responsible for the interaction of Oct1 with fluorescent substrates and for the transport of these substrates, respectively.

The inhibition constants of fifteen chosen interactors with five fluorescent substrates are presented in Table 3.1. Comparing with ASP+, ethidium bromide (EtBr) inhibition tests resulted with K_i values for steroid hormones in similar range as with ASP+. Prazosin showed lower effect on EtBr uptake, with 4-fold higher K_i value of 4.01 µM. The inhibition assays with EtBr also revealed higher K_i values for diltiazem (K_i = 458 µM), acetylcholine (K_i = 2287 µM) and cimetidine (K_i = 3594 µM), whereas mitoxantrone and tetraethylammonium showed lower K_i values than with ASP+ (Table 3.1).

Berberine showed more similar interaction with tested compounds in comparison with ASP+. Inhibition constants for steroid hormones were in similar range as with ASP+ and EtBr. The difference can be seen in the interaction with mitoxantrone, which resulted with 10-fold higher K_i value than with EtBr and only 3-fold higher than with ASP+. On the other hand, acetylcholine inhibited berberine uptake with lower K_i value of 276.2 µM, which is 9-fold lower than with EtBr and less than 3-fold lower than with ASP+ (Table 3.1). It should be noted that quinidine and vandetanib did not affect the uptake of berberine by Oct1, which is indication of different interaction between these compounds and the active site of Oct1. The inhibition assays with DAPI revealed more different interactions than with previously tested substrates. Progesterone (K_i = 1225 µM) and β-estradiol (K_i = 954.6 µM) showed much lower interaction with DAPI (Table 3.1), whereas testosterone and androstenedione, together with prazosin and tetraethylammonium, did not have any effect on DAPI uptake by Oct1, which was another indication of difference in the interaction between DAPI and Oct1. The fifth fluorescent substrate, rhodamine 123 (Rh123), revealed higher interaction with all tested compounds, which in turn resulted with lower inhibition constants in comparison with other substrates. The interaction with steroid hormones resulted in K_i values in low micromolar range from 0.23 µM for androstenedione to

maximum of 1.66 µM for testosterone (Table 3.1). The other tested xenobiotics showed more potent Rh123 uptake inhibition, which resulted in calculated K_i values up to 20-fold lower than with other substrates (Table 3.1).

Table 3.1. Comparison of the inhibition constants (K_i) obtained for typical endo- and xenobiotic Oct1 interactors using five identified model fluorescent substrates.

	K_i (µM)				
Substrate	**ASP**	**EtBr**	**Rh123**	**Berberine**	**DAPI**
Corticosterone	16,53	4,56	1,25	9,55	4,40
Progesterone	1,99	1,25	0,25	5,30	1225,00
β-Estradiol	44.35	17,12	1,54	38,94	954,60
Testosterone	13.19	12,83	1,66	12,80	n.e.
Androsteniedione	5,13	3,60	0,23	6,40	n.e.
Prazosin	0.9	4,01	0,10	0,30	n.e.
Mitoxantrone	54,33	16,80	3,44	173,20	15,75
Quinidne	139,50	188,80	3,42	n.e.	292,00
Diltiazem	61,89	458,10	n.t.	105,50	24,00
Propranolol	119,40	266,80	n.t.	44,13	63,51
TEA	820,50	337,10	60,94	641,80	n.e.
Acetylcholine	710,80	2287,00	100,00	276,20	5586,00
Cimetidine	522.2	3594,00	15,00	414,40	1860,00
Dasatinib	29,10	28,60	1,36	11,80	n.t.
Vandetanib	3,74	7,70	0,40	n.e.	n.t.

Correlation analysis among the obtained K_i values of all five fluorescent substrates confirmed previous indications of differences in the interaction between Oct1 and the tested substrates. Analysis showed high level of correlation between K_i values of DAPI and Rh123 with correlation coefficient of 0.96, following with the correlation between ASP+ and berberine (r = 0.92) and the same r values of 0.82 for the correlation between ASP+ and Rh123 and DAPI. The other comparisons of K_i values resulted with lower correlation coefficients, with the lowest r value of 0.5 between EtBr and Rh123, indicating the differences in the interaction of these substrates and Oct1 (Table 3.2).

Table 3.2. Comparison of correlation coefficients among five model Oct1 fluorescent substrates for Ki set of typical Oct1 interactors presented in Table 3.1.

	ASP	**EtBr**	**Rh123**	**Berberine**	**DAPI**
ASP+	1	0,66	0,87	0,92	0,87
EtBr		1	0,50	0,55	0,64
Rh123			1	0,65	0,96
Berberine				1	0,55
DAPI					1

3.9. Determining the type of interaction

In order to determine the type of interaction with Oct1, we compared kinetic parameters of ASP+ uptake in the presence and in the absence of different interacting compounds, where their concentrations were equal to their previously calculated K_i values. If an interacting compound is a competitive inhibitor of ASP+ we can assume that it is being transported by Oct1, in which case the K_i value of the interacting compound actually represents its K_m value. The analysis was performed with identified fluorescent substrates, except with ethidium bromide due to overlapping of fluorescence emission wavelengths. All tested fluorescent dyes were confirmed as competitive inhibitors of Oct1 ASP+ transport, thus confirming to be the substrates of Oct1 (Table 3.3). Interaction analysis was also performed with physiological compounds and xenobiotics that showed potent inhibitory effect on the uptake of ASP+. Obtained kinetic constants of ASP+ uptake showed competitive inhibition of Oct1 by corticosterone, whereas uncompetitive inhibition was reported for 19-methlytestosterone (Fig. 3.25B), tetrapentylammonium and tripropyltin chloride (Table 3.3). The rest of tested compounds showed mixed type of inhibition, which resulted in changes in both K_m and V_m values of the ASP+ kinetics (Table 3.3, Fig. 3.25C and D). The interaction with steroid hormones – progesterone, androstenedione and β-estradiol – caused the increase of K_m value together with lowering of the V_m value of the ASP+ uptake. Tetrabutylammonium had different effect on the ASP+ kinetic constants, with drastic decrease of ASP+ affinity, together with elevation of V_m, which indicated that TBA could have specific effect on ASP+ active site on Oct1 and cause the activation of ASP+ transport. Interaction with tributyltin chloride showed opposite results. TBT affected the ASP+ kinetics through elevation of Oct1 affinity for ASP+ and drastic decrease in V_m (Table 3.3).

Table 3.3. Determination of type of interaction for set of zebrafish Oct1 interactors. Kinetic parameters of ASP+ uptake are given as K_m (μM), V_m (pmol ASP+/mg protein/min), and 95% confidence intervals (c.i.) for each. The mark "I" denotes inhibitors, the "S" denotes Oct1 substrates and the ''M'' denotes mixed type of inhibition. Data are mean ± SD from triplicate determinations.

Interactor	K_m (ASP+)	c.i.	V_m (ASP+)	c.i.	Type of interaction
Control	23	17 -29	568,1	507 - 628	
Rhodamine 123	34,55	24 - 45	645,7	547 - 744	S
Berberine	30,17	18 - 42	461,2	377 - 546	S
DAPI	53,86	36 - 71	715,6	580 - 851	S
Progesterone	37,38	19 - 56	379,8	285 - 475	M
Andorstenedione	35,08	21 - 48	341,1	276 - 406	M
Corticosterone	49,96	34 - 66	435,1	356 - 514	S
β-Estradiol	34,36	23 - 46	289,8	241 - 338	M
19-methyltestosterone	24,67	14 - 35	286,9	236 - 337	I
Tetrabutylammonium	101,8	68 - 135	1002	770 - 1233	M
Tetrapentylammonium	31,18	16 - 47	342,5	258 - 427	I
Tributyltin chloride	7,69	5,6 - 9,7	92,16	85 - 98	M
Tripropyltin chloride	21,6	16 - 27	67,41	61 - 74	I

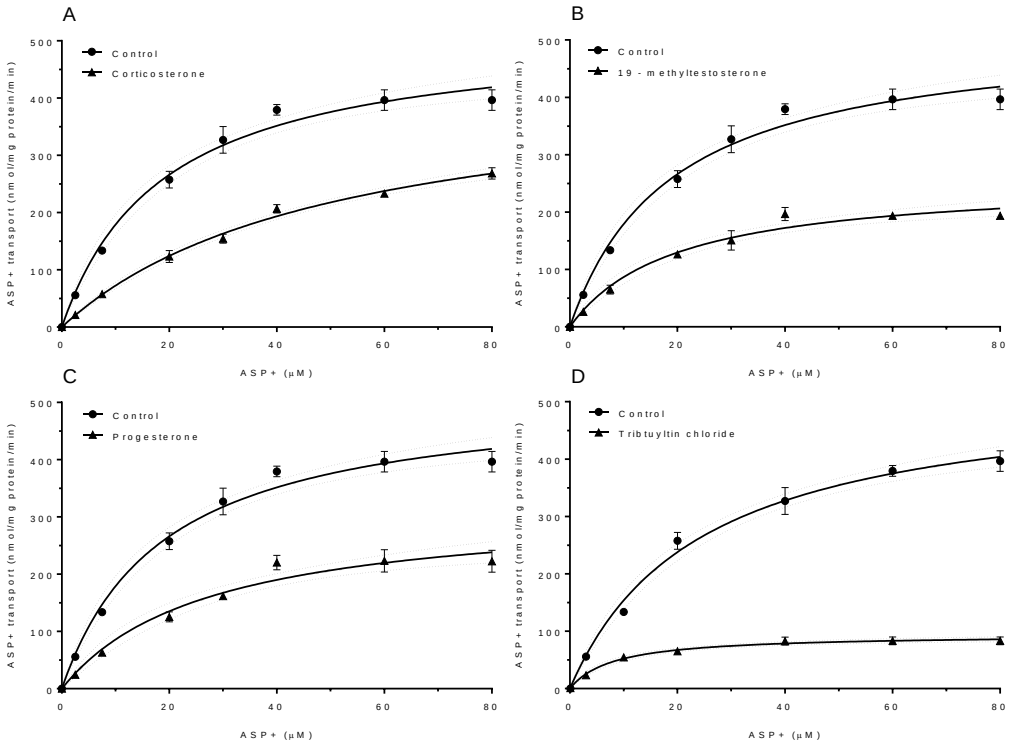

Figure 3.25. Example of dose-response curves used to determine type of interaction with Oct1. A) corticosterone as competitive inhibitor, B) 19-methyltestosterone as uncompetitive inhibitor, C) progesterone showing mixed type of inhibition, D) tributyltin chloride showing mixed type of inhibition.

3.10. Functional characterization of human OCT1 and OCT2

For further characterization of zebrafish Oct1, we performed functional characterization of human organic cation transporters 1 and 2 (OCT1 and 2) in HEK293 heterologous expression system. Our goal was to compare transport kinetics with novel fluorescent substrates of zebrafish Oct1 and interactions with compounds that showed to be potent interactors of zebrafish Oct1. The results of these comparisons are then used for characterization of the active site of zebrafish Oct1 and to elucidate transport mechanism and type of interaction in further studies, based on homology modeling and molecular docking experiments.

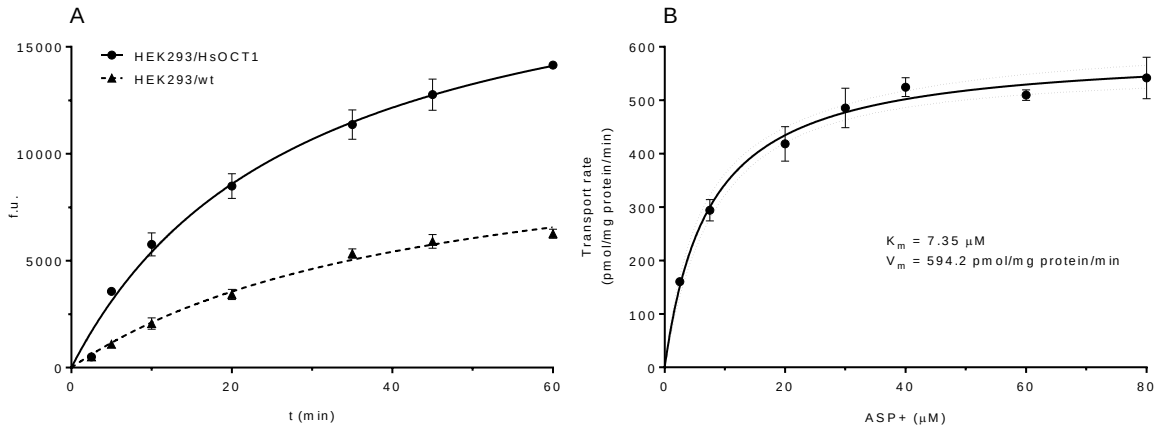

Figure 3.26. Michaelis-Menten kinetics of human OCT1 mediated uptake of fluorescent dye ASP+. A) Time dependent uptake of ASP+ by HEK293 cell overexpressing OCT1 and by wild type HEK293 cells. ASP+ accumulation is expressed as increase in fluorescence (fluorescence units – f.u.) over time (min). B) Dose-response of OCT1 ASP+ uptake expressed as transport rate (pmol/mg protein/min) over ASP+ concentration (µM) after 10 min incubation with ASP+.

The uptake assays with fluorescent dyes revealed some crucial differences between human and zebrafish OCTs/Octs. Initial uptake screen of fluorescent substrates revealed that human OCT1 transported all fluorescent substrates, previously reported in the characterization of zebrafish Oct1, with highest affinities and transport rates for ASP+ and Rh123 (Figs. 3.9 and 3.10). Human OCT1 transported ASP+ with affinity of 7.35 µM and V_m of 594.2 pmol/mg protein/min which was lower than reported V_m value of zebrafish Oct1 (Figs. 3.26 and 3.27). Rh123 was transported by human OCT1 with even higher affinity than ASP+ (K_m = 167.3 nM), which was in the same range as reported Rh123 affinity of zebrafish Oct1 (Fig. 3.10). However, the uptake screen of potential fluorescent substrates showed that human OCT2 does not transport ASP+ and berberine. The uptake screen was positive for the transport of DAPI and EtBr, together with Rh123 as the most potent fluorescent human Oct2 substrate.

Human OCT2 transported Rh123 with low K_m value of 1.56 µM, which was nearly 10-fold higher than Rh123 affinities of human OCT1 and zebrafish Oct1. However, human OCT2 transported Rh123 much faster than other human and zebrafish orthologs, with V_m value of 1349 pmol/mg protein/min (Fig. 3.28).

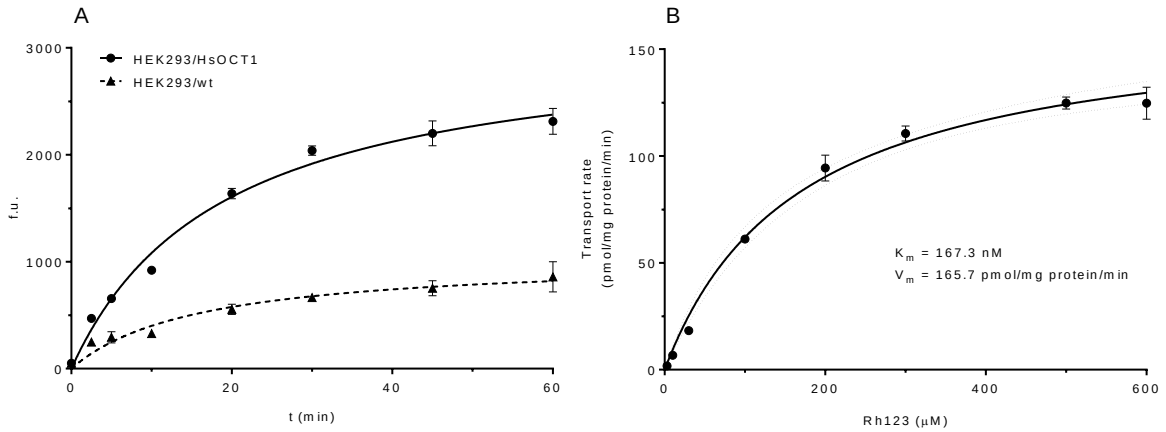

Figure 3.27. Michaelis-Menten kinetics of human OCT1 mediated uptake of fluorescent dye Rh123. A) Time dependent uptake of Rh123 by HEK293 cell overexpressing OCT1 and by wild type HEK293 cells. Rh123 accumulation is expressed as increase in fluorescence (fluorescence units – f.u.) over time (min). B) Dose-response of OCT1 Rh123 uptake expressed as transport rate (pmol/mg protein/min) over Rh123 concentration (µM) after 15 min incubation with Rh123.

Since Rh123 showed to be a potent substrate of both human OCT orthologs and zebrafish Oct1, we proceeded with the functional characterization and human vs. zebrafish comparisons based on the results obtained with Rh123 as model substrate. The dose-response assays showed the differences in Rh123 uptake inhibition between investigated transporters, which emphasized potential differences in the active sites and transport dynamics of observed OCTs/Octs. The graphical representation of interaction differences among human OCTs can be seen in Figure 3.29.

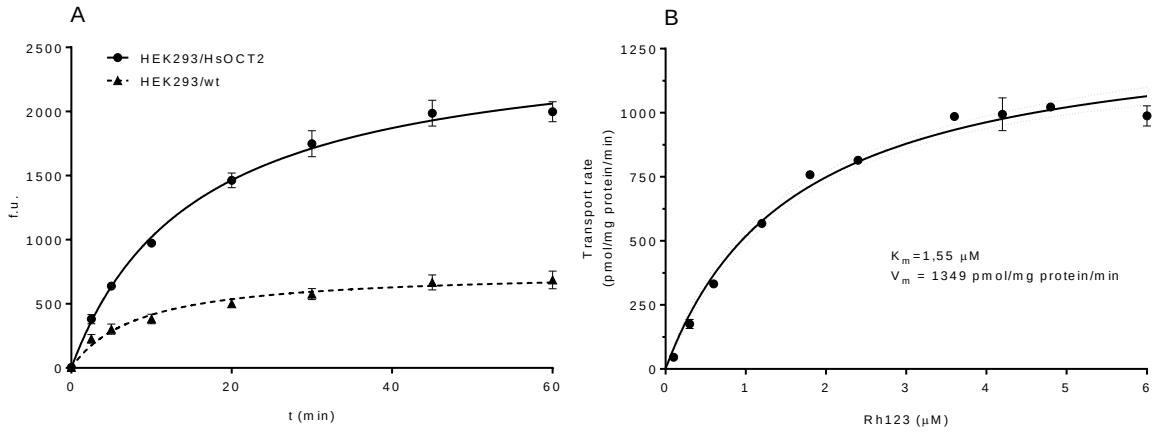

Figure 3.28. Michaelis-Menten kinetics of human OCT2 mediated uptake of fluorescent dye Rh123. A) Time dependent uptake of Rh123 by HEK293 cell overexpressing OCT2 and by wild type HEK293 cells. Rh123 accumulation is expressed as increase in fluorescence (fluorescence units – f.u.) over time (min). B) Dose-response of OCT2 Rh123 uptake expressed as transport rate (pmol/mg protein/min) over Rh123 concentration (µM) after 15 min incubation with Rh123.

Most of the analyzed steroid hormones showed similar interaction pattern in the comparison of human and zebrafish OCTs/Octs. Corticosterone, progesterone, testosterone, androstenedione and 19-methyltestosterone inhibited Rh123 uptake by hOCT2 and drOct1 in similar low micromolar range, opposing the higher K_i values obtained with hOCT1, which were in higher micromolar range and in some cases almost 400-fold higher than K_i values of hOCT2 (Table 3.4). The exceptions were reported for β-estradiol, which inhibited human OCT1 and OCT2 with similar K_i values of 6.06 µM and 5.98 µM, respectively, whereas K_i value of drOct1 was 1.54 µM (Table 3.4). Another exception was observed for dihydrotestosterone, which was the only steroid hormone that showed the highest inhibition of Rh123 uptake by hOCT1, with K_i value of 0.58 µM, whereas drOct1 and hOCT2 inhibition constants for dihydrotestosterone were 5.3 µM and 7.08 µM, respectively (Table 3.4). Prazosin and mitoxantrone showed the highest Rh123 uptake inhibition with drOct1, whereas these compounds inhibited human OCTs in higher range (Table 3.4). Quaternary ammonium cations showed similar pattern as steroid hormones, with lower inhibition constants with drOct1 and hOCT2 (Table 3.4). Tetraethylammonium inhibited hOCT1 with high K_i value of 633.9 µM, whereas the K_i values with drOct1 and hOCT2 were 10-fold and 20-fold lower, respectively. Dibutyltin chloride showed to be most potent inhibitor of drOct1 with K_i value of 1.9 µM, following with inhibition of hOCT2 (K_i = 4.6) and hOCT1 (K_i = 343 µM), whereas tributyltin chloride showed the highest inhibition of hOCT2 with *Ki* value of 0.47 µM, following with the inhibition of hOCT1 (K_i = 1.64 µM) and drOct1 (K_i = 6.37 µM).

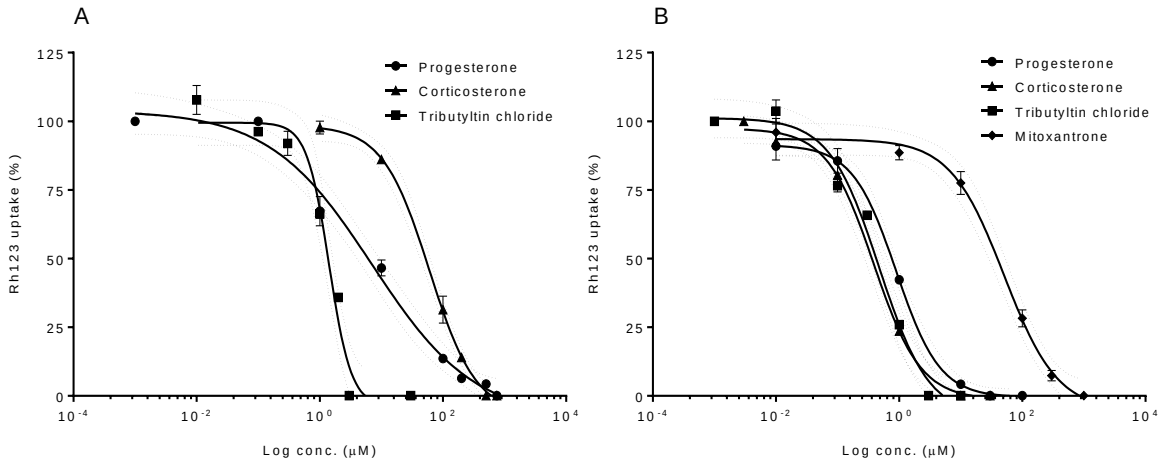

Figure 3.29. Progesterone, corticosterone and tributyltin chloride concentration dependent inhibition of: A) human OCT1 mediated Rh123 uptake, B) human OCT2 mediated Rh123 uptake. Data are expressed as percentage (%) of Rh123 uptake over logarithm of interactor concentrations (µM) after 15 min of co-exposure. Each data point represents mean ± SD from triplicate determinations.

Table 3.4. Comparison of inhibition constants (K_i) of Rh123 uptake for zebrafish Oct1 and human OCT1 and 2.

	Rh123 Ki (µM)		
	drOct1	**hOCT1**	**hOCT2**
Corticosterone	1,25	60,1	0,15
Progesterone	0,25	7,14	0,9
Testosterone	1,66	42,04	0,61
Androstenedione	0,23	23,15	0,14
β-Estradiol	1,54	6,06	5,98
19-methyltestosterone	2,1	11,2	0,11
Dihydrotestosterone	5,3	0,58	7,08
Acethylcholine	93,53	n.t.	14,12
Prazosine	0,1	7	11,95
Mitoxantrone	3,44	71,5	50,43
Tetraethylammonium	60,94	633,9	31,66
Tetrabutylammonium	2,01	46,6	4,28
Tetrapentylammonium	0,68	24,7	2,85
Dibutyltin chloride	1,9	343	4,6
Tributyltin chloride	6,37	1,64	0,47

3.11. *In silico* analysis of zebrafish Oct1 structure and active site

3.11.1. Homology modeling

Further characterization of zebrafish Oct1 transport mechanism and elucidation of types of interactions between the transporter and tested compounds, required more detailed investigation of protein structure, especially the structure of the active site(s) of the transporter. Since there are no known crystal structures of eukaryotic Octs, we performed the homology modeling in order to acquire 3D representation of zebrafish Oct1 and human OCT1 and 2, in order to compare their structures and determine the similarities and differences responsible for the determined differences in interaction of these three transporters with tested compounds. Modeling was performed using the tertiary structure of LacY (PDB entry 1PV6) from *E. coli.* The obtained 3D protein model offered new insight in the structure of analyzed transporters and their active sites, pinpointing the crucial amino acid residues in the active site cleft.

All three modeled proteins revealed their characteristic spatial organizations, showing tertiary structure with dominating α-helices. The model showed that OCTs/Octs were consisted of 12 transmembrane helices that formed active site cleft of the transporters (Fig. 3.30). We identified crucial amino acid residues inside the active site cleft, that were previously confirmed to interact with OCT/Oct substrates in the active site. Identified sterically accessible amino acids Phe161, Trp219, Tyr223, Thr227, Arg440, Ile443, Phe447, Gln448 and Asp475 in the active site cleft of drOct1, and their homologous counterparts on hOCT1 and 2, were used for determination of docking sphere that will be used for analysis of molecular docking of identified fluorescent substrates and potent interactors.

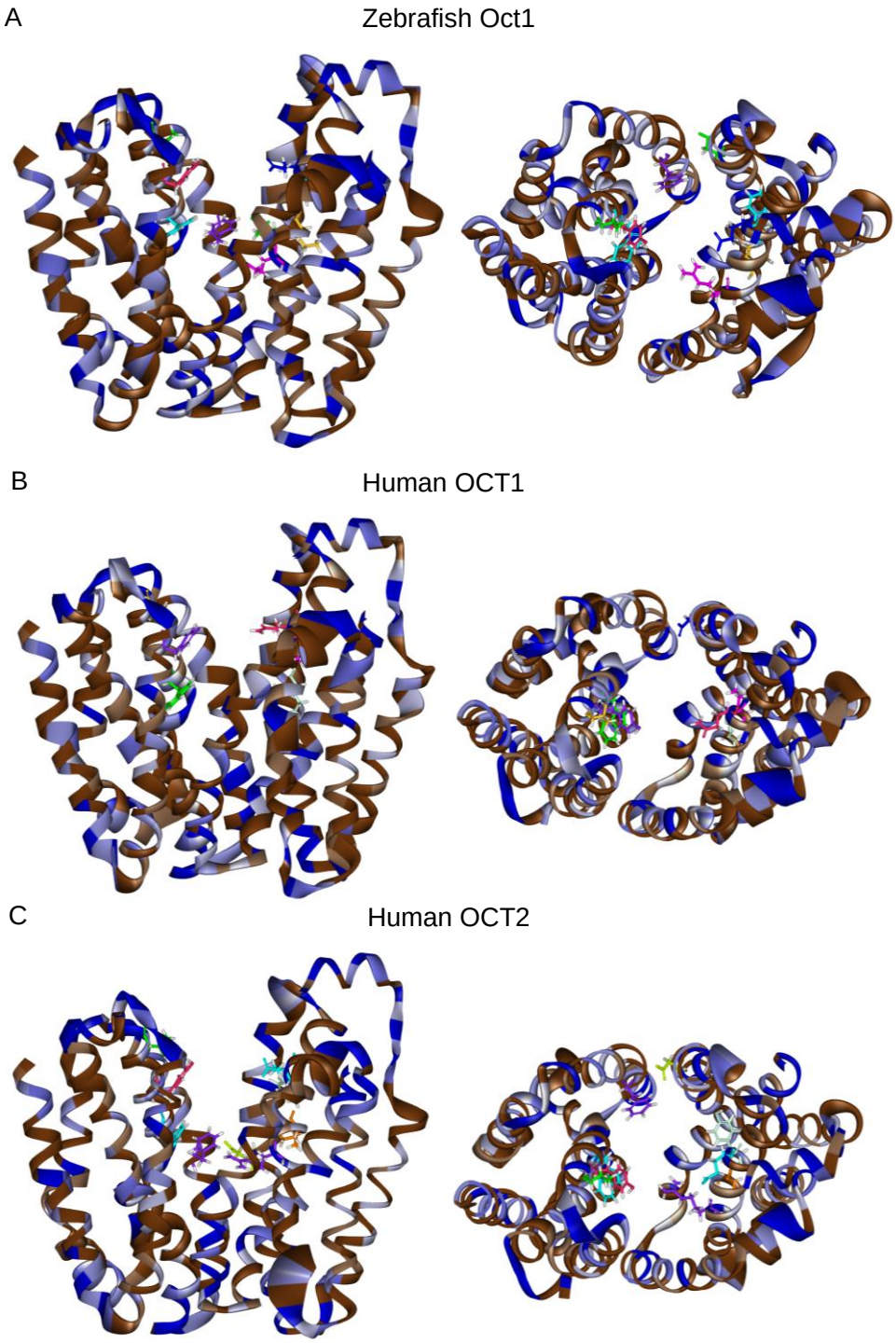

Figure 3.30. Structure models of: A) zebrafish Oct1, B) human OCT1, C) human OCT2 with amino acids that are crucial for substrate affinity.

3.11.2. Molecular docking

Determined OCT/Oct models were used as basis for molecular docking, in order to determine all potential amino acid residues that interact with identified fluorescent substrates and other interactors. As it can be seen on the resulting secondary structure, OCTs/Octs have one large extracellular loop between TMH1 and 2. However, in molecular docking analysis this loop sterically blocked the entrance of investigated interactors into the active site cleft of the proteins. In order to avoid this obstacle in the extracellular loop, we modified the model and removed the loop, which made active site cleft more accessible for docking analysis. Importantly, the removal of the extracellular loop did not change the tertiary structure of the protein and organization of twelve transmembrane helices and active site cleft remained unaffected by the described model modification. We analyzed molecular docking of all five fluorescent substrates and five potent interactors which strongly inhibited the uptake of the substrates by OCTs/Octs. We tested two members of steroid hormones, androstenedione and corticosterone, two members of potent xenobiotic interactors, prazosin and tributyltin chloride and MPP+ as previously identified model substrate of mammalian OCTs/Octs (Table 3.8 – 3.10). The results of molecular docking of five fluorescent substrates and endo- and xenobiotic interactors on zebrafish Oct1 and human OCT1 and 2 are presented on Table 3.4 – 3.7. These results represent amino acid residues that are crucial for the interaction of active site of examined proteins with fluorescent substrates. The identified interactions among crucial amino acid residues and examined substrates ranged from H-bond interactions, where amino acids in the active site acted both as donors and acceptors of hydrogen atom, to aromatic π-π interactions. The majority of amino acids in the active site were identified as residues in the close vicinity of docked interactor, indicating possible non-polar steric interactions.

Table 3.5. Molecular docking results for zebrafish Oct1 with five fluorescent substrates in 1 – 3 analyzed docking positions. The ''D'' represents amino acid residues that are donors of hydrogen in H-bond, the ''A'' represents an acceptor of hydrogen in H-bond, the ''π-π'' represents aromatic interactions between amino acid residues and tested substrate. Close residues represent amino acids in the close proximity of docked substrate.

Zebrafish Oct1		
Ligand	Interactions	
ASP+ (two poses)	D) none A) none π-π) Trp355 Close residues) Phe161, Ser165, Ile166, Met220, Trp355, Arg440, Ile443, Thr444, Gly466, Val467, Cys470, Ser471	D) none A) none π-π) none Close residues) Tyr36, Phe161, Val215, Lys216, Trp219, Met220, Gly466, Cys470, Ser471
Berberine (one pose)	D) Trp219 A) none π-π) none Close residues) Phe161, Trp219, Met220, Tyr223, Val240, Gln243, Leu351, Trp355, Phe407, Ile443, Thr444, Phe447, Cys470	
DAPI (two poses)	D) Thr444, A) Phe161, Glu448 π-π) none Close residues) Phe161, Leu162, Ser165, Ile166, Trp355, Ile443, Thr444, Phe447, Glu448, Cys470, Ser471	D) none A) none π-π) none Close residues) Phe161, Leu162, Ser165, Ile166, Trp219, Met220, Tyr223, Trp355, Cys470, Ser471
EtBr (one pose)	D) none A) none π-π) Trp355, Arg440, Phe447 Close residues) Phe161, Leu351, Trp355, Phe407, Gly439, Arg440, Ile443, Thr444, Phe447, Cys470	
Rh123 (one pose)	D) none A) none π-π) none Close residues) Phe161, Lys216, Trp219, Met220, Tyr223, Trp355, Ile443, Thr444, Cys470, Ser471	

Table 3.6. Molecular docking results for human OCT1 with five fluorescent substrates in 1 – 3 analyzed docking positions. The ''D'' represents amino acid residues that are donors of hydrogen in H-bond, the ''A'' represents an acceptor of hydrogen in H-bond, the ''π-π'' represents aromatic interactions between amino acid residues and tested substrate. Close residues represent amino acids in the close proximity of docked substrate.

Human OCT1			
Ligand	Interactions		
ASP+ **(one pose)**	D) none A) none π-π) Trp354 Close residues) Leu164, Met218, Leu350, Ile442, Thr443, Ile446, Gly465, Val466, Cys469, Ser470		
Berberine **(one pose)**	D) none A) none π-π) none Close residues) Phe159, Leu164, Met218, Trp354, Ile442, Thr443, Ile446, Gln447, Arg462, Gly465, Val466, Cys469, Ser470		
DAPI **(3 poses)**	D) none A) Ser163, Leu164 π-π) none Close residues) Ser163, Leu164, Gly167, Tyr168, Met218, Arg346, Ile446, Gln447, Cys450, Val461, Arg462, Gly465, Cys469	D) none A) Ser163, Leu164, Gln447, Cys450, π-π) none Close residues) Ser163, Leu164, Gly167, Tyr168, Met218, Arg346, Ile446, Gln447, Cys450, Val461, Gly465, Val466, Cys469	D) none A) Thr443 π-π) Trp354 Close residues) Phe159, Leu164, Met218, Leu350, Trp354, Ile442, Thr443, Ile446, Gly465, Val466, Cys469, Ser470
EtBr **(one pose)**	D) none A) none π-π) none Close residues) Phe159, Leu164, Met218, Trp354, Ile442, Thr443, Ile446, Gln447, Cys450, Gly465, Cys469, Ser470		
Rh123 **(one pose)**	D) Ser470 A) Thr443 π-π) none Close residues) Phe159, Lys214, Trp217, Tyr221, Met218, Trp354, Thr443, Ile446, Gln447, Gly465, Cys469, Ser470		

Table 3.7. Molecular docking results for human OCT2 with five fluorescent substrates in 1 – 3 analyzed docking positions. The ''D'' represents amino acid residues that are donors of hydrogen in H-bond, the ''A'' represents an acceptor of hydrogen in H-bond, the ''π-π'' represents aromatic interactions between amino acid residues and tested substrate. Close residues represent amino acids in the close proximity of docked substrate.

Human OCT2			
Ligand	Interactions		
ASP+ (3 poses)	D) none A) none π-π) Trp355, Tyr447 Close residues) Phe160, Ser164, Met165, Leu219, Leu351, Trp355, Ile443, Thr444, Tyr447, Gly466, Val467, Cys470, Ser471	D) none A) none π-π) none Close residues) Tyr37, Phe160, Ser214, Lys215, Trp218, Leu219, Arg440, Tyr447, Gly466, Cys470	D) none A) none π-π) none Close residues) Tyr37, Phe160, Ser214, Lys215, Trp218, Leu219, Arg440, Tyr447, Gly466, Cys470
Berberine (3 poses)	D) none A) none π-π) Tyr447 Close residues) Phe160, Met165, Leu219, Trp355, Ile443, Thr444, Tyr447, Arg463, Gly466, Val467, Cys470, Ser471	D) none A) none π-π) none Close residues) Tyr37, Phe160, Ser214, Lys215, Trp218, Leu219, Trp355, Ile443, Thr444, Met445, Tyr447	D) none A) none π-π) none Close residues) Tyr37, Phe160, Lys215, Trp218, Leu219, Trp355, Thr444, Met445, Tyr447, Glu448, Cys470
DAPI (3 poses)	D) none A) Glu448 π-π) none Close residues) Phe160, Phe161, Ser164, Met165, Leu219, Trp355, Thr444, Met445, Tyr447, Glu448, Cys470, Ser471, Asp475	D) none A) Thr444, Glu448, Ser471, π-π) none Close residues) Phe160, Ser164, Met165, Leu219, Trp355, Thr444, Met445, Tyr447, Glu448, Cys470, Ser471	D) none A) Thr444, Glu448, Ser471 π-π) none Close residues) Phe160, Phe161, Ser164, Met165, Leu219, Trp355, Thr444, Met445, Tyr447, Glu448, Cys470, Ser471
EtBr (2 poses)	D) none A) none π-π) Phe160, Tyr447 Close residues) Phe160, Trp218, Leu219, Tyr222, Leu351, Trp355, Ile443, Thr444, Tyr447, Glu448, Cys470	D) none A) none π-π) Phe160 Close residues) Tyr37, Phe160, Tyr447, Lys215, Trp218, Leu219, Tyr222, Trp355, Cys470	
Rh123 (2 poses)	D) none A) Ser214 π-π) Lys215, Trp218, Arg440 Close residues) Tyr37, Phe160, Ser214, Lys215, Trp218, Leu219, Tyr222, Ile223, Trp355, Arg440, Thr444	D) none A) Ser214, Trp218 π-π) Lys215, Trp218 Close residues) Tyr37, Phe160, Ser214, Lys215, Trp218, Leu219, Tyr222, Trp355, Arg440, Thr444, Tyr447, Cys470	

Table 3.8. Molecular docking results for zebrafish Oct1 with five endo- and xenobiotic interactors in 1 – 3 analyzed docking positions. The ''D'' represents amino acid residues that are donors of hydrogen in H-bond, the ''A'' represents an acceptor of hydrogen in H-bond, the ''π-π'' represents aromatic interactions between amino acid residues and tested interactor. Close residues represent amino acids in the close proximity of docked interactor.

Zebrafish Oct1			
Ligand	Interactions		
Androstenedione (2 poses)	D) none A) none π-π) none Close residues) Phe161, Trp219, Leu351, Trp355, Phe407, Arg440, Ile443, Thr444, Phe447, Glu448, Cys470	D) none A) none π-π) none Close residues) Phe161, Trp219, Leu351, Trp355, Arg440, Ile443, Thr444, Phe447, Glu448, Cys470	
Corticosterone (3 poses)	D) none A) none π-π) none Close residues) Phe161, Leu351, Trp355, Arg440, Ile443, Thr444, Phe447, Glu448, Val451, Leu465, Gly466, Cys470	D) none A) none π-π) none Close residues) Phe161, Ser165, Ile166, Trp219, Met220, Trp355, Ile443, Thr444, Phe447, Glu448, Val467, Cys470, Ser471	D) none A) none π-π) none Close residues) Phe161, Ser165, Trp219, Met220, Leu351, Trp355, Phe407, Arg440, Ile443, Thr444, Phe447, Glu448, Cys470
MPP+ (one pose)	D) none A) none π-π) none Close residues) Phe161, Ile443, Thr444, Phe447, Glu448, Gly466, Val467, Cys470, Ser471		
Prazosine (2 poses)	D) none A) none π-π) Tyr170 Close residues) Phe161, Ser165, Ile166, Gly169, Tyr170, Met220, Trp355, Arg440, Ile443, Thr444, Phe447, Glu448, Val467, Cys470, Ser471	D) Arg440, Ser471 A) none π-π) Tyr36, Trp219 Close residues) Tyr36, Phe161, Leu162, Ser165, Ile166, Trp219, Trp355, Arg440, Ile443, Phe447, Glu448, Gly466, Val467, Cys470, Ser471, Asp475	
Tributyltin (3 poses)	D) none A) none π-π) none Close residues) Phe161, Lys216, Trp219, Met220, Tyr223, Trp355, Cys470, Ser471	D) none A) none π-π) none Close residues) Phe161, Lys216, Trp219, Met220, Tyr223, Trp355, Cys470, Ser471	D) none A) none π-π) none Close residues) Tyr36, Phe161, Val215, Lys216, Trp219, Met220, Tyr223, Trp355, Arg440, Cys470, Ser471

Table 3.9. Molecular docking results for human OCT1 with five endo- and xenobiotic interactors in 1 – 3 analyzed docking positions. The ''D'' represents amino acid residues that are donors of hydrogen in H-bond, the ''A'' represents an acceptor of hydrogen in H-bond, the ''π-π'' represents aromatic interactions between amino acid residues and tested interactor. Close residues represent amino acids in the close proximity of docked interactor.

Human OCT1			
Ligand	Interactions		
Androstenedione **(one pose)**	D) none A) none π-π) none Close residues) Met218, Trp354, Arg439, Ile442, Thr443, Ile446, Gln447, Cys469		
Corticosterone **(one pose)**	D) Arg439 A) none π-π) none Close residues) Met218, Leu350, Trp354, Arg439, Ile442, Thr443, Ile446, Gln447, Cys450, Gly465, Cys469,		
MPP+ **(one pose)**	D) none A) none π-π) none Close residues) Leu164, Met218, Trp354, Ile442, Ile446, Gln447, Gly465, Val466, Cys469, Ser470		
Prazosine **(2 poses)**	D) none A) none π-π) none Close residues) Phe159, Lys214, Trp217, Met218, Tyr221, Trp354, Ile446, Gln447, Cys450, Val461, Gly465, Cys469, Ser470	D) none A) none π-π) none Close residues) Phe159, Lys214, Trp217, Met218, Tyr221, Trp354, Ile446, Gln447, Cys450, Val461, Leu464, Gly465, Cys469, Asp474	
Tributyltin **(3 poses)**	D) none A) none π-π) none Close residues) Phe159, Leu164, Lys214, Trp217, Met218, Trp354, Ile442, Thr443, Ile446, Gln447, Gly465, Val466, Cys469, Ser470	D) none A) none π-π) none Close residues) Phe159, Leu164, Met218, Leu350, Trp354, Ile442, Thr443, Ile446, Gln447, Cys450, Val461, Gly465, Cys469, Ser470, Asp474	D) none A) none π-π) none Close residues) Phe159, Leu164, Lys214, Trp217, Met218, Trp354, Ile442, Ile446, Gln447, Gly465, Cys469, Ser470, Asp474

Table 3.10. Molecular docking results for human OCT2 with five endo- and xenobiotic interactors in 1 – 3 analyzed docking positions. The ''D'' represents amino acid residues that are donors of hydrogen in H-bond, the ''A'' represents an acceptor of hydrogen in H-bond, the ''π-π'' represents aromatic interactions between amino acid residues and tested interactor. Close residues represent amino acids in the close proximity of docked interactor.

Human OCT2			
Ligand	Interactions		
Androstenedione (one pose)	D) none A) none π-π) none Close residues) Tyr37, Phe160, Lys215, Trp218, Leu219, Tyr222, Trp355, Arg440, Tyr447, Glu448		
Corticosterone (3 poses)	D) Lys215 A) none π-π) none Close residues) Phe160, Lys215, Trp218, Leu219, Trp355, Arg440, Ile443, Thr444, Tyr447, Glu448, Cys470	D) Lys215, Arg440 A) Tyr37 π-π) Close residues) Tyr37, Phe160, Lys215, Trp218, Leu219, Tyr222, Trp355, Arg440, Thr444, Tyr447, Cys470	D) Lys215, Arg440 A) Tyr37 π-π) Close residues) Tyr37, Phe160, Lys215, Trp218, Leu219, Tyr222, Trp355, Arg440, Ile443, Thr444, Tyr447, Cys470
MPP+ (3 poses)	D) none A) none π-π) Tyr447 Close residues) Phe160, Tyr222, Trp355, Ile443, Thr444, Met445, Tyr447, Glu448, Cys470	D) none A) none π-π) none Close residues) Phe160, Trp355, Ile443, Thr444, Tyr447, Glu448, Gly466, Cys470, Ser471, Asp475	D) none A) none π-π) Tyr447 Close residues) Phe160, Trp355, Ile443, Thr444, Tyr447, Glu448, Gly466, Cys470, Ser471, Asp475,
Prazosine (2 poses)	D) Lys215 A) none π-π) Phe160 Close residues) Tyr37, Phe160, Ser164, Met165, Ser214, Lys215, Trp218, Leu219, Tyr222, Trp355, Tyr447, Cys470, Ser471, Asp475	D) Lys215 A) none π-π) Phe160 Close residues) Tyr37, Phe160, Ser214, Lys215, Trp218, Leu219, Tyr222, Trp355, Glu448, Asp475	
Tributyltin (3 poses)	D) none A) none π-π) none Close residues) Tyr37, Phe160, Lys215, Trp218, Leu219, Tyr222, Trp355, Arg440, Ile443, Thr444, Tyr447	D) none A) none π-π) none Close residues) Tyr37, Phe160, Ser214, Lys215, Trp218, Leu219, Tyr222, Ile223, Trp355, Arg440, Tyr447, Cys470	D) none A) none π-π) none Close residues) Phe160, Ser164, Met165, Trp218, Leu219, Leu351, Trp355, Arg440, Ile443, Thr444, Tyr447, Glu448, Gly466, Cys470, Ser471, Asp475

4. Discussion

This study represents the first functional characterization of organic cation transporters from Slc22 family in fish. The obtained knowledge on zebrafish organic cation transporters will provide new insight into important roles of Octs related crucial physiological, defensive and pathological functions in zebrafish, which could be positively correlated with OCT/Oct functions in higher vertebrates and human. Such direct correlation of the obtained knowledge from zebrafish to human requires the accurate assignment of gene orthologies. Previous studies identified two zebrafish *Oct* genes, *Oct1*, annotated as *Slc22a2*, and *Oct2*, annotated as *Slc22a3* (Popovic, 2014). Comparing with other vertebrate species, the occurrence of three *OCT/Oct* members starts with reptiles. In *X. laevis* and *T. rubripes* only one Oct ortholog was identified, and two *Oct* members were found in *G. morhua*, *T. nigroviridis*, and *G. aculeatus*, apart from zebrafish. Surprisingly, *O. latipes* and *C. intestinalis* showed the lack of *Oct* genes in their genomes (Popovic, 2014). Two identified zebrafish *Oct* genes clustered more closely together with *Oct* members of other fish species, *T. nigroviridis* and *G. aculeatus*, within a larger cluster which includes *OCT1/Oct1* and *OCT2/Oct2* members of other vertebrate species, including the human members. However, zebrafish *Oct2* showed closer phylogenetic relations with vertebrate *OCT3/Oct3* genes. The separation of *OCT3/Oct3* was determined in phylogenetic analyses of other vertebrate species, indicating that zebrafish *Oct2* may be more orthologically related to members of *OCT3/Oct3* (Wu *et al*., 2009; Popovic, 2014).

Based on the obtained phylogenetic data, it was not possible to reliably determine direct orthologies between human and zebrafish *OCT/Oct* genes, especially in case of relationship between human *OCT1* and *OCT2* and zebrafish *Oct1* and *Oct2*, which clustered together with *Oct1* and *Oct2* members of other vertebrates, disabling confident determination of direct phylogenetic relations between zebrafish *Oct1* and human *OCT1* or *OCT2* (Fig. 3.1). Additional uncertainties in the assignment of direct OCT/Oct orthologs by phylogenetic analysis were present due to teleost genome duplication (TGD), for which it is confirmed that can cause errors in phylogenetic determinations of direct gene orthologies (Catchen *et al*., 2011). After the whole genome duplication of teleost species, further evolutionary processes caused more complex orthological relations among zebrafish and higher vertebrate genes. It was shown that only 25% of duplicated zebrafish genes survived these evolutionary processes (Ravi and Venkatesh, 2008). Reciprocal gene loss (RGL) is also confirmed among fish species, making it more difficult to determine orthological relationships (Semon and Wolfe, 2007). Additionally, reported rapid and asymmetric evolution of duplicated genes contribute to complex phylogenetic relations between fish and higher vertebrate genes, which requires more detailed investigation of zebrafish gene orthologies (Steinke *et al*., 2006). Conserved synteny analysis provided more detailed insight in orthological relations between *OCT/Oct* genes. Previous research by Eraly *et al*. (2003) and Wu *et al*. (2009) revealed the tendency of *SLC22/Slc22* to form clusters of similar genes, consecutively localized

on the same chromosome. Reported clustering of *SLC22/Slc22* genes with similar functional properties and tissue expressions points to potential coordinated regulation of genes within the cluster (Tirona, 2011; Nigam, 2015). Synteny analysis of human, *T. nigroviridis* and stickleback genes revealed clustered organization of *OCT/Oct* genes (Fig. 3.2). Contrary to determined localizations of other analyzed fish species, *T. nigroviridis* and stickleback, zebrafish *Oct* members showed diverse localization on two separate chromosomes, indicating difference in evolution of zebrafish *Oct* genes (Fig. 3.2). To the best of our knowledge, separation of *Oct* genes is present only in zebrafish, cave fish (*Astyanax mexicanus*) and tilapia (*Oreochromis niloticus*) which is contrary to organization of *Oct* and *SLC22/Slc22* genes in general. This unique event in the evolution of organic cation transporters could lead to different and more specific functions, especially regarding Oct2, whose synteny analysis showed specific genetic neighborhood in respect to Oct1, with more similar genetic neighborhood to human and other analyzed fish species (Fig. 3.2). Additionally, due to partition of zebrafish *Oct* cluster, the potential coordinated regulation of *Oct* genes will not be present in zebrafish, which could result in separate and specific regulations of individual *Oct* genes and in different tissue expression and functional properties of zebrafish *Oct1* and *Oct2*, which was confirmed in this study. Analysis of conserved gene order between human and zebrafish *OCT/Oct* genes offered better understanding of their orthological relationship. Specific difference was once again determined for synteny of zebrafish *Oct2*, located on chromosome 17. Synteny analysis revealed unique genetic neighborhood of zebrafish *Oct2*, with two genes, *txlnbb* and *fuca2*, located downstream of *Oct2* and in the same reversed orientation, whereas human orthologs of *TXLNB* and *FUCA2* are located on the opposite side, upstream of human *OCT* cluster. Additional conserved synteny analysis showed that Oct2 is in direct syntenic relationship only with two fish species, cave fish and tilapia, with the same orientation and genetic neighborhood. Our analysis suggests that zebrafish *Oct2* underwent different evolutionary path after separation from *Oct1* on chromosome 20. Conclusion on *Oct2* separation is based on very similar synteny analysis of zebrafish *Oct1* and other investigated fish species, together with human *OCT* cluster, showing the same gene neighborhood with some variations in adjacent gene positions (Fig. 3.2). The main difference in respect to conserved synteny of zebrafish *Oct1* and human *OCT* cluster is lack of zebrafish *igf2r* gene in neighborhood of *Oct1*, whereas it is present in gene neighborhood of other analyzed species. Other identified neighboring genes of zebrafish *Oct1* are localized similarly as human orthologs, with single shift of *vgll2a/VGL2* and *rfx6/RFX6*. The same genes were identified in syntenic relationship of *Oct* clusters of *T. nigroviridis* and stickleback, with minor shifts in gene order (Fig. 3.2). However, due to organization of human *OCT* cluster with similar genetic neighborhood as in other analyzed fish species, there was no conclusive relationship which could determine the direct orthologs of individual human *OCT* members and zebrafish and/or other fish orthologs.

More conclusive orthological relationships could be deduced using determined *Oct* tissue expression profiles in different zebrafish tissues. Tissue expression pattern of zebrafish *Oct1* points to closer relationship with human *OCT2* (Koepsell *et al*., 2007). Dominant expression of zebrafish *Oct1* in kidneys was actually the highest determined expression among all zebrafish *Slc22* members (Popovic, 2014). Over 2-fold higher expression of *Oct1* in female kidneys confirmed previous conclusions of gender related tissue differences in mammalian *OCT2/Oct2*. However, the determined expression of mammalian *OCT2/Oct2* showed dominance in expression in male tissues (Urakami *et al*., 1999), opposite to our findings that showed clear and dominant *Oct1* expression in female kidney. On the other hand, clear dominance of *Oct1* in male liver, brain and testes was in correlation with expressional patterns of mammalian *OCTs/Octs*, suggesting possible long term steroid hormone regulation of zebrafish *Oct2* transcript and protein expression, together with more specific activities, as was previously observed for rat *OCT2* (Urakami *et al*., 2000). Zebrafish *Oct1* showed high expression in male liver, with more drastic differences in gender related expression. High expression of *Oct1* in liver is more in correlation with tissues expression of human *OCT1,* which showed the highest expression in sinusoidal membranes of hepatocytes (Meyer-Wentrup *et al*., 1998). However, contrary to reported long term regulation by steroid hormones and interaction with androgen receptor of human and rat *OCT2/Oct2* (Asaka *et al*., 2006), human and rat *OCT2/Oct2* are not regulated by steroid hormones and their regulation is connected with upregulation by hepatocyte nuclear factor-4a (HNF-4a) (Saborowski *et al*., 2006) and peroxisome proliferator agonist receptor (PPAR) response element (Nie *et al*., 2005), respectively. Reported observations regarding tissue expression pattern of zebrafish *Oct1* revealed greater similarities between *Oct1* and human ortholog *OCT2*, emphasizing closer orthological relations which can be additionally supported with previously determined phylogenetic and syntenic relationships. Tissue expression data also point to the crucial role of *Oct1* in excretion and reabsorption of various endo- and xenobiotics through renal excretion. Regardless of temporarily unknown cellular localization of *Oct1* within zebrafish tissues, high expression of *Oct1* together with the reported nature of the uptake transport implies the role of *Oct1* in renal excretion in zebrafish by mediating uptake of various chemicals and physiological compounds from the blood into the renal cells, as reported for mammalian orthologs (Motohashi *et al*., 2002). Taking into the account the presence of only two zebrafish Oct orthologs in respect to three orthologs in higher vertebrates, and moderate to low expression of Oct2, there is a possibility of Oct1 functioning as both human OCT1 and OCT2. Additionally, high expression of zebrafish *Oct1* in kidney (as hOCT2) and liver (as hOCT1), together with moderate expressions in zebrafish testes and brain, points to potential compensatory function of zebrafish *Oct1*.

Surprisingly, zebrafish *Oct2* showed more different tissue expression pattern than *Oct1*, indicating a different role of these transporters in zebrafish. *Oct2* generally showed much lower tissue expression pattern in all analyzed tissues (Fig. 3.7). The highest expression was determined in gonads, with expression level in testes corresponding to moderate expression of *Oct1* in testes. Gender-dependent differences in tissue expression pattern were also observed for *Oct2* in kidney and liver, suggesting potential long term regulation of *Oct2* expression by steroid hormones, as in the case of rat *Oct2* (Urakami *et al*., 2000). Apart from moderate expression in zebrafish testes, followed by low and gender-dependent expression in kidney, *Oct2* showed very low expression in all other, especially toxicologically relevant tissues such as intestine and gills, that surprisingly did not show significant expression of any investigated transporters. Therefore, the obtained tissue expression pattern of *Oct2* indicated completely different role of this transporter opposed to *Oct1* and other mammalian *OCT1/Oct1* and *OCT2/Oct2* orthologs. Lower expression in toxicologically relevant tissues, together with the obtained phylogenetic relations of *Oct2*, put this transporter more closely to mammalian *OCT3/Oct3* ortholog (Verhaagh *et al*., 1999). However, research on mammalian *OCT3/Oct3* using *Oct3* knockout mice showed higher expression and crucial activity in heart (Zwart *et al*., 2001) and certain brain tissues, where it plays important role in uptake of possibly more physiologically relevant compounds, such as monoamine neurotransmitters, with potential role in the uptake of various drugs in these tissues (Inazu *et al*., 2003).

Taking together the determined tissue expression pattern of both, *Oct1* and *Oct2*, potential roles of individual transporter can be deduced, pointing to crucial role of *Oct1* in ADME processes, especially in renal excretion and biliary elimination of potentially deleterious endo- and xenobiotic compounds. Additionally, tissue expression profile of zebrafish *Oct1* suggests potential compensatory role in respect to human *OCT1*. Since zebrafish possesses only two *Oct* members and the expression profile of *Oct2* points to a minor role of this transporter in kidney and liver, it can be hypothesized that Oct1 performs the role of both human OCT transporters (OCT1 and OCT2) in liver and kidney, respectively.

Further functional characterization of zebrafish organic cation transporters allowed better insight in role and transport activity of Oct1 and Oct2. Investigation of fluorescent cationic dyes revealed the ability of Oct1 to transport five identified fluorescent substrates. Surprisingly, Oct2 did not show activity with any of tested substrates. The lack of Oct2 transport activity was additionally confirmed by immunocytochemical cell localization of overexpressed Oct1 and Oct2 in HEK293 cells. Immunocytochemistry revealed that Oct2 was not localized within the cell plasma membranes, instead Oct2 proteins remained inside the cell in the cytoplasm or possibly within vesicles (Figure 3.8B). The inability of Oct2 membrane localization pointed to possible unsuitable heterologous expression system for functional characterization of zebrafish Oct2. Furthermore, HEK293 cells are not polarized and lack

defined apical and basolateral membranes, while mammalian OCTs/Octs are mostly localized on basolateral membranes of the cells in the expressing tissues (Nies *et al*., 2011). There is a possibility that zebrafish Oct2 is more sensitive to specific polarized localization, which could be the reason for inability of Oct2 localization within HEK293 cell membranes and stay in the cytoplasm. Secondary structure analysis revealed uncommon organization of Oct2, with only 9 transmembrane helices and more unorganized C-terminal end localized outside of the cell and two short α-helical structures, which are not long enough to form transmembrane domains (Fig. 3.4). Additionally, we determined five N-glycosylation sites within the large extracellular loop of Oct2 and two more sites on the C-terminal end of the protein, whereas Oct1 possesses only three N-glycosylation sites within the large extracellular loop, which is in correlation with mammalian OCTs/Octs (Fig. 3.6) (Nies *et al*., 2011). The differences in secondary structure between Oct1 and Oct2 together with lack of polarization of HEK293 cells could be the cause of Oct2 functional absence in used expression system. Therefore, our next research steps were focused on detailed characterization of Oct1.

Unlike Oct2, Oct1 was localized within plasma membranes in the transiently transfected HEK293 cells (Fig 3.8A) and showed active transport of all five investigated fluorescent substrates (Figs. 3.9 – 3.13). Oct1 transported ASP+ with high affinity of 25.97 µM which was higher than reported ASP+ K_m value of 1 µM for rat OCT1 (Mehrens *et al.*, 2000) and in lower range than reported for human OCT1 with K_m value of 12.5 µM (Salomon et al., 2012). On the other hand, Oct1 showed much higher affinity for mitochondrial fluorescent dye rhodamine 123 (K_m = 0.1 µM) which is in similar range as reported for human OCT1 (K_m = 0.54 µM) and OCT2 (K_m = 0.61 µM) (Jouan *et al*., 2014). Further, the uptake assays revealed ethidium bromide as potent substrate of Oct1 with K_m value of 0.1 µM, the same affinity as reported for rhodamine 123 (Rh123), indicating potentially similar mode of interaction of these substrates and active site/region of Oct1. Ethidium bromide is also reported as potent fluorescent substrate of all three human OCTs, with OCT1 showing K_m value of 0.8 µM, closest to zebrafish Oct1 ortholog, followed by OCT2 (K_m = 1.7 µM) and OCT3 (K_m = 2 µM) (Lee *et al*., 2009). Another determined Oct1 substrate in our study was DAPI, with low K_m value of 0.78 µM, also in the same range as Rh123 and ethidium bromide. DAPI was also confirmed as substrate of human OCTs with higher Km value of 8.94 µM (Yasujima *et al*., 2011), and as a valuable model substrate of human MATE transporters (Yasujima *et al*., 2010). The fifth identified Oct1 fluorescent substrate, berberine, showed high affinity interaction, with K_m value of 3.96 µM which is in similar micromolar range as ASP+ and in higher range than Rh123, ethidium bromide and DAPI. These data indicate that ASP+ and berberine might interact with active region of Oct1 in different ways than other three substrates which may provide valuable information in determining the active region and crucial amino acid residues that interact with identified substrates. Determined K_m value of berberine uptake is in the same range as human OCT2

K_m value of 4.4 µM, whereas human OCT1 showed 3-fold higher K_m value for berberine transport of 14.8 µM (Nies *et al*., 2011).

Based on the determined uptake preferences and basic kinetic parameters of identified fluorescent substrates, we performed inhibition analysis on a wide range of potential Oct1 substrates and non-transported inhibitors. The list of tested substances that might show interaction with zebrafish Oct1 was based on their properties as organic cations and/or previously recorded interaction with other mammalian OCTs/Octs. Using our expression system – Oct1 transiently transfected in HEK293 cells – we showed inhibition of ASP+ and Rh123 uptake by steroid hormones (Figs. 3.18 – 3.20). The results showed that endogenous steroid hormone progesterone acts as a potent inhibitor of transport of fluorescent substrates by zebrafish Oct1 (Table 3.1). Presented results of progesterone effect on uptake of five identified fluorescent substrates showed different strengths of interaction with different substrates, ranging from very low K_i value with Rh123 (0.25 µM) to high K_i value of 1.23 mM with DAPI. The observed divergence points to probable different interactions with substrate binding region of Oct1. Furthermore, it also suggests that different kind of substrate interaction may affect the interaction with other investigated substrates or inhibitors. The effect of variable substrate interaction with the exposed and relatively big substrate binding region of OCTs/Octs was reported before for rat Oct2 (Volk *et al*., 2009), and our results provide potential confirmation of this kind of interaction. Additional confirmation of complex interactions with substrates and non-transported inhibitors, which probably bind to the active site in different ways and cause different types of interaction, was confirmed by observing the variability in Michaelis-Menten kinetic parameters of ASP+ uptake in presence of different interactors (Table 3.3; Fig. 3.25). Progesterone specifically showed mixed type of inhibition by elevating the K_m value and lowering the V_m value of ASP+ uptake, suggesting that progesterone does not compete for the same binding site as ASP+, but it affects the transport of ASP+ by possible conformational changes and steric interaction within substrate binding region of Oct1. Due to the determined mixed type of inhibition by progesterone, it is not sure if the progesterone is being transported into the cell by zebrafish Oct1, or it acts as non-transported inhibitor. Similar to our findings, progesterone was shown to be potent inhibitor of human OCTs, with low K_i values of 3.1, 27 and 4.3 µM for OCT1, OCT2 and OCT3, respectively (Hayer-Zillgen *et al.*, 2002). The inhibition constants of human OCT1 and OCT3 are in the same range as determined inhibition of zebrafish Oct1 with K_i of 2 µM (Table 3.1). Based on the observed effects of progesterone, it may be hypothesized that zebrafish Oct1 plays important physiological role in maintenance of basic physiological homeostasis of sex steroid hormones, thus affecting reproduction and embryogenesis. Apart from its putative physiological role, presence of progesterone and its synthetic analogs has been identified in environment in high concentrations, suggesting that they may affect hormonal hemostasis and

embryonic development in fish species (Zhao *et al*., 2015). This conclusion is further supported by inhibition of Oct1 by synthetic medroxyprogesterone, which showed approximately 50% of ASP+ uptake inhibition (Fig. 3.14). Therefore, Oct1 may play important ecotoxicological role as key mediator of uptake of environmental progesterone and other steroid hormones as well as important mediator in their excretion (Zeilinger *et al*., 2009; DeQuattro *et al*., 2012). Additionally, environmentally relevant concentration of progesterone and its synthetic analogs may disrupt physiological functions of Oct1 that may in turn have profound effects on organic cation homeostasis.

We also showed the interaction of Oct1 with androgen hormones androstenedione and testosterone which inhibited ASP+ uptake with low K_i values of 5.13 and 13.19 µM, respectively (Fig. 3.18). Investigated hormones also showed different intensities of inhibition with different fluorescent substrates, whereas they did not inhibit DAPI uptake by Oct1. Differences in the interaction, together with lack of interaction with DAPI transport, further confirmed the potential variability in the interaction between the Oct1 substrate binding region and substrates/inhibitors. Additionally, Michaelis-Menten ASP+ uptake kinetics confirmed mixed type of interaction with androstenedione, by elevating the K_m value and lowering the V_m value of ASP+ uptake (Table 3.3). The K_i value of Oct1 testosterone inhibition is in the same range as K_m value of testosterone uptake by human OCT1 (K_m = 10 µM), with similar affinity of OCT2 (K_m = 3 µM) and slightly lower affinity of OCT3 (K_m = 44 µM) (Koepsell *et al*., 2007). Oct1 also showed interaction with synthetic analog of testosterone, 19-methyltestosterone, with higher K_i value of 56.06 µM, showing that conjugated methyl group on C19 probably affects binding of 19-methyltestosterone to binding region of Oct1. The main source of methyltestosterone in environment is aquaculture which utilizes synthetic testosterone conjugates in order to control the number of male fish in population, using methyltestosterone as xenoandrogen compound (Homklin *et al*., 2009; Khalil *et al*., 2011; Biswas *et al*., 2014). Since we have shown the interaction of zebrafish Oct1 with 19-methyltestosterone, along with other androgen hormones, it is possible that Oct1 plays important role in absorption and excretion of these hormones. *Vice versa*, the hormones could cause disruptions of organic cation homeostasis maintained by Oct1, ether by inhibition of Oct mediated transport of other organic cations or by regulation of tissue expression. We also showed interaction of Oct1 with another sex hormone, β-estradiol, which caused the inhibition of ASP+ uptake with inhibition constants of 44.35 µM (Fig. 3.20B). Determined K_i value of β-estradiol pointed to similar inhibition of human OCT2 (K_i > 30 µM), whereas it showed to be more potent inhibitor of human OCT1 and OCT3 with K_i values of 3 – 4 µM (Hayer-Zillgen *et al*., 2002). However, β-estradiol showed higher inhibition of Rh123 uptake by Oct1 (K_i = 1.54 µM), whereas it caused over 600-fold lower inhibition of DAPI uptake (K_i = 954 µM), which further confirms the complexity of interaction of Oct1 variable binding region with different fluorescent substrates and potential interactors (Table

3.1). Furthermore, due to determined mixed type of inhibition between β-estradiol and Oct1, the transport of this sex hormone cannot be confirmed with certainty. Regardless of these findings, it can be concluded that β-estradiol plays important role in the physiological functions of Oct1 as possible substrate or a highly potent inhibitor, which can be crucial factor in the regulation of Oct1 activity. Due to determined potent interaction of β-estradiol with zebrafish Oct1 and recorded rising concentrations of synthetic hormones in the aquatic environment, such as 17a estradiol, 17 β-estradiol and 17 α-ethinyl estradiol, which are present in wastewaters in concentration range of ng/L (Kolpin *et al*., 2002), there is a possibility that these synthetic hormones could have crucial impact on homeostasis of organic cations in zebrafish through the disturbance of Oct1 physiological functions. Oppositely, Oct1 could be important element in excretion of these xenoestrogens.

Previous studies confirmed corticosterone as potent inhibitor of all three human OCTs, with K_i values of OCT1 and OCT2 of 7 – 22 μM, and 34 μM, respectively, in similar range as reported interaction for zebrafish Oct1, whereas OCT3 showed much higher inhibition by corticosterone (K_i = 0.12 – 0.29 μM) (Hayer-Zillgen *et al*., 2002). Similar to human OCT1 and OCT2, we determined corticosterone inhibition of ASP+ uptake by Oct1 with K_i value of 16.5 μM (Fig. 3.20B). Surprisingly, corticosterone did not show drastic differences in inhibition with different fluorescent substrates. All determined K_i values were in similar range, with the lowest recorded inhibition of Rh123 (K_i = 1.25 μM) (Table 3.1). Additionally, corticosterone has shown to be the only substrate of Oct1 among tested steroid hormones, which pointed to unique interaction of corticosterone and binding region of Oct1. Our findings further supported the conclusion that Oct1 plays important role in absorption, distribution and excretion of sex hormones and steroid hormones in general, while determined inhibition constants of investigated steroids point to high similarity of zebrafish Oct1 to human OCT1 and OCT2, thus suggesting a possible compensatory role of zebrafish Oct1.

Other physiological compounds, outside the group of steroid hormones, showed less potent interaction with zebrafish Oct1 which was evident in initial inhibition screen of endogenous compounds (Fig. 3.14). The most potent interaction among tested endogenous compounds was determined for neurotransmitter acetylcholine (K_i = 710.3 μM) and tyrosine metabolite tyramine (K_i = 1016 μM) (Fig. 3.21). Similar range of acetylcholine inhibition is reported for human OCT1 and OCT3 with K_i values of 580 μM and 490 μM, respectively, whereas OCT2 transported acetylcholine with K_m value of 117 μM. Considering the role of acetylcholine as a neurotransmitter in the central and peripheral nervous system and reported expression of Oct1 in zebrafish brain, a potential role of Oct1 in transport of acetylcholine in zebrafish nervous system may be hypothesized. Additional findings that acetylcholine mediates signaling of basic cell functions, outside the nervous system in various non-neuronal mammalian cells such as epithelial and endothelial cells (Lips *et al*., 2005), point to possible

role of Oct1 in acetylcholine signaling in other zebrafish tissues. The second endogenous metabolite, tyramine, is not reported as interactor of any mammalian OCT/Oct. However, tyramine is reported as a potent substrate of human extraneuronal transporter for monoamine transmitters (EMT) (Gründermann *et al.,* 1998) which is a member of ASF superfamily of proteins, same as SLC transporters, indicating that similar structure and possible function could be the reason for the observed interaction of tyramine and zebrafish Oct1.

Oct1 showed high affinity interactions with numerous xenobiotics. In the inhibition analysis we specifically distinguished one group of hazardous environmental contaminants, organotin compounds. The organotin compounds have a wide variety of industrial uses, therefore considerable amounts end up in the environment. That is especially evident in the aquatic environments, where they are widely used because of their bactericidal and fungicidal properties as key elements of antifouling boat paints (Kimbrough 1975). Maximum toxicological activity is determined for trisubstituated compounds in any R_4SnX_{4-n} series. Interestingly, tributyltin chloride, together with dibutyltin chloride appear to be the most potent inhibitors of zebrafish Oct1, with K_i values of 3.9 µM and 0.4 µM, respectively (Fig. 3.22). This is the first determined interaction of Oct transporters with these hazardous environmental contaminants which points to potentially crucial role of Oct1 in toxic response to organotin compounds, with emphasis on most potent members, dibutyltin and tributyltin chloride, that were shown as very harmful toxic compounds, causing the toxicity effect at very low concentrations of 0.04 – 0.16 ng/L in the aquatic environment (Hoch, 2001). Furthermore, due to highly potent inhibition of Oct1 by tributyltin and dibutyltin chloride, it is possible that these compounds together with other members of organotin group could have tremendous effect on normal physiological functions of Oct1 in zebrafish. Therefore, it is highly necessary to investigate in more detail relationship between organotin compounds and organic cation transporters in zebrafish.

Another group of reported xenobiotic compounds which showed interaction with zebrafish Oct1 are quaternary ammonium cations with tetrapentylammonium (TPA) as the most potent representative which inhibited ASP+ transport by Oct1 with K_i value of 8.35 µM, following with tetrabutylammonium (TBA) (K_i = 28.05 µM) and tetraethylammonium (TEA) (K_i = 820.5 µM), whereas other members with shorter side chains exhibited inhibition constants in higher millimolar range (Fig. 3.23B). This effect of positive correlation between rising inhibition and increase in size of inhibiting molecules could be due to elevated steric disruptions within binding region of the transporter. This effect is also present in inhibition of human OCTs by quaternary ammonium salts, with most potent inhibition by the largest compound with longest sidechains, TPA, whereas lowest inhibition was recorded with tetramethylammonium (Koepsell, 2007). Studies of mammalian OCTs/Octs identified TEA a transported substrate of organic cation transporters, with most potent transport by OCT2 with K_m

value of 27 – 76 µM, followed with OCT1 (K_m = 229 µM) and OCT3 (K_i = 1400 µM), which points that affinity of zebrafish Oct1 for TEA is in the concentration range between human OCT1 and OCT3 (Koepsell *et al*., 2007). Our results showed variable inhibition of Oct1 by TEA with different fluorescent substrates (Table 3.1). Interestingly, there was no observable inhibition by TEA with DAPI, indicating that interaction of TEA with Oct1 binding region had no effect on binding and transport of DAPI. Additionally determined interactions of Oct1 with xenobiotic compounds were with antimalarial drug pyrimethamine which showed to be a potent inhibitor of ASP+ uptake with K_i value of 0.9 µM and sympatholytic drug prazosin with K_i value of 2.48 µM (Fig. 3.23A). Prazosin showed the highest inhibition of human OCT1 with K_i value of 1.8 µM, followed by OCT3 with K_i value of 13 µM, whereas OCT2 showed lower inhibition with prazosin with K_i values above 100 µM (Koepsell, 2004), indicating similarities with zebrafish Oct1 and potential role of prazosin as Oct1 inhibitor which could affect the maintained homeostasis of organic cation in tissues with dominant expression of Oct1. Histamine H_2-receptor agonist, cimetidine, showed highest inhibition of Rh123 uptake (K_i = 15 µM), whereas K_i values with other fluorescent substrates were in much higher micromolar and even millimolar ranges (Table 3.1). Cimetidine is frequently used pharmaceutical with predicted environmental concentrations in low micromolar range (Kim *et al*., 2007). Therefore cimetidine could have adverse effect on physiological functions of zebrafish Oct1, thus effecting homeostasis of organic and inorganic cations in zebrafish. The research of drug-drug interactions with small-molecule tyrosine kinase inhibitors revealed interaction with mammalian OCTs/Octs (Minematsu and Giacomini, 2011). We determined interaction of Oct1 with dasatinib and vandetanib, which inhibited the uptake of fluorescent substrates. The highest inhibition of vandetanib was determined with Rh123 with K_i value of 0.4 µM, which is one of the highest Oct1 inhibitions determined by this study. Uptake inhibition by dasatinib and vandetanib with other fluorescent substrates was also high with K_i values in lower micromolar range, whereas vandetanib showed no effect on berberine uptake, indicating the differences in the interaction with binding region of Oct1.

Taking together all determined inhibition data of various endo- and xenobiotic compounds, it can be concluded that steroid hormones have great effect on zebrafish Oct1. The type of determined strong interactions with both male and female steroid hormones remains yet to be elucidated. However, taking into account tissue expression profile of Oct1, with dominant gender-dependent expression in kidney and liver, and reports from the previous studies of other mammalian OCTs/Octs, it can be postulated that the relationship between zebrafish Oct1 and steroid hormones is crucial for the normal functions of Oct1, either through regulation of tissue expression or by being potent substrates or non-transported inhibitors of Oct1. Previous findings in other mammalian OCT/Oct orthologs suggest crucial physiological and toxicological role of organic cation transporters as important elements of

ADME processes and key mediators of organic and inorganic cation homeostasis (Koepsell, 2013). However, nature and structure of OCT/Oct active binding site in a form of substrate binding region complicates the elucidation of the type of interaction with determined interactors, due to variable and complex interactions between substrates and non-transported inhibitors with multiple binding sites within a big substrate binding region. The complexity of Oct1 – interactor relationship is confirmed by comparison of different inhibition constants obtained in inhibition assays with five different fluorescent substrates, which in most of combinations showed weak correlation (Tables 3.1 and 3.2). These findings point to complexity of substrate/inhibitor interactions with binding region of Oct1, showing that different kind of interaction with transported fluorescent or non-fluorescent substrate will have unique effect on the type of interactions with other potential substrate or non-transported inhibitor (Koepsell *et al*., 2007). Additional confirmation of variable interactions between zebrafish Oct1 and interacting compounds due to possible complexity of the binding region was done by Michaelis-Menten kinetic experiment which determined mixed type of inhibition for numerous investigated compounds (Table 3.3; Fig. 3.25).

In order to determine type of interaction with investigated compounds, together with a more detailed characterization of Oct1 substrate binding region, we constructed 3D models of zebrafish Oct1 and human OCT1 and OCT2 proteins, based on homology modeling with bacterial lactose permease (LacY) from MFS superfamily of membrane transporters. Obtained models revealed similar tertiary structures of human and zebrafish OCTs/Octs, showing universal structure of MFS transporters, with twelve transmembrane alpha helices whose steric organization forms a large binding region within the transporter (Fig. 3.30). Additionally, we performed functional characterization of human OCT1 and OCT2 in HEK293 heterologous expression system. We tested substrate specificities with identified fluorescent substrates, using the set of previously determined interactors based on zebrafish research. Crucial difference obtained from determination of fluorescent substrate interaction with human OCT1 and OCT2 was lack of transport of ASP+ and berberine by OCT2 which indicated that OCT2 may have a different active site, unable to bind and transport ASP+ and berberine. Inability to determine the transport of ASP+ and berberine by hOCT2 suggests that these fluorescent dyes might interact with the previously reported low affinity binding site within hOCT2 binding region (Koepsell, 2011). That implies they may be transported with much lower affinities, in high micromolar or even millimolar range (Ciarimboli *et al*., 2012), which was impossible to determine in this study due to solubility of the dyes. These findings revealed that ASP+ and berberine interact with human OCT2 in different ways and potentially different amino acid residues within hOCT2 active region. In order to determine and compare K_i values of chosen compounds, we used Rh123 as a model fluorescent substrate which showed low K_m value of 0.17 µM for OCT1 and higher K_m value of 1.55 µM for OCT2 (Figs. 3.27 and

3.28). The comparison of zebrafish Oct1 and human OCT1 and OCT2 determined K_i values revealed crucial differences in compound interactions among these transporters (Table 3.4; Fig 3.29). In the group of steroid hormones general difference can be observed in higher K_i values of human OCT1 in respect to K_i values of OCT2 and zebrafish Oct1 in similar ranges, with exception for β-estradiol that showed similar K_i values of human OCTs, and dihydrotestosterone which demonstrated the lowest K_i of 0.7 µM with human OCT1 (Table 3.4). Similar relations in K_i values were observed for xenobiotic compounds, with higher K_i values with human OCT1, although with certain exceptions with prazosin and tributyltin chloride (Table 3.4).

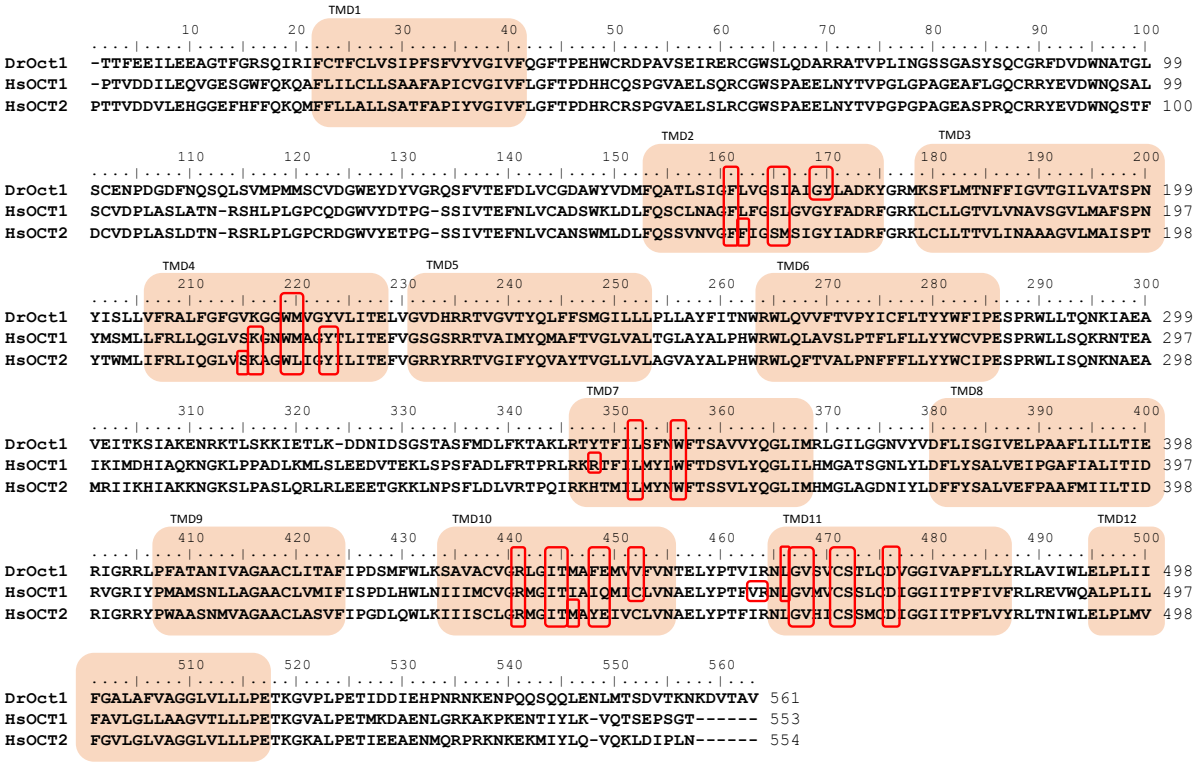

Figure 4.1. Presentation of molecular docking data with multiple sequence alignment of zebrafish Oct1 and human OCT1 and 2. Amino acid residues that showed interaction with tested compounds are marked with red rectangles.

Previous studies used mutagenesis and homology modeling with molecular docking in order to determine position and shape of the substrate binding region of rat OCT1 (Koepsell, 2011). Eight crucial amino acid residues (Phe160, Trp218, Tyr222, Thr226, Arg440, Leu447, Gln448 and Asp475) that changed substrate affinities and transport rates upon substitution in mutagenesis studies were identified (Popp *et al.*, 2005; Volk *et al.*, 2009). These amino acid residues of rat Oct1 are conserved in human and zebrafish OCTs/Octs and play crucial role in interaction between substrate and the

substrate binding region (Koepsell, 2011). Homology modeling of zebrafish Oct1 and human OCT1 and OCT2 provided the 3D models of the transporters, which were used as basis for molecular docking of five determined fluorescent substrates and five potent interactors (Tables 3.5. – 3.10). Using molecular docking of five fluorescent substrates and five determined interacting compounds, we identified potentially crucial amino acid residues within substrate binding regions of zebrafish Oct1 and human OCT1 and OCT2 (Fig. 3.30). Initial docking of five fluorescent substrates identified several interacting amino acid residues within determined active site of the transporter. Identified amino acid residues were in correlation with previous studies, showing that a conserved set of amino acid residues has important role in interaction of OCT/Oct transporters with potential substrates or inhibitors (Koepsell, 2011). The highest number of interacting sites was localized on TMD10 and TMD11, together with fewer determined interacting sites on TMD2, TMD4 and TMD7 (Fig. 4.1). These transmembrane domains are crucial for the formation of the binding pocket of OCTs/Octs. Furthermore, TMD11 of rat Oct1, with hinge domain formed by Cys474, Asp475, Leu476, Gly477 and Gly478, has shown to be crucial for substrate binding and conformational changes during the transport (Gorbunov *et al*., 2008; Egenberger *et al*., 2012). We determined that Lys215, Trp218, Arg440 and Ser470 have important role in interaction with fluorescent substrates as donors of hydrogen atom in H-bond, whereas Phe160, Ser163, Leu164, Arg440, Thr443, Gln447 and Cys550 contribute to formation of H-bond between OCT/Oct active region and interacting compounds as acceptors of hydrogen atom (Tables 3.5 - 3.7). Amino acid residues such as Phe160, Tyr170, Trp219, Trp355, Arg440, Phe/Tyr447 were shown to form aromatic bonds between OCT/Oct and tested compounds, which revealed the importance of these amino acid residues as well as correlation with previous studies on the structure of human and rat OCT/Oct binding regions (Popp *et al*., 2005; Volk *et al*., 2009). Additionally, several amino acid residues are located within docking sites of substrates and form steric interactions, which also make them important in substrate interactions. Molecular docking of five identified OCT/Oct interactors revealed new interactions between amino acid residues within active region and tested interactors, with dominant number of close amino acid residues which showed steric interactions with tested interactors. Most of the crucial amino acid residues determined in previous studies on rat and human OCTs/Octs were identified as close residues within docking sites of tested interactors (Tables 3.8 – 3.10). Amino acid residues which formed H-bonds with tested interactors were Arg440 and Tyr219, along with newly identified residues Lys215 and Ser471 which acted as hydrogen donors in formed H-bonds. Aromatic interactions with tested interactors were formed by Phe160 and Tyr447, with newly identified Tyr36 and Tyr170 (Tables 3.8 – 3.10). Interestingly, docking results showed that interaction between tested transporters and androstenedione and tributyltin chloride were based solely on interaction with close amino acid residues within their docking sites (Tables 3.8 – 3.10).

In summary, phylogenetic and conserved synteny analyses showed orthological relationships of zebrafish Oct1 with toxicologically relevant mammalian and other vertebrate orthologs. On the other hand, phylogenetic clustering of zebrafish Oct2 with OCT3/Oct3 orthologs, along with determined tissue expression, points to a less significant role of zebrafish Oct2 in ADME processes. High expression of zebrafish Oct1 in major toxicologically relevant tissues, with emphasis on the highest expression in kidney, points to crucial role of this transporter in absorption, reabsorption and excretion of organic cations in zebrafish. In comparison with tissue expression profiles of human OCT1 and OCT2 which are dominant in liver and kidney, respectively, determined expression pattern of zebrafish Oct1 points to potential compensatory role of Oct1 which may cover function of both human OCT1 and OCT2. Performed uptake assays revealed zebrafish Oct1 as potent transporter of cationic and neutral fluorescent substrates, offering methodological basis for functional characterization of zebrafish Oct1. Inhibition assays revealed high affinity interactions of Oct1 with steroid hormones, indicating the potential role of Oct1 in mediation of steroid hormone homeostasis which could function as important transporter in gonads and hormone synthesizing organs, as well as in biliary and renal excretion end reabsorption. From the ecotoxicological aspect, Oct1 may be crucial target for xenobiotic disruption by environmental hormones and their synthetic analogs. Inhibition assays also revealed Oct1 as important element in zebrafish ADME processes, with the proposed key role in defense against hazardous environmental and endobiotic compounds through biliary and renal excretion. Finally, determined 3D model of zebrafish Oct1 and human Oct1 and OCT2 provided new insight in structure and complexity of substrate binding regions of analyzed transporters, and confirmed complex interactions with potential substrates and inhibitors which affects determination of type of interaction between the transporter and identified interactors. Further analysis of Oct1 active site and transport mechanism through extensive mutagenesis studies will be needed in order to thoroughly elucidate the type of interaction and further characterize zebrafish Oct1.

5. Conclusions

The work presented in this dissertation offered the first comprehensive insight in the role(s) of organic cation transporters in fish, and in particular zebrafish as an important model organism. More specifically, the most important conclusions of this study are:

1. Two identified zebrafish organic cation transporters, Oct1 and Oct2, are encoded with *Slc22a2* and *Slc22a3* genes, respectively. *Oct1* gene shows phylogenetic relationship with human and other vertebrates' OCT1/Oct1 and OCT2/Oct2 cluster, whereas zebrafish *Oct2* gene shows closer relationship with OCT3/Oct3 cluster;

2. Conserved synteny analysis revealed syntenic relationships between zebrafish genes, *Oct1* on chromosome 20 and separated Oct2 gene on chromosome 17, and human OCT cluster on chromosome 6. In comparison with synteny analysis of other fish Oct genes, zebrafish Oct2 possess different genetic neighborhood and is the only gene which is separated from the other homolog. These novel findings indicate different evolutionary path of zebrafish Oct2 and point to potentially different functions of Oct2 in zebrafish. However, synteny analysis could not provide evidence of direct orthologies between zebrafish and human genes due to consecutive clustering of human genes within the same genetic neighborhood;

3. High expression of zebrafish Oct1 in major toxicologically relevant tissues, with emphasis on the highest expression in kidney, point to crucial role of this transporter in absorption, reabsorption and excretion of organic cations in zebrafish. In comparison with tissue expression profiles of human OCT1 and OCT2 which are dominant in liver and kidney, respectively, determined expression pattern of zebrafish Oct1 points to potential compensatory role of Oct1 which may cover function of both human OCT1 and OCT2;

4. Performed uptake assays revealed zebrafish Oct1 as potent transporter of cationic and neutral fluorescent substrates, and served as the basis of functional characterization of zebrafish Oct1.

5. Inhibition assays revealed high affinity interactions of Oct1 with steroid hormones, indicating the potential role of Oct1 in mediating steroid hormone homeostasis which could function as important transporter in gonads and hormone synthesizing organs, as well as in biliary and renal excretion end reabsorption. From the ecotoxicological aspect, Oct1 may be crucial cellular target for xenobiotic disruption by environmental hormones and their synthetic analogs;

6. Determined 3D model of zebrafish Oct1 and human Oct1 and OCT2 provided new insight in structure and complexity of substrate binding region of analysed transporters, and confirmed complex interactions with potential substrates and inhibitors which affects determination of type of interaction between the transporter and identified interactors.

6. References

Abbas, L., Whitfield, T. T., 2009. Nkcc1 (Slc12a2) is required for the regulation of endolymph volume in the otic vesicle and swim bladder volume in the zebrafish larva. Development 136, 2837–2848.

Abramson, J., Smirnova, I., Kasho, V., Verner, G., Kaback, H. R., Iwata, S., 2003. Structure and mechanism of the lactose permease of Escherichia coli. Science 301, 610–615.

Alnouti, Y., Petrick, J. S., Klaassen, C. D., 2006. Tissue distribution and ontogeny of organic cation transporters in mice. Drug Metab. Dispos. 34, 477–482.

Amphoux, A., Vialou, V., Drescher, E., Bruss, M., La Cour, C. M., Rochat, C., Millan, M. J., Giros, B., Bonisch, H., Gautron, S., 2006. Differential pharmacological in vitro properties of organic cation transporters and regional distribution in rat brain. Neuropharmacology 50, 941-952.

Anisimova, M., Gascuel, O., 2006. Approximate likelihood-ratio test for branches: A fast, accurate, and powerful alternative. Syst. Biol. 55, 539–552.

Arndt, P., Volk, C., Gorboulev, V., Budiman, T., Popp, C., Ulzheimer-Teuber, I., Akhoundova, A., Koppatz, S., Bamberg, E., Nagel, G., Koepsell, H., 2001. Interaction of cations, anions, and weak base quinine with rat renal cation transporter rOCT2 compared with rOCT1. Am. J. Physiol. Renal Physiol. 281, F454–F468.

Asaka, J.-i., Terada, T., Okuda, M., Katsura, T., Inui, K., 2006. Androgen receptor is responsible for rat organic cation transporter 2 gene regulation but not for rOCT1 and rOCT3. Pharm. Res. 1–8.

Barut, B. A. and Zon, L. I., 2000. Realizing the potential of zebrafish as a model for human disease. Physiol. Genomics 2, 49-51.

Bayaa, M., Vulesevic, B., Esbaugh, A., Braun, M., Ekker, M., Grosell, M., and Perry, S. F., 2009. The involvement of SLC26 anion exchangers in Cl/HCO3 exchange in zebrafish (Danio rerio) larvae. J. Exp. Biol. 212, 1940–1948.

Biswas, A., Behera, S., Das, P., Meena, D. K., Behera, B. K., 2014. Effect of Methyl Testosterone (17α-MT) on the Phenotype, Bioindices and Gonads of Adult Male Dwarf Gourami (*Colisa lalia*). Emir. J. Food. Agric. 26, 459-464.

Boussif, O., Lezoualc'h, F., Zanta, M. A., Mergny, M.D., Scherman, D., Demeneix, B., Behr, J. P., 1995. A versatile vector for gene and oligonucleotide transfer into cells in culture and in vivo: Polyethylenimine. Proc. Natl. Acad. Sci. 92, 7297-301.

Bradford, M. M., 1976. A rapid and sensitive method for the quantitation of microgram quantities of protein utilizing the principle of protein-dye binding. Anal. Biochem. 72: 248–254.

Brooks, B. R. Bruccoleri, R. E., Olafson, B. D., States, D. J., Swaminathan, S., Karplus ,M. J., 2004. CHARMM: A program for macromolecular energy, minimization, and dynamics calculations. Comp. Chem. 4, 187-217.

Busch, A. E., Karbach, U., Miska, D., Gorboulev, V., Akhoundova, A., Volk, C., Arndt, P., Ulzheimer, J. C., Sonders, M. S., Baumann, C., Waldegger, S., Lang, F., Koepsell, H., 1998. Human neurons express the polyspecific cation transporter hOCT2, which translocates monoamine neurotransmitters, amantadine, and memantine. Mol. Pharmacol. 54, 342–352.

Catchen, J. M., Conery, J. S., Postlethwait, J. H., 2009. Automated identification of conserved synteny after whole-genome duplication. Genome Res. 19, 1497–1505.

Cetinkaya, I., Ciarimboli, G., Yalcinkaya, G., Mehrens, T., Velic, A., Hirsch, J. R., Gorboulev, V., Koepsell, H., Schlatter, E., 2003. Regulation of human organic cation transporter hOCT2 by PKA, PI3K, and calmodulin-dependent kinases. Am. J. Physiol. Renal Physiol. 284, F293–F302.

Chen, J. J., Li, Z., Pan, H., Murphy, D. L., Tamir, H., Koepsell, H., Gershon, M. D., 2001. Maintenance of serotonin in the intestinal mucosa and ganglia of mice that lack the high-affinity serotonin transporter: abnormal intestinal motility and the expression of cation transporters. J. Neurosci. 21, 6348–6361.

Ciarimboli, G., Struwe, K., Arndt, P., Gorboulev, V., Koepsell, H., Schlatter, E., Hirsch, J. R., 2004. Regulation of the human organic cation transporter hOCT1. J. Cell. Physiol. 201, 420–428.

Ciarimboli, G., Koepsell, H., Iordanova, M., Gorboulev, V., Durner, B., Lang, D., Edemir, B., Schroter, R., VanLe, T., Schlatter, E., 2005. Individual PKC-phosphorylation sites in organic cation transporter 1 determine substrate selectivity and transport regulation. J. Am. Soc. Nephrol. 16, 1562–1570.

Ciarimboli, G., Lancaster, C. S., Schlatter, E., Franke, R. M., Sprowl, J. A., Pavenstädt H., Massmann, V., Guckel D., Mathijssen R. H., Yang, W., Pui, C. H., Relling M. V., Herrmann, E., Sparreboom, A., 2012. Proximal tubular secretion of creatinine by organic cation transporter Oct2 in cancer patients. Clinic. Cancer res. 18, 1101-1108.

Davis, R. H., 2004. The age of model organisms. Nat. Rev. Genet.5, 69–76.

Dequattro, Z. A., Peissig, E. J., Antkiewicz, D. S., Lundgren, E. J., Hedman, C. J., Hemming, J. D. C., Barryz, T. P., 2012. Effects of progesterone on reproduction and embryonic development in the fathead minnow (*Pimephales promelas*). Environ. Toxicol. Chem. 31, 851–856.

Di Giullio, R. T., Hinton, D. E., 2008. The Toxicology of Fishes. CRC Press, Boca Raton, FL 33487‑2742.

Donner, M. G., Keppler, D., 2001. Up-regulation of basolateral multidrug resistance protein 3 (Mrp3) in cholestatic rat liver. Hepatology 34, 351-359.

Dresser, M. J., Zhang, L., Giacomini, K. M., 1999. Molecular and functional characteristics of cloned human organic cation transporters. Pharmaceutical biotechnology 12, 441-449.

Dresser, M. J., Gray, A. T., Giacomini, K. M., 2000. Kinetic and selectivity differences between rodent, rabbit, and human organic cation transporters (OCT1). J. Pharmacol. Exp. Ther. 292, 1146–1152.

Edgar, R. C., 2004. MUSCLE: a multiple sequence alignment method with reduced time and space complexity. BMC Bioinformatics 5:113.

Egenberger, B., Gorboulev, V., Keller, T., Gorbunov, D., Gottlieb, N., Geiger, D., Mueller, T. D., Koepsell, H., 2012. A substrate binding hinge domain is critical for transport-related structural changes of organic cation transporter 1. J. Biol. Chem. 287, 31561-31573.

Embry, M. R., Belanger, S. E., Braunbeck, T. A., Galay-Burgos, M., Halder, M., Hinton, D. E., Léonard, M. A., Lillicrap, A., NorbergKing, T., and Whale, G., 2010. The fish embryo toxicity test as an animal alternative method in hazard and risk assessment and scientific research. Aquat. Toxicol. 97, 79–87.

Eraly, S. A., Hamilton, B., A., Nigam, S. K., 2003. Organic anion and cation transporters occur in pairs of similar and similarly expressed genes. Biochem. Biophys. Res. Commun. 300, 333-342.

Feig, M. and Brooks, C. L., 2004. III Recent advances in the development and application of implicit solvent models in biomolecule simulations. Curr. Opin. Struct. Biol. 14:217-224.

Fujita, T., Urban, T. J., Leabman, M. K., Fujita, K., Giacomini, K. M., 2006. Transport of drugs in the kidney by the human organic cation transporter, OCT2 and its genetic variants. J. Pharm. Sci. 95, 25–36.

Furuichi, Y., Sugiura, T., Kato, Y., Shimada, Y., Masuda, K., 2010. OCTN2 is associated with carnitine transport capacity of rat skeletal muscles. Acta Physiol. 200, 57–64.

Gasser, P. J., Lowry, C. A., Orchinik, M., 2006. Corticosterone sensitive monoamine transport in the rat dorsomedial hypothalamus: potential role for organic cation transporter 3 in stress-induced modulation of monoaminergic neurotransmission. J. Neurosci. 26, 8758–8766.

Gelhaar, D. K., Verkhivker, G. M., Rejto, P. A., Sherman, C. J., Foge,l D. B., Fogel, L. J., Freer, S. T., 1995. Molecular recognition of the inhibitor AG-1343 by HIV-1 Protease: Conformationally flexible docking by evolutionary programming. Chem. Biol. 2, 317-324.

Gelhaar, D. K., Bouzida, D., Rejto, P. A., 1999. Rational Drug Design: Novel Methodology and Practical Applications. In Parrill L, Rami Reddy M. (Eds.) Series title: ACS symposium series, 719. American Chemical Society, Washington, DC. pp. 292-311.

Giacomini, K. M., Huang, S.-M., Tweedie, K., M., G., 2010. Membrane transporters in drug development. Nature Reviews, Drug Discovery, 9, 216-236.

Gorboulev, V., Shatskaya, N., Volk, C., Koepsell, H., 2005. Subtype specific affinity for corticosterone of rat organic cation transporters rOCT1 and rOCT2 depends on three amino acids within the substrate binding region. Mol. Pharmacol. 67, 1612–1619.

Gorboulev, V., Ulzheimer, J. C., Akhoundova, A., Ulzheimer-Teuber, I., Karbach, U., Quester, S., Baumann, C., Lang, F., Busch, A. E., Koepsell, H., 1997. Cloning and characterization of two human polyspecific organic cation transporters. DNA Cell Biol. 16, 871–881.

Gorboulev, V., Volk, C., Arndt, P., Akhoundova, A., Koepsell, H., 1999. Selectivity of the polyspecific cation transporter rOCT1 is changed by mutation of aspartate 475 to glutamate. Mol. Pharmacol. 56, 1254–1261.

Gorbunov, D., Gorboulev, V., Shatskaya, N., Mueller, T., Bamnerg, E., Friedrich, T., Koepsell, H., 2008. High-affinity cation binding to organic cation transporter 1 induces movement of helix 11 and blocks transport after mutations in a modeled interaction domain between two helices. Mol. Pharmacol. 73, 50–61.

Green, R. M., Lo, K., Sterritt, C., Beier, D. R., 1999. Cloning and functional expression of a mouse liver organic cation transporter. Hepatology 29, 1556–1562.

Grover, B., Auberger, C., Sarangarajan, R., Cacini, W., 2002. Functional impairment of renal organic cation transport in experimental diabetes. Pharmacol. Toxicol. 90, 181–186.

Groves, C. E., Suhre, W. B., Cherrington, N. J., Wright, S. H. Sex differences in the mRNA, protein, and functional expression of organic anion transporter (Oat) 1, Oat3, and organic cation transporter (Oct) 2 in rabbit renal proximal tubules. J. Pharmacol. Exp. Ther. 316, 743–752.

Gründemann, D., Hahne, C., Berkels, R., Schomig, E., 2003. Agmatine is efficiently transported by non-neuronal monoamine transporters extraneuronal monoamine transporter (EMT) and organic cation transporter 2 (OCT2). J. Pharmacol. Exp. Ther. 304, 810–817.

Gründemann, D., Schechinger, B., Rappold, G. A., Schömig, E., 1998. Molecular identification of the corticosterone sensitive extraneuronal catecholamine transporter. Nat. Neurosci. 1, 349-351.

Guindon, S., Gascuel, O. 2003. A Simple, Fast, and Accurate Algorithm to Estimate Large Phylogenies by Maximum Likelihood. Syst. Biol. 52: 696–704.

Hagenbuch, B. and Meier, P.J., 2004. Organic anion transporting polypeptides of the OATP/ SLC21 family: phylogenetic classification as OATP/ SLCO superfamily, new nomenclature and molecular/functional properties. Pflugers Arch. 447, 653–65.

Hall, T. A. 1999. BioEdit: a user-friendly biological sequence alignment editor and analysis program for Windows 95/98/NT. Nucleic Acids Symp. 41: 95–98.

Hayer, M., Bonisch, H., Bruss, M., 1999. Molecular cloning, functional characterization and genomic organization of four alternatively spliced isoforms of the human organic cation transporter 1 (hOCT1/SLC22A1). Ann. Hum. Genet. 63, 473– 482.

Hayer-Zillgen, M., Bruss, M., Bonisch, H., 2002. Expression and pharmacological profile of the human organic cation transporters hOCT1, hOCT2 and hOCT3. Br. J. Pharmacol. 136, 829–836.

Heidiger, M., A., Romero, M. F., Peng, J. B., Takanaga, H., Bruford, E. A., 2004. The ABCs of solute carriers: physiological, pathological and therapeutic implications of human membrane transport proteinsIntroduction. Pflungers Arch. 447, 465-468.

Hirano, M., Maeda, K., Shitara, Y., Sugiyama, Y., 2006. Drug-drug interaction between pitavastatin and various drugs via OATP1B1. Drug Metab. Dispos. 34, 1229–36.

Hoch, M., 2001. Organotin compounds in the environment – an overview. Applied Geochemistry 16, 719-743.

Hodgson, E., 2010. Introduction to Biotransformation (Metabolism). In: Krieger R, editor. Hayes' Handbook of Pesticide Toxicology. Elsevier Inc., Vol. Volume 1. pp. 865–875.

Höglund, P. J., Nordstrom, K. J. V., Schioth, H. B., Fredriksson, R., 2010. The Solute Carrier Families Have a Remarkably Long Evolutionary History with the Majority of the Human Families Present before Divergence of Bilaterian Species. Mol. Biol. Evol. 28, 1531–1541.

Homklin, S., Wattanodorn, T., Ong, S.K., Limpiyakorn, T., 2009. Biodegradation of 17alpha-methyltestosterone and isolation of MT-degrading bacterium from sediment of Nile tilapia masculinization pond. Water Sci. Technol. 59, 261-5.

Huang, P., Xiao, A., Zhou, M., Zhu Z., Lin, S., Zhang B., 2011. Heritable gene targeting in zebrafish using customized TALENs. Nat. Biotechnol. 29, 699-700.

Hwang, P. P., 2009. Ion uptake and acid secretion in zebrafish (Danio rerio). J. Exp. Biol. 212, 1745–1752.

Inazu, M., Takeda, H., Matsumiya, T., 2003. Expression and functional characterization of the extraneuronal monoamine transporter in normal human astrocytes. J. Neurochem. 84, 43–52.

Ivanis, G., Braun, M., Perry, S. F., 2008. Renal expression and localization of SLC9A3 sodium/hydrogen exchanger and its possible role in acid-base regulation in freshwater rainbow trout (Oncorhynchus mykiss). Am. J. Physiol. 295, R971–R978.

Jakoby, W. B., Ziegler, D. M., 1990. The enzymes of detoxication. J. Biol. Chem. 265, 20715-20718.

Jain, A. N. J., 1996. Scoring noncovalent protein-ligand interactions: a continuous differentiable function tuned to compute binding affinities. Comput. -Aided Mol. Des. 10, 427-440.

Ji, L., Masuda, S., Saito, H., Inui, K., 2002. Down-regulation of rat organic cation transporter rOCT2 by 5/6 nephrectomy. Kidney Int. 62, 514–524.

Jonker, J. W., Wagenaar, E., Mol, C. A. A. M., Buitelaar, M., Koepsell, H., Smit, J. W., Schinkel, A. H., 2001. Reduced hepatic uptake and intestinal excretion of organic cations in mice with a targeted disruption of the organic cation transporter 1 (oct1[Slc22a1]) gene. Mol. Cell. Biol. 21, 5471–5477.

Jonker, J. W., Wagenaar, E., van Eijl, S., Schinkel, A. H., 2003. Deficiency in the organic cation transporters 1 and 2 (oct1/oct2 [slc22a1/slc22a2]) in mice abolishes renal secretion of organic cations. Mol. Cell Biol. 23, 7902–7908.

Jouan, E., Le Vee, M., Denizot, C., Da Violante, G., Fardel, O., 2014. The mitochondrial fluorescent dye rhodamine 123 is a high-affinity substrate for organic cation transporters (OCTs) 1 and 2. Fundamental and Clinical Pharmacology. Fundam. Clin. Pharmacol. 28, 65-77.

Kanai, Y. and Hediger, M. A., 2004. The glutamate/neutral amino acid transporter family SLC1: molecular, physiological and pharmacological aspects. Pflugers Arch 447, 469–479.

Karbach, U., Kricke, J., Meyer-Wentrup, F., Gorboulev, V., Volk, C., Loffing-Cueni, D., Kaissling, B., Bachmann, S., Koepsell, H., 2000. Localization of organic cation transporters OCT1 and OCT2 in rat kidney. Am. J. Physiol. Renal Physiol. 279, F679–F687.

Kassahn, K. S., Dang, V. T., Wilkins, S. J., Perkins, A. C., Ragan, M. A., 2009. Evolution of gene function and regulatory control after whole-genome duplication: comparative analyses in vertebrates. Genome Res. 19, 1404–1418.

Kato, Y., Yoshida, K., Watanabe, C., Sai, Y., Tsuji, A., 2004. Screening of the interaction between xenobiotic transporters and PDZ proteins. Pharm. Res. 21, 1886–1894.

Keller, T., Elfeber, M., Gorboulev, V., Reilander, H., Koepsell, H., 2005. Purification and functional reconstitution of the rat organic cation transporter OCT1. Biochemistry 44, 12253–12263.

Kerb, R., Brinkmann, U., Chatskaia, N., Gorbunov, D., Gorboulev, V., Mornhinweg, E., Keil, A., Eichelbaum, M., Koepsell, H., 2002. Identification of genetic variations of the human organic cation transporter hOCT1 and their functional consequences. Pharmacogenetics 12, 591–595.

Khalil, W. K. B., Hasheesh, W. S., Marie, M.- A. S., Abbas, H. H., Zahran, E. A., 2011. Assessment the impact of 17α-methyltestosterone hormone on growth, hormone concentration, molecular and histopathological changes in muscles and testis of Nile tilapia; *Oreochromis niloticus.* Life Sci. J. 8, 329-343.

Kim, Y., Kyungho, C., Jung, J., Park, S., Kim, P.-G., Park, J., 2007. Aquatic toxicity of acetaminophen, carbamazepine, cimetidine, diltiazem and six major sulfonamides, and their potential ecological risks in Korea. Environ. Int. 33, 370–375.

Kimbrough, R. D., 1976. Toxicity and Health Effects of Selected Organotin Compounds: A Review. Environ. Health Perspect. 14, 51-56.

Kitaichi, K., Morishita, Y., Doi, Y., Ueyama, J., Matsushima, M., Zhao, Y.-L., Takagi, K., Hasegawa, T., 2003. Increased plasma concentration and brain penetration of methamphetamine in behaviorally sensitized rats. Eur. J. Pharmacol. 464, 39–48.

Koehler, M. R., Wissinger, B., Gorboulev, V., Koepsell, H., Schmid, M., 1997. The two human organic cation transporter genes SLC22A1 and SLC22A2 are located on chromosome 6q26. Cytogenet. Cell Genet. 79, 198–200.

Koepsell, H., 2011. Substrate recognition and translocation by polyspecific organic cation transporters. Biol. Chem. 392, 95-101.

Koepsell, H., 2013. The SLC22 family with transporters of organic cations, anions and zwitterions. Mol. Asp. Med. 34, 413–435.

Koepsell, H., Busch, A., Gorboulev, V., Arndt, P., 1998. Structure and Function of Renal Organic Cation Transporters. News Physiol. Sci. 13, 11-16.

Koepsell, H., Lips, K., Volk, C., 2007. Polyspecific organic cation iransporters: structure, function, physiological roles, and biopharmaceutical implications. Pharm. Res. 24, 1227–1251.

Koepsell, H., Schmitt, B. M., Gorboulev, V., 2003. Organic cation transporters. Rev. Physiol. Biochem. Pharmacol. 150, 36–90.

Kolpin, D.W., Furlong, E.T., Meyer, M.T., Thurman, E.M., Zaugg, S.D., Barber, L.B., Buxton, H.T., 2002. Pharmaceuticals, hormones, and other organic wastewater contaminants in U.S. streams, 1999e2000: a national reconnaissance. Environ. Sci. Technol. 36, 1202-1211.

Krammer, A., Kirchhoff, P. D., Jiang, X., Venkatachalam, C. M., Waldman, M., 2005. LigScore: a novel scoring function for predicting binding affinities J. Mol. Graph. Model. 23:395-407.

Kummer, W., Wiegand, S., Akinci, S., Wessler, I., Schinkel, A. H., Wess, J., Koepsell, H., Haberberger, R. V. Lips, K. S., 2006. Role of acetylcholine and polyspecific cation transporters in serotonin-induced bronchoconstriction in the mouse. Respir. Res. 7, 65.

Kwon, M., Choi, Y. A., Choi M.-K., Song I.-S., 2015. Organic cation transporter-mediated drug–drug interaction potential between berberine and metformin. Arch. Pharm. Res. 38, 849-856.

Lecureur, V., Sun, D., Hargrove, P., Schuetz, E. G., Kim, R. B., Lan, L. B., Schuetz, J. D., 2000. Cloning and expression of murine sister of P-glycoprotein reveals a more discriminating transporter than MDR1/P glycoprotein. Mol Pharmacol 57, 24-35.

Lee, W.-K., Reichold, M., Edemir, B., Ciarimboli, G., Warth, R., Koepsell, H., Thevenod, F., 2009. Organic cation transporters OCT1, 2, and 3 mediate high-affinity transport of the mutagenic vital dye ethidium in the kidney proximal tubule. Am J Physiol Renal Physiol 296, F1504–F1513.

Leslie, E.M., Deeley, R.G., Cole, S. P. C., 2005. Multidrug resistance proteins: role of P-glycoprotein, MRP1, MRP2, and BCRP (ABCG2) in tissue defense. Toxicol. Appl. Pharmacol., 204, 216–237.

Liao, B. K., Deng, A. N., Chen, S. C., Chou, M. Y., and Hwang, P. P., 2007. Expression and water calcium dependence of calcium transporter isoforms in zebrafish gill mitochondrion rich cells. BMC Genomics. 8, 354.

Lieschke, G. J. and Currie, P. D., 2007. Animal models of human disease: zebrafish swim into view. Nat. Rev. Genet. 8, 353-367.

Lin, J.H. and Yamazaki, M., 2003. Role of P-glycoprotein in pharmacokinetics: clinical implications. Clin. Pharmacokinet. 42, 59-98.

Lips, K. S., Volk, C., Schmitt, B. M., Pfeil, U., Arndt, P., Miska, D., Ermert, L., Kummer, W., Koepsell, H., 2005. Polyspecific cation transporters mediate luminal release of acetylcholine from bronchial epithelium. Am. J. Respir. Cell Mol. Biol. 33, 79–88.

Loncar, J., Popovic, M., Zaja, R., Smital, T., 2010. Gene expression analysis of the efflux transporters in rainbow trout (Oncorhynchus mykiss). Comp. Biochem. Physiol. C-Toxicol. Pharmacol. 151, 209.

Louis, A., Muffato, M., Roest, C. H., 2013. Genomicus: five genome browsers for comparative genomics in eukaryota. Nucleic Acids Res. 41, 700–705.

Martel, F., Keating, E., Calhau, C., Grundemann, D., Schomig, E., Azevedo, I., 2001. Regulation of human extraneuronal monoamine transporter (hEMT) expressed in HEK293 cells by intracellular second messenger systems. Naunyn-Schmiedebergs Arch. Pharmacol. 364, 487–495.

Mehrens, T., Lelleck, S., Cetinkaya, I., Knollmann, M., Hohage, H., Gorboulev, V., Boknik, P., Koepsell, H., Schlatter, E., 2000. The affinity of the organic cation transporter rOCT1 is increased by protein kinase C-dependent phosphorylation. J. Am. Soc. Nephrol. 11, 1216–1224.

Meyer-Wentrup, F., Karbach, U., Gorboulev, V., Arndt, P., Koepsell, H., 1998. Membrane localization of the electrogenic cation transporter rOCT1 in rat liver. Biochem. Biophys. Res. Commun. 248, 673–678.

Miyazaki, H., Sekine, T., Endou, H., 2004. The multispecific organic anion transporter family: properties and pharmacological significance. Trends Pharmacol. Sci. 25, 654-662.

Minematsu, T., Giacomini, K. M., 2011. Interactions of tyrosine kinase inhibitors with organic cation transporters and multidrug and toxic compound extrusion proteins. Mol. Cancer Ther. 10, 531-539.

Motohashi, H., Sakurai, Y., Saito, H., Masuda, S., Urakami, Y., Goto, M., Fukatsu, A., Ogawa, O., Inui, K., 2002. Gene expression levels and immunolocalization of organic ion transporters in the human kidney. J. Am. Soc. Nephrol. 13, 866–874.

Muegge, I., Martin, Y. C., 1999. A general and fast scoring function for protein-ligand interactions: a simplified potential approach. J. Med. Chem. 42, 791-804.

Muegge, I., 2006. PMF scoring revisited. J. Med. Chem. 49, 5895-5902.

Muller, P.Y., Janovjak, H., Miserez, A.R., Dobbie, Z., 2002. Processing of gene expression data generated by quantitative real-time RT-PCR. Bio. Techniques 32, 1372-79.

Müller, J., Lips, K. S., Metzner, L., Neubert, R. H. H., Koepsell, H., Brandsch, M., 2005. Drug specificity and intestinal membrane localization of human organic cation transporters (OCT). Biochem. Pharmacol. 70, 1851–1860.

Nagel, G., Volk, C., Friedrich, T., Ulzheimer, J. C., Bamberg, E., Koepsell, H., 1997. A reevaluation of substrate specificity of the rat cation transporter rOCT1. J. Biol. Chem. 272, 31953–31956.

Nakamura, T., Yoshida, K., Yabuuchi, H., Maeda, T., Tamai, I., 2008. Functional characterization of ergothioneine transport by rat organic cation/carnitine transporter Octn1 (slc22a4). Biol. Pharm. Bull. 31, 1580-1584.

Nelson, J. S., 2006. Fishes of the World. John Wiley & Sons, New York.

Nichane, M., Van Campenhout, C., Pendeville, H., Voz, M. L., Bellefroid, E. J., 2006. The Na^+/PO_4 cotransporter slc20a1 gene labels distinct restricted subdomains of the developing pronephros in Xenopus and zebrafish embryos. Gene Expr. Patterns 6, 667–672.

Nie, W., Sweetser, S., Rinella, M., Green, R. M., 2005. Transcriptional regulation of murine Slc22a1 (Oct1) by peroxisome proliferator agonist receptor-alpha and -gamma. Am. J. Physiol. Gastrointest. Liver Physiol. 288, G207–G212.

Nies, A. T. and Keppler, D., 2007. The apical conjugate efflux pump ABCC2 (MRP2). Pflugers Arch. 453, 643-659.

Nies, A.T., Koepsell, H., Damme, K., Schwab, M., 2011. Organic cation transporters (OCTs, MATes), *in vitro* and *in vivo* evidence for the importance in drug therapy. Handb.exp. Pharmacol 201, 105–167.

Nigam, S. K., 2015. What do drug transporters really do? Nature Reviews 14, 29-44.

Nigam, S. K., Bahatnagar, V., 2013. How much do we know about drug handling by SLC and ABC drug transporters in children? Clin. Pharmacol. Ther. 94, 27-29.

Nina, M., Beglov, D., Roux, B. J., 1997. Atomic Born radii for continuum electrostatic calculations based on molecular dynamics free energy simulations. Phys. Chem. B. 101, 5239-5248.

Okabe, M., Szakacs, G., Reimers, M.A., Suzuki, T., Hall, M.D., Abe, T., Weinstein, J.N., Gottesman, M.M., 2008. Profiling SLCO and SLC22 genes in the NCI-60 cancer cell lines to identify drug uptake transporters. Mol. Cancer Ther. 7, 3081–3091.

Okuda, M., Saito, H., Urakami, Y., Takano, M., Inui, K., 1996. cDNA cloning and functional expression of a novel rat kidney organic cation transporter, OCT2. Biochem. Biophys. Res. Commun. 224, 500–507.

Otsuka, M., Matsumoto, T., Morimoto, R., Arioka, S., Omote, H., Moriyama, Y., 2005. A human transporter protein that mediates the final excretion step for toxic organic cations. Proc. Natl. Acad. Sci. USA 102, 17923–17928.

Pelis, R. M., Zhang, X., Danqprapai, Y., Wright, S. H., 2006. Cysteine accessibility in the hydrophilic cleft of the human organic cation transporter 2. J. Biol. Chem. 281, 35272–35280.

Pochini, L., Scalise, M., Galluccio, M., Pani, G., Siminovitch, K. A., Indiveri, C., 2012. The human OCTN1 (SLC22A4) reconstituted in liposomes catalyzes acetylcholine transport which is defective in the mutant L503F associated to the Crohn's disease. Biochim. Biophys. Acta. 1818, 559-565.

Popović, M., 2014. Identification, characterization and ecotoxicological relevance of membrane transport protein families slc21 and slc22 in zebrafish (Danio rerio Hamilton, 1822). PhD Thesis.

Popovic, M., Zaja, R., Fent, K., Smital, T., 2013. Molecular characterization of zebrafish Oatp1d1 (Slco1d1), a novel organic anion-transporting polypeptide. J Biol Chem. 22, 33894-33911.

Popp, C., Gorboulev, V., Muller, T. D., Gorbunov, D., Shatskaya, N., Koepsell H., 2005. Amino acids critical for substrate affinity of rat organic cation transporter 1 line the substrate binding region in a model derived from the tertiary structure of lactose permease. Mol. Pharmacol. 67, 1600–1611.

Pritchard, J. B. and Miller, D. S., 1996. Renal secretion of organic anions and cations. Kidney International 49, 1649–1654.

Ravi, V., Venkatesh, B., 2008. Rapidly evolving fish genomes and teleost diversity. Curr. Opin. Genet. Dev. 18, 544–50.

Romano, A., Barca, A., Storelli, C., Verri, T., 2014. Teleost fish models in membrane transport research: the PEPT1(SLC15A1) H^+ -oligopeptide transporter as a case study. J. Physiol. 592, 881-897.

Saborowski, M., Kullak-Ublick, G. A., Eloranta, J. J., 2006. The human organic cation transporter-1 gene is transactivated by hepatocyte nuclear factor-4α. J. Pharmacol. Exp. Ther. 317, 778–785.

Sali, A., Blundell, T. L., 1993. Comparative protein modeling by satisfaction of spatial restraints. Mol. Biol. 234, 779-815.

Salomon, J. J., Endter, S., Tachon, G., Falson, F., Buckley, S. T., Ehrhardt, C., 2012. Transport of the fluorescent organic cation 4-(4-(dimethylamino)styryl)-N-methylpyridinium iodide (ASP+) in human respiratory epithelial cells. Eur. J. Pharm. Biopharm. 81, 351-359.

Sambrook, J. F., Fritsch, E.F., Maniatis, T. 1989. Molecular Cloning - A Laboratory Manual. Cold Spring Harbor Laboratory Press. Cold Spring Harbor, NY, USA.

Sata, R., Ohtani, H., Tsujimoto, M., Murakami, H., Koyabu, N., Nakamura, T., Uchiumi, T., Kuwano, M., Nagata, H., Tsukimori, K., Nakano, H., Sawada, Y., 2005. Functional Analysis of Organic Cation Transporter 3 Expressed in Human Placenta. JPET 315, 888–895.

Sato, Y., Hashiguchi, Y., Nishida, M., 2009. Temporal pattern of loss/persistence of duplicate genes involved in signal transduction and metabolic pathways after teleost-specific genome duplication. BMC Evol Biol 9, 127.

Schmitt, B. M., Koepsell, H., 2005. Alkali cation binding and permeation in the rat organic cation transporter rOCT2. J. Biol. Chem. 280, 24481–24490.

Semon, M., and Wolfe, K. H., 2007. Rearrangement rate following the whole-genome duplication in teleosts. Mol. Biol. Evol. 24, 860–867.

Shen, M. Y., Sali, A., 2006. Statistical potential for assessment and prediction of protein structures. Protein Sci. 15, 2507-2524.

Shin, N., Oh, J-H., Lee, Y-J., 2015. Role of drug transporters: an overview based on knockout animal model studies. Int. J. Pharm. Investig. 45, 101-114.

Shmukler, B. E., Kurschat, C. E., Ackermann, G. E., Jiang, L., Zhou, Y., Barut, B., StuartTilley, A. K., Zhao, J., Zon, L. I., Drummond, I. A., Vandorpe, D. H., Paw, B. H., Alper, S. L., 2005. Zebrafish slc4a2/ae2 anion exchanger: cDNA cloning, mapping, functional characterization, and localization. Am. J. Physiol. 289, 835–849.

Shu, Y., Leabman, M. K., Feng, B., Mangravite, L. M., Huang, C. C., Stryke, D., Kawamoto, M., Johns, S. J., DeYoung, J., Carlson, E., Ferrin, T. E., Herskowitz, I., Giacomini, K. M., 2003. Pharmacogenetics of membrane transporters investigators. Evolutionary conservation predicts function of variants of the human organic cation transporter, OCT1. Proc. Natl. Acad. Sci. USA 100, 5902–5907.

Schlessinger, A., Yee, S.W., Sali, A., Giacomini, K. M., 2013. SLC Classification: An Update. Clin. Pharmacol. Ther. 94, 19-23.

Slitt, A. L., Cherrington, N. J., Hartley, D. P., Leazer, T. M., Klaassen, C. D., 2002. Tissue distribution and renal developmental changes in rat organic cation transporter mRNA levels. Drug Metab. Dispos. 30, 212–219.

Smith, N.F., Figg, W.D., Sparreboom, A., 2005. Role of the liver-specific transporters OATP1B1 and OATP1B3 in governing drug elimination. Expert Opin. Drug. Metab. Toxicol. 1, 429-45.

Steinke, D., Salzburger, W., Braasch, I., and Meyer, A., 2006. Many genes in fish have species-specific asymmetric rates of molecular evolution. BMC Genomics 7, 20.

Sugawara-Yokoo, M., Urakami, Y., Koyama, H., Fujikura, K., Masuda, S., Saito, H., Naruse, T., Inui, K., Takata, K., 2000. Differential localization of organic cation transporters rOCT1 and rOCT2 in the basolateral membrane of rat kidney proximal tubules. Histochem. Cell Biol. 114, 175–180.

Suhre, W. M., Ekins, S., Chang, C., Swaan, P. W., Wright, S. H., 2005. Molecular determinants of substrate/inhibitor binding to the human and rabbit renal organic cation transporters hOCT2 and rbOCT2. Mol. Pharmacol. 67, 1067–1077.

Sukardi, H., Chng, H.T., Chan, E.C.Y., Gong, Z., Lam, S.H., 2011. Zebrafish for drug toxicity screening: bridging the in vitro cell-based models and in vivo mammalian models. Expert Opin. Drug Metab. Toxicol. 7, 579–89.

Sun, S., Wang, K., Lei, H., Li, L., Tu, M., Zeng, S., Zhou, H., Jiang, H., 2014. Inhibition of organic cation transporter 2 and 3 may be involved in the mechanism of the antidepressant-like action of berberine. Prog. Neuro-Psychopharmacol. Biol. Psychiatry 49, 1–6.

Sweet, D. H., Miller, D. S., Pritchard, J. B., 2001. Ventricular choline transport: a role for organic cation transporter 2 expressed in choroid plexus. J. Biol. Chem. 276, 41611–41619.

Tachikawa, M., Takeda, Y., Tomi, M., Hosoya, K., 2010. Involvement of OCTN2 in the transport of acetyl-L-carnitine across the inner blood-retinal barrier. Invest. Ophthalmol. Vis. Sci. 51, 430–36.

Tahara, H., Kusuhara, H., Endou, H., Koepsell, H., Imaoka, T., Fuse, E., Sugiyama, Y., 2005. A species difference in the transport activities of H2 receptor antagonists by rat and human renal organic anion and cation transporters. J. Pharmacol. Exp. Ther. 315, 337–345.

Tamai, I., 2012. Pharmacological and pathophysiological roles of carnitine/organic cation transporters (OCTNs: SLC22A4, SLC22A5 and Slc22a21). Biopharm. Drug Dispos.34, 29-44.

Tanihara, Y., Masuda, S., Sato, T., Katsura, T., Ogawa, O., Imui, K., 2007. Substrate specificity of MATE1 and MATE2-, human multidrug and toxin extrusions/H(+)-organic cation antiporters. Biochem Pharmacol 74, 359-371.

Terashita, S., Dresser, M. J., Zhang, L., Gray, A. T., Yost, S. C., Giacomini K. M., 1998. Molecular cloning and functional expression of a rabbit renal organic cation transporter. Biochim. Biophys. Acta 1369, 1–6.

Tiefenbach, J., Moll, P. R., Nelson, M. R., Hu, C., Baev, L., Kislinger, T., Krause, H. M., 2010. A live zebrafish-based screening system for human nuclear receptor ligand and cofactor discovery. PLoS ONE 5, e9797.

Tirona, R. G., 2011. Molecular mechanisms of drug transporter regulation. Handb.exp. Pharmacol 201, 373-402.

Tom, R., Bisson, L., Durocher, Y., 2008. Transfection of adherent HEK293-EBNA1 cells in a six-well plate with branched PEI for production of recombinant proteins. Cold Spring Harb Protoc. 3.

Turner, J. R., 2009. Intestinal mucosal barrier function in helatih and disease. Nature Reviws Immunology 9, 799-809.

Tusnady, G.E. and Simon, I., 2001. The HMMTOP transmembrane topology prediction server. Bioinformatics 17, 849-850.

Ullrich, K. J., Rumrich, G., David, C., Fritzsch, G., 1993. Bisubstrates: substances that interact with renal contraluminal organic anion and organic cation transport systems. Pfltigers Arch 425, 280-299.

Urakami, Y., Akazawa, M., Saito, H., Okuda, M., Inui, K., 2002. cDNA cloning, functional characterization, and tissue distribution of an alternatively spliced variant of organic cation transporter hOCT2 predominantly expressed in the human kidney. J. Am. Soc. Nephrol. 13, 1703–1710.

Urakami, Y., Nakamura, N., Takahashi, K., Okuda, M., Saito, H., Hashimoto, Y., Inui, K., 1999. Gender differences in expression of organic cation transporter OCT2 in rat kidney. FEBS Lett. 461, 339–342.

Urakami, Y., Okuda, M., Saito, H., Inui, K., 2000. Hormonal regulation of organic cation transporter OCT2 expression in rat kidney. FEBS Lett. 473, 173–176.

Verhaagh, S., Schweifer, N., Barlow, D. P., Zwart, R., 1999. Cloning of the Mouse and Human Solute Carrier 22a3 (Slc22a3/SLC22A3) Identifies a Conserved Cluster of Three Organic Cation Transporters on Mouse Chromosome 17 and Human 6q26–q27. Genomics 55, 209–218.

Verri, T., Terova, G., Romano, A., Barca, A., Pisani, P., Storelli, C., Saroglia, M., 2012. The SoLute Carrier (SLC) family series in teleost fish. In Functional Genomics in Aquaculture, ed. Saroglia, M., Liu, Z., pp. 219–320. John Wiley & Sons, Oxford.

Vialou, V., Amphoux, A., Zwart, R., Giros, B., Gautron, S., 2004. Organic cation transporter 3 (Slc22a3) is implicated in salt intake regulation. J. Neurosci. 24, 2846–2851.

Volff, J. N., 2005. Genome evolution and biodiversity in teleost fish. Heredity 94, 280–294.

Volk, C., Gorboulev, V., Budiman, T., Nagel, G., Koepsell, H., 2003. Different affinities of inhibitors to the outwardly and inwardly directed substrate binding site of organic cation transporter 2. Mol. Pharmacol. 64, 1037–1047.

Volk, C., Gorboulev, V., Kotzsch, A., Müller, T. D., Koepsell, H., 2009. Five Amino Acids in the Innermost Cavity of the Substrate Binding Cleft of Organic Cation Transporter 1 Interact with Extracellular and Intracellular Corticosterone. Mol. Pharmacol. 76, 75–289.

Wu, W., Baker, M. E., Eraly, S. A., Bush, K. T., Nigam, S. K., 2009. Analysis of a large cluster of SLC22 transporter genes, including novel USTs, reveals species-specific amplification of subsets of family members. Physiol. Genomics. 38, 116–124.

Xia, C. Q., Liu, N., Yang, D., Miwa, G., Gan, L. S., 2005. Expression, localization and functional characteristics of breast cancer resistance protein in Caco-2 cells. Drug Metab. Dispos. 33, 637–643.

Yamashiro, W., Maeda, K., Hirouchi, M., Adachi, Y., Sugiyama, Y., 2006. Involvement of transporters in the hepatic uptake and biliary excretion of valsartan, a selective antagonist of the angiotensin II AT1 receptor, in humans. Drug Metab. Dispos. 34, 1247-1254.

Yasujima, T., Ohta, K., Inoue, K., Yuasa, H., 2011. Characterization of Human OCT1-Mediated Transport of DAPI as a Fluorescent Probe Substrate. J. Pharm. Sci. 100, 4006-4012.

Yasujima, T., Ohta, K.-y., Inoue, I., Ishimaru, M., Yuasa, H., 2010. Evaluation of 4,6-Diamidino-2-phenylindole as a Fluorescent Probe Substrate for Rapid Assays of the Functionality of Human Multidrug and Toxin Extrusion Proteins. DMD 38, 715–721.

Yonezawa, A., Inui, K., 2013. Novel riboflavin transporter family RFVT/SLC52: identification, nomenclature, functional characterization and genetic diseases of RFVT/SLC52. Mol Aspects Med. 34, 693-701.

Zeilinger, J., Steger-Hartmann, T., Maser, E., Goller, S., Vonk, R., Lange, R., 2009. Effects of Synthetic Gestagens on Fish Reproduction. Environ. Toxicol. Chem. 28, 2663–2670.

Zhang, L., Dresser, M. J., Gray, A. T., Yost, S. C., Terashita, S., Giacomini, K. M., 1997a. Cloning and functional expression of a human liver organic cation transporter. Mol. Pharmacol. 51,913–921.

Zhang, L., Dresser, M. J., Chun, J. K., Babbitt, P. C., Giacomini, K. M., 1997b. Cloning and functional characterization of a rat renal organic cation transporter isoform (rOCT1A). J. Biol. Chem. 272, 16548–16554.

Zhang, T., Xiang, C. D., Gale, D., Carreiro, S., Wu, E. Y., Zhang, E. Y., 2008. Drug transporter and cytochrome P450 mRNA expression in human ocular barriers: implications for ocular drug disposition. Drug Metab. Dispos. 36, 1300–1307.

Zhao, Y., Castiglioni, S., Fent, K., 2015. Synthetic progestins medroxyprogesterone acetate and dydrogesterone and their binary mixtures adversely affect reproduction and lead to histological and transcriptional alterations in zebrafish (Danio rerio). Environ. Sci. Technol. 49, 4636−4645.

Zhu, H.-J., Appel, D. I., Grundemann, D., Markowitz, J. S., 2010. Interaction of organic cation transporter 3 (SLC22A3) and amphetamine. J. Neurochem. 114, 142-149.

Zwart, R., Verhaagh, S., Buitelaar, M., Popp-Snijders, C., Barlow, D. P., 2001. Impaired activity of the extraneuronal monoamine transporter system known as uptake-2 in Orct3/Slc22a3-deficient mice. Mol. Cell Biol. 21, 4188–4196.

7. Summary

Members of SLC (Solute carrier) superfamily are membrane transporters responsible for the uptake and extrusion of enormous variety of organic and inorganic substrates. The SLC22 family consists of members of major facilitator superfamily (MFS) clan which encompasses all SLCs, together with other membrane proteins and is one of the largest clans of membrane transporters found in humans. Regardless of the maximal amino acid sequence homology of 25%, all members of SLC22 family have similar secondary and tertiary protein structures. They are monomeric polypeptides that have 12 transmembrane α-helices which form transmembrane domains and are incorporated in plasma membranes of the cell. Order and steric arrangement of transmembrane helices define polyspecific active site clefts of transporters.

Organic cation transporters (OCTs) are members of the SLC22A family within SLC superfamily. These internal membrane proteins are responsible for uptake of broad and overlapping range of endo- and xenobiotics. Despite their cricial role in the ADME (Absorption, Distribution, Metabolism, Excretion) and toxicological response of organisms, their detailed ecotoxicological relevance and characteristics are still unknown.Therefore, we focused our research on molecular characterization of organic cation transporters in zabrafish (*Danio rerio*) as newly emerged and valuable model organism.

Using methods such as phylogenetic analysis, qRT-PCR, and transfection in heterologous expression system, we developed transport assays based on fluorescent probes in order to identify potential substrates and inhibitors of ecotoxicological relevance and elucidate transport mechanism of zebrafish Octs as key elements in physiological and ADME preocesses of organic cations.

Phylogenetic analysis revealed specific clustering of vertebrate *SLC22* genes. Zebrafish Octs clustered with other vertebrate *OCTs/Octs*, and with *OCTN/Octn* and *OCT6/Oct6* gene groups of other vertebrates. The analysis of gene block conservation and changes during evolution provided an insight to syntenic relationships among fish and human *OCT/Oct* genes. Synteny analysis showed that zebrafish *Oct1* ortholog is located on chromosome 20, and it showed conserved synteny with human *OCT* cluster. Neighboring genes of zebrafish *Oct1* matched the neighboring genes of the human ortholog cluster. Another zebrafish ortholog *Oct2* is located on chromosome 17. Synteny analysis of *Oct2* showed conserved syntenic relationship with human *OCT* cluster which was confirmed by analysis of neighboring genes locations.

Secondary structure analysis of Oct1 showed that Oct1 forms twelve transmembrane α-helices. Analysis of Oct2 revealed the differences between these two proteins. The major differences are in number of transmembrane helices, with nine transmembrane helices of Oct2. N-glycosylation analysis identified three potential N-glycosylation sites on Oct1 extracellular loop and analysis of Oct2 revealed total of seven N-glycosylation sites.

Tissue expression analysis revealed the highest expression of *Oct1* in kidney, with clear expression differences among genders. Very high expression of *Oct1* was observed in zebrafish liver, with dominant expression in male liver. Tissue expression of Oct2 was highest in testes, following with kidney and other analyzed tissues in lower range of expression, starting from intestine and following with liver, gills, brain and the lowest observed expression in ovaries. High expression of zebrafish Oct1 in major toxicologically relevant tissues, with emphasis on the highest expression in kidney, points to crucial role of this transporter in absorption, reabsorption and excretion of organic cations in zebrafish.

Inhibition assays revealed high affinity interactions of Oct1 with steroid hormones, indicating the potential role of Oct1 in mediation of steroid hormone homeostasis which could function as important transporter in gonads and hormone synthesizing organs, as well as in biliary and renal excretion end reabsorption. From the ecotoxicological aspect, Oct1 may be crucial target for xenobiotic disruption by environmental hormones and their synthetic analogs. Inhibition assays also revealed Oct1 as important element in zebrafish ADME processes, with the proposed key role in defense against hazardous environmental and endobiotic compounds through biliary and renal excretion.

Finally, determined 3D model of zebrafish Oct1 and human Oct1 and OCT2 provided new insight in structure and complexity of substrate binding region of analysed transporters, and confirmed complex interactions with potential substrates and inhibitors which affects determination of type of interaction between the transporter and identified interactors.

8. Sažetak

Članovi SLC (*eng. Solute Carriers*) superobitelji membranskh prijenosnika su odgovorni za unos i ekskreciju velikog broja organskih i anorganskih supstrata. Članovi SLC22 obitelji su članovi MFS klana memranskih proteina koji zajedno s drugim membranskim proteinima obuhvaća sve SLCs proteine i predstavlja jedan od najvećih klanova membranskih transportera kod čovjeka. Bez obzira na maksimalne homologije proteina od 25%, svi članovi SLC22 obitelji imaju slične sekundarne i tercijarne strukture. Oni su monomerni polipeptidi sastavljeni od 12 transmembranskih α-uzvojnica koje tvore transmembranske domene i ugrađene su staničnu membranu. Poredak i sterički raspored transmembranskih uzvojnica definiraju polispecifično aktivno mjesto ovih prijenosnika

Prijenosnici organskih kationa (OCT, *engl. Organic Cation Transporters*) su članovi obitelji SLC22A unutar SLC superobitelji. Ovi membranski proteini odgovorni su za unos širokog i preklapajućeg raspona endo- i ksenobiotika. Usprkos njihovoj kritičnoj ulozi u ADME (apsorpcija, distribucija, metabolizam, ekskrecija), kao i toksikološkom odgovoru organizama, njihov detaljan ekotoksikološki značaj i karakteristike su još nepoznate. Stoga smo usredotočili naše istraživanje na molekularnu karakterizaciju prijenosnika organskih kationa u ribe vrste zebrica (*Danio rerio*) kao značajnog modelnog organizma.

Filogenetskom analizom, qRT-PCR-om, transfekcijom u heterolognome ekspresijskom sustavu razvili smo testove na temelju fluorescentnih modelnih supstrata, kako bi se utvrdili potencijalni supstrati i inhibitori, ekotoksikološka važnost i razjasnili transportni mehanizmi Oct prijenosnika zebrice kao ključnih elemenata u fiziološkim i ADME procesima organskih kationa.

Analiza sekundarne strukture zebričinog Oct1 pokazala je da Oct1 formira 12 karakterističnih transmembranskih regija, dok je analiza Oct2 ukazala na prisutne razlike u sekundarnoj strukturi između ova dva proteina. Glavna razika bila je u broju transmembranskih uzvojnica, kojih Oct2 ima samo 9. Analizom N-glikozilacijskih mjesta utvrdili smo tri N-glikozilacijska mjesta na velikoj ekstracelularnoj petlji Oct1, dok je kod Oct2 identificirano sedam N-glikozilacijskih mijesta.

Analizom tkivne ekspresije utvrđena je visoka ekspresija Oct1 u bubregu zebrice, s jasnim spolnim razlikama. Visoka ekspresija je također zabilježena u jetri, s dominacijom u jetri mužjaka zebrice. Tkivna ekspresija Oct2 pokazala je najvišu ekspresiju Oct2 u testisima i bubrezima, kao i nisku razinu ekspresije u crijevima, jetri, škrgama, mozgu i najniže razinu ekspresije u ovarijima. Visoka ekspresija Oct1 u toksikološki bitnim tkivima, s naglaskom na najvšu zabilježenu ekspresiju u bubregu, ukazuje na važnu ulogu ovog prijenosnika u apsorpciji, reapsorpiji i ekskreciji organskih kationa u zebrici.

Testovi inhibicije pokazali su interakcije visokog afiniteta između Oct1 i steroidnih hormona, upućujući na potencijalno važnu ulogu Oct1 u održavanju hormonske homeostaze, odnosu prijenosu steroidnih hormona u gonadama kao mjestima sinteze steroidnih hormona, kao i u bilijarnoj i renalnoj ekskreciji

i reapsorpciji steroidnih hormona. Ekotoksikološki značaj Oct1 ogleda se u tome da bi Oct1 mogao biti glavna meta okolišno sve više prisutnih hormona i njihovih sintetičkih analoga. Inhibicijski testovi također su utvrdili Oct1 kao važan element u ADME procesima zebrice, s predloženom ključnom ulogom u obrani protiv brojnih štetnih endo- i ksenobiotika.

Na kraju, dobiveni trodimenzionalni model zebričinog Oct1 prijenosnika i humanih OCT1 i OCT2 omogućio je novi pogled na strukturu, i posebice kompleksnost susptratne regije analiziranih proteina, čime su potvrđene kompleksne interakcije između aktivnih mijsta prijenosnika i potencijalnih supstrata i inhibitora, što utječe na određivanje tipa interakcija.

9. Abbreviations

Ac	Anolis carolinensis
Ala	Alanine
Arg	Arginine
ASF	Amphiphilic solute facilitator
Asn	Aparagine
Asp	Aspartate
ASP+	4-(4-(dimethylamino)styryl)-N-methylpyridinium iodide
cAMP	Cyclic adenosine monophosphate
cDNA	complementary Deoxyribonucleic acid
cGMP	Cyclic guanosine monophosphate
Ci	Ciona intestinalis
Cys	Cysteine
DAPI	Diamidino-2-phenylindole
DMEM	Dulbecco's modified Eagle medium
DNA	Deoxyribonucleic acid
Dr	Danio rerio
DTT	Dithiothreitol
EDTA	Ethylenediaminetetraacetic acid
EF1α	Elongation factor 1α
EtBr	Ethidium bromide
FBS	Fetal Bovine Serum
FITC	Fluorescein isothiocyanate
Ga	Gastrosteus aculeatus
GFP	Green fluorescent protein
Gg	Gallus gallus
Gln	Glutamine
Gly	Glycine
Gm	Gadus morhua
HEK293	Human Embryonic Kidney 293
HEPES	Hydroxyethyl piperazineethanesulfonic acid
His	Histidine
HKG	Housekeeping gene
Hs	Homo sapiens
I	Inhibitor
IgG	Immunoglobulin G

IgG-HRP	Immunoglobulin G - horseradish peroxidase
Lys	Lysine
MFS	Multifacilitator superfamily
Mm	Mus musculus
MNE	Mean normalized expression
MPP+	1-methyl-4-phenylpyridinium
mRNA	messanger Ribonucleic acid
ne	no effect
nt	not tested
NH_4Cl	Ammonium chloride
NP-40	Nonidet P-40
OAT/Oat	Organic anion transporter
OATP/Oatp	Organic anion transporting polypeptide
OCT/Oct	Organic cation transporter
OCTN/Octn	Organic carnitine transporter
Ol	Oryzas latipes
ORCTL/Orctl	Organic cation like transporter
PBS	Phosphate-buffered saline
PCR	Polymerase chain reaction
PEI	Polyethyleneimine
PGE2	Prostaglandine E2
qRT-PCR	Quantitative Real-Time polymerase chain reaction
Rh123	rhodamine123
Rn	Rattus norvegicus
RNA	Ribonucleic acid
S	Substrate
SD	Standard deviation
SDS	Sodium dodecyl sulphate
SE	Standard error
SLC	Solute carrier
TBA	Tetrabutylammonium
TCL	Total cell lysate
TEA	Tetraethylammonium
TMD	Transmembrane domain

Tn	Tetraodon nigroviridis
TPA	Tetrapentylammonium
Tr	Takifugu rubripes
Tris	Tris(hydroxymethyl)aminomethane
Tyr	Tyrosine
Val	Valine
WGD	Whole genome duplication
wt	wild type
X-gal	5-bromo-4-chloro-3-indolyl-β-D-galactopyranoside
Xl	Xenopus laevis
Xt	Xenopus tropicalis

10. Supplement

Table 1. Protein annotation and accession numbers of protein sequences used in the phylogenetic analysis of SLC22/Slc22 family in vertebrate. Species abbreviations: Hs, *Homo sapiens*; Mm *Mus musculus*; Gg, *Gallus gallus*; Ac, *Anolis carolinensis*; Xl*, Xenopus laevis;* Dr*, Danio rerio;* Tn*, Tetraodon nigroviridis;* Tr*, Takifugu rubripes;* Ga*, Gastrosteus aculeatus;* Ol*, Oryzas latipes.*

Protein annotation	Accession number
HsOAT1	NP_004781.2
HsOAT2	NP_006663.2
HsOAT3	NP_004245.2
HsOAT4	NP_060954.1
HsOAT5	NP_001034841.3
HsOAT6	NP_001004326.4
HsOAT7	NP_543142.2
HsURAT1	NP_653186.2
HsORCTL3	NP_004247.2
HsORCTL4	NP_004794.2
HsOCT1	NP_003048.1
HsOCT2	NP_003049.2
HsOCT3	NP_068812.1
HsOCTN1	NP_003050.2
HsOCTN2	NP_003051.1
HsOCT6	NP_149116.2
MmOat1	NP_032792.2
MmOat2	NP_659105.2
MmOat3	NP_112471.3
MmOat5	NP_659034.1
MmOat6	NP_941052.1
MmUrat1	NP_033229.3
MmOrctl3	NP_598741.2
MmOrctl4	NP_001032838.1
MmOct1	NP_033228.2
MmOct2	NP_038695.1
MmOct3	NP_035525.1
MmOctn1	NP_062661.1
MmOctn2	NP_035526.1
MmOctn3	NP_062697.1
MmOct6	NP_081848.1
GgOat2	NP_001186367.1
GgOrctl3	XP_418528.3
GgOrctl4	XP_418529.3
GgOct1	XP_419621.3
GgOct2	XP_419622.2
GgOct3	XP_419620.4
GgOctn1	NP_001139603.1
GgOctn2	NP_001039293.1

Table continuing on the next page

AcOat1	ENSACAP00000006348
AcOat2	ENSACAP00000004498
AcOat3	ENSACAP00000013862
AcOrctl3	ENSACAP00000009649
AcOatl1	ENSACAP00000008001
AcOct1	ENSACAP00000003531
AcOct2	ENSACAP00000003545
AcOct3	ENSACAP00000003332
AcOctn1	ENSACAP00000019006
AcOctn2	ENSACAP00000012434
AcOct6	ENSACAP00000010768
XlOat1	NP_001087663.1
XlOat3	NP_001087661.1
XlOct1	NP_001087673.1
XlOctn1	NP_001088049.1
XlOctn2	NP_001080898.1
XlOct6	AAH80416.1
DrOat1	AAH95733.1
DrOat2a	NP_001077330.1
DrOat2b	XP_001340340.3
DrOat2c	XP_001337343.1
DrOat2d	XP_001337264.3
DrOat2e	NP_956643.1
DrOat3	NP_996960.1
DrOrctl3	NP_001070840.2
DrOrctl4	XP_001346178.2
DrOct1	NP_998315.1
DrOct2	NP_001107932.1
DrOctn1	XP_001340836.1
DrOctn2	NP_957143.1
DrOct6	NP_001020659.1
GaOat1	ENSGACP00000027657
GaOat2b	ENSGACP00000015157
GaOat2c	ENSGACP00000023551
GaOat3	ENSGACP00000027316
GaOct1	ENSGACP00000007873
GaOct2	ENSGACP00000007823
GaOctn1	ENSGACP00000027599
GaOctn2	ENSGACP00000027601
GaOct6	ENSGACP00000015320

Table continuing on the next page

OlOat1	ENSORLP00000015952
OlOat2e	ENSORLP00000024217
OlOat3	ENSORLP00000007641
OlOrctl3	ENSORLP00000012386
OlOrctl4	ENSORLP00000014717
OlOctn2	ENSORLP00000001412
OlOctn1	ENSORLP00000001455
OlOct6	ENSORLP00000017631
TrOat1	ENSTRUP00000000970
TrOat2c	ENSTRUP00000035983
TrOat2d	ENSTRUP00000035982
TrOat3	ENSTRUP00000043583
TrOrctl3	ENSTRUP00000044590
TrOct1	ENSTRUP00000022458
TrOctn1	ENSTRUP00000005016
TrOctn2	ENSTRUP00000009792
TrOct6	ENSTRUP00000047083
TnOat1	ENSTNIP00000010475
TnOat2a	ENSTNIP00000007735
TnOat2b	ENSTNIP00000012754
TnOat2c	ENSTNIP00000015332
TnOat2d	ENSTNIP00000015333
TnOrctl3a	ENSTNIP00000001359
TnOrctl3b	ENSTNIP00000015723
TnOrctl3c	ENSTNIP00000015723
TnOrctl4	ENSTNIP00000010741
TnOct1	ENSTNIP00000000542
TnOct2	ENSTNIP00000001184
TnOctn1a	ENSTNIP00000017277
TnOctn1b	ENSTNIP00000001229
TnOct6	ENSTNIP00000015214
CiOrcrtl1	XP_002132109.1
CiOrcrtl2	XP_004225970.1
CiOct6a	XP_002123867.2
CiOct6b	ENSCINP00000031808

11. *Curriculum vitae*

First name: Ivan
Family name: Mihaljevic
Date of birth: July 30th 1985
Place of birth: Vukovar, Croatia
Nationality: Croatian
Present position: Ph.D. student, Laboratory for Molecular Ecotoxicology, Division for Marine and Environmental Research, Ruder Boskovic Institute, Zagreb, Croatia.

Education:

- PhD - Postgraduate Interdisciplinary Doctoral Study of "Molecular Biosciences", joint study of the J. J. Strossmayer University of Osijek, Ruđer Bošković Institute, Zagreb and University of Dubrovnik – in progress

- Master's degree in biology, J. J. Strossmayer University of Osijek, Department of biology, 2011

- Bachelors's degree in biology, J. J. Strossmayer University of Osijek, Department of biology, 2008

Projects:

- *Ecotoxicological significance of ABC transport proteins in aquatic organisms,* (2007-2013) Project supported by the Ministry of Science Education and Sports, Project leader Tvrtko Smital, PhD;
- *Identification and characterization of cyanobacterial toxins based on their interaction with basic cellular detoxification systems in zebrafish (Danio rerio) and zooplankton Daphnia magna*. Swiss National Science Foundation (SNSF), SCOPES 2014-2016 Joint Research Project, Project leader Tvrtko Smital, PhD;
- Identification and functional characterization of (eco)toxicologically relevant polyspecific membrane transport proteins in zebrafish (Danio rerio). Croatian science foundation project (2014. - 2018.), Project leader Tvrtko Smital, PhD.

Awards and scholarships:

2012 – Student scholarship given by Croatian society for biochemistry and molecular biology for the attendance (presentation) at the *FEBS3+ Meeting – From molecules to life and back,* Opatija, Croatia.

2010 – Rector's award

2006 – 2010 University scholarship

Platform presentations at scientific conferences:

1. Congress of the Croatian Society of Biochemistry and Molecular Biology (HDBMB2014), 24.-27.9.2014. Zadar, Croatia, The role of organic cation transporters (Octs, SLC22a) in zebrafish (*Danio rerio*
2. Heart of Europe Zebrafish Meeting, 17.-19.9.2014., Warsaw, Poland, The role of organic cation transporters (Octs, SLC22a) in zebrafish (Danio rerio)
3. The 1st Croatian symposium on membrane transporters, 6.-7.6.2013., Zagreb, Croatia. Uloga transportera organskih kationa (Oct, Slc22a) u zebrice (*Danio rerio*)
4. Göttinger Transporttage, 13.-14.10.2013., Gottingen, Germany, Functional characterization of novel uptake transporters in zebrafish (*Danio rerio*): Oat2a, Oat2d, and Oat2e

5. 11th Greta Pifat-Mrzljak International School of Biophysics, 30.9.-9.10.2012., Primošten, Croatia, Functional characterization of novel uptake transporters in zebrafish (*Danio rerio*).
6. FEBS 3+ Meeting, 13.-16.12.2012., Opatija, Croatia, Functional characterization of a novel uptake transporter Oat2a (SLC22a7) in zebrafish (*Danio rerio*)

Publications:

Glisic, B., Mihaljevic, I., Popovic, M., Zaja, R., Loncar J., Fent, K., Kovacevic, R., Smital, T. 2015. Characterization of Glutathione-S-transferases in zebrafish (*Danio rerio*). Aquat. Toxicol. 158, 50-62.

Memberships:

Croatian society for biochemistry and molecular biology
Croatian biophysical society